"NOTICE. When Government or other drawings, specifications or other data are used for any purpose other than in connection with a definitely related Government procurement operation, the U.S. Government thereby incurs no responsibility, nor any obligation whatsoever; and the fact that the Government may have formulated, furnished, or in any way supplied the said drawings, specifications or other data is not to be regarded by implication or otherwise as in any manner licensing the holder or any other person or corporation, or conveying any rights or permission to manufacture, use or sell any patented invention that may in any way be related thereto."

WADC TECHNICAL REPORT 58-166

RESPONSE OF STRUCTU[illegible] O AIRCRAFT GENERATED SHOC[illegible] WAVES

ARDA ASSOCIATES

A[illegible] 959

CONTRACT [illegible] AF(616)-5197

AERO MEDI[illegible] LABORATORY
WRIGHT AIR [illegible] OPMENT CENTER
AIR RESEARCH AN[illegible] 'LOPMENT COMMAND
UNITED ST[illegible] AIR FORCE
WRIGHT-PATTERS[illegible] FORCE BASE, OHIO

WADC TECHNICAL REPORT 58-169

RESPONSE OF STRUCTURES TO AIRCRAFT GENERATED SHOCK WAVES

ARDE ASSOCIATES

APRIL 1959

CONTRACT NO. AF 33(616)-5197
PROJECT NO. 7230
TASK NO. 71780

AERO MEDICAL LABORATORY
WRIGHT AIR DEVELOPMENT CENTER
AIR RESEARCH AND DEVELOPMENT COMMAND
UNITED STATES AIR FORCE
WRIGHT-PATTERSON AIR FORCE BASE, OHIO

McGregor & Werner, Inc., Dayton, O.

FOREWORD

This study of the response of structures to aircraft generated shock waves was performed under USAF Contract No. 33(616)-5197 by authority of Project No. 7230, Task No. 71780, "Effects of the Sonic Boom Pressure Wave Phenomenon on Structures and on Man". Lt. F. J. Leech served as Project Engineer for the Bio-Acoustics Branch, Aero Medical Laboratory, Wright Air Development Center.

Contributing personnel from ARDE ASSOCIATES were: B. J. Aleck, D. Gleich, M. Scheinberg, L. Schneider, J. Aleck and W. Fee.

ABSTRACT

A study of the response of structures to aircraft generated shock waves (popularly called "sonic boom") is presented. Peak, free-stream, shock wave pressures producing failure of various structural elements of buildings are given. The failure pressures are functions of shock wave and structural parameters. Methods and basic data for predicting shock wave failure pressures of structural elements are also presented. Experimental structural failure data and aircraft generated shock wave and wind damage information are employed in conjunction with theoretical considerations to obtain the predicted failure pressures.

Extensions of blast wave theory are made to account for the differences in shape and pressure levels between aircraft generated N-waves and blast waves. The pressure loads on structures produced by aircraft generated shock waves (necessary for structural response predictions) are computed within the general framework of blast wave procedures.

PUBLICATION REVIEW

This report has been reviewed and is approved.

FOR THE COMMANDER:

FRED W. BERNER
Technical Director
Aero Medical Laboratory

TABLE OF CONTENTS

LIST OF ILLUSTRATIONS

LIST OF TABLES

LIST OF SYMBOLS

A	Amplification Factor
A_L	Upper Limit of amplification factor
a	Sonic velocity
a	Plate span
a_{ij}	Mode shape coefficients
a_1, b_1, c_1	Constants
B	Building width
b	Linear dimension
C	Sum of absolute values of participation factors
C_D	Drag coeficient
c	Distance from centroid to outer fiber
D	Distance between bow and tail shock wave
D	Plate flexural rigidity
d	Building separation distance
d_1	Building spacing
E	Young's modulus
$F(t)$	Forcing function
F_{max}	Maximum value of F(t)
$F(\alpha)$	Function of aspect ratio
F_H	Horizontal roof force
F_t	Translational force
F_v	Vertical roof force
$f(t)$	Time function

f	Natural frequency (cyclic)
G	Shear Modulus
g	Gravitational constant
g_{cl}, g_{ss}	Shape factors
H	Building height
H	Higher mode factor
H'	Characteristic building dimension
H_R	Sloped roof height
h	Thickness
h	Window pane height
h_{cl}, h_{ss}	Frequency factors
I	Moment of inertia
i, j	Indices indicating modes
K	Shear factor
k	Spring constant
k	Eigenvalue
L	Building length
L	Linear dimension
L_x, L_y	Plate spans in x and y directions
l	Body length
M	Mach number
M	Moment
M	Total mass
M	Modification factor
m	Mass per unit length of beam

N	Number of buildings
n	Index indicating mode number
P	Total load
P_o	Ambient pressure
PF	Participation factor
p	Pressure
p'	Stagnation pressure
p_{bi}	Inside back face building pressure
p_{bo}	Outside back face building pressure
p_D	Drag pressure
p_f	Failure pressure
p_{fi}	Inside front face building pressure
p_{fo}	Outside front face building pressure
p_H	Horizontal pressure on sloped roof
p_N	Normal pressure on sloped roof
p_r	Reflected pressure
p_s	Free-stream pressure
$\overset{\circ}{p}_s$	Peak value of free-stream pressure
p_t	Translational pressure
p_{to}	Outside top face building pressure
p_u	Static failure pressure
p_v	Vertical pressure on sloped roof
P_{10}, P_{30}	Outside face pressures on building (nonnormal incidence)
q	Dynamic pressure, shear flow, or uniformly distributed load
S, S', S''	Characteristic building dimensions

S_u	Ultimate strength
s	Stress
T	Natural period
t	Time
t	Thickness
t_b	Build up time
t_L	L/U
t_1, t'_1, t_2, t_3, t_p	Characteristic times
U	Shock wave velocity
v	Displacement
W	Total load
w	Weight
w	Window pane width
X	Distance
x, y	Space coordinates
α	Roof pitch angle
a	Aspect ratio
β	Angle of incidence of shock wave
β	Moment coefficient
Δ	Deflection
∇^4	$\left(\frac{\partial^2}{\partial x^2}+\frac{\partial^2}{\partial y^2}\right)\left(\frac{\partial^2}{\partial x^2}+\frac{\partial^2}{\partial y^2}\right)$
δ	Pressure attenuation
δ	Rise function
θ	Angle of incidence of shock wave

Λ	Open area ratio of wall
η	Duration of N-Wave
μ	Mass per unit area of plate
μ_s	Shielding factor
ν	Poisson's ratio
ζ_{ij}	Normal mode shapes
$\tau,\ \tau_1, \tau_1', \tau_2, \tau_2'$	Decay times
ϕ_{ij}	Time functions
ω	Natural frequency (radians)

SECTION 1

INTRODUCTION

With aircraft now flying at supersonic speeds, the public has become aware of the problems created by the resulting pressure disturbances. There has been an increasing number of reports of loud noises or booms on the ground in the vicinity of flying aircraft. This phenomenon is produced by shock waves emanating from aircraft in supersonic flight. These shock waves propagate at sonic speeds to the ground and produce noise or booms. Hence, the name "sonic boom".

An understanding and evaluation of these shock waves and their effects on structures are vital to the solution of practical Air Force problems. Air operations must frequently be carried out in the vicinity of residential communities. An evaluation of possible shock wave damage to civilian structures is necessary to establish rules for flying at supersonic speeds with minimal concomitant annoyance and to check the validity of claims for damage alleged to have been caused by these shock waves. Damage to military installations and aircraft is also of concern since this too effects Air Force operations.

A recent study[6]* has been made of the relation between aircraft parameters and the aircraft generated shock waves. The pressure of a shock wave that exists near ground level just prior to contact with a structure is termed the free-stream pressure. The purpose of this study is to investigate the relation between the free-stream pressure wave parameters and the response of structures to these pressures. The primary objective is to provide bounding values for the free-stream pressures which produce damage to structures and structural elements.

The investigation is broken down into four phases as follows: (1) the determination of the transient loads on structures, (2) the evaluation of structural parameters, (3) the computation of structural response, and (4) the prediction of failure pressures and their correlation with experimental data.

The transient loads are obtained in terms of building and shock wave parameters by the transformation of the free-stream pressures to pressure distributions on structures. This is accomplished by employing blast wave concepts of reflections and pressure rise and attenuation. Blast wave methods are used since a literature survey and contacts with personnel working in the field indicate that no experimental data or practical computational procedures are available concerning pressure distributions on structures subjected to aircraft generated shock waves. Extensions of blast wave theory are made to account for the difference in shape and pressure amplitude of the shock wave compared to a blast wave. Consideration is also given to the loading produced by nonnormal incidence of a shock wave to a structure when the trace on the ground of the inclined front is parallel to the front face of the building. This loading condition is not specifically treated in blast wave procedures.

The structural parameters studied are size, materials, type of construction, material properties and natural frequencies. Experimental data is employed, where available, as basic information for strength and frequency evaluation.

The dynamic response of structural elements to the transient loadings is computed in terms of dynamic amplification factors. The amplification factors are obtained by analytic methods for simple loadings. An analog computer or graphical procedure (utilizing phase plane theory) is employed for the more complex loadings.

---

*Numerical superscripts correspond to like numbered references in Appendix I.

Manuscript submitted in January 1959 for publication as a WADC Technical Report.

Damping effects are ignored in all dynamic response calculations.

Shock wave free-stream failure pressures are obtained by modifying the equivalent static failure pressures (based on static load ultimate strengths) for the effects of reflection of the shock wave by the structure, dynamic amplification, and increase in material strength produced by rapid rate of loading. Use is made of experimental data, where available, in the evaluation of the failure pressures. Wind load and shock wave damage reports are also correlated.

The free-stream pressures producing failure are given for specific values of structural and shock wave parameters. Methods and basic data are presented for use in the prediction of failure pressures for other combinations of shock wave and structural variables.

The shock wave pressure levels generated by low-flying aircraft are low at ground level. Structural theory confirms experimental evidence that plaster walls are the most critically loaded components of residential structures, while glass and window frames are critical in all types of structures. Therefore, these structural elements are emphasized in this report.

SECTION 2

SHOCK WAVE LOADS ON STRUCTURES

FREE-STREAM PRESSURE

1. General

The amplitudes of the shock waves generated by aircraft flying at supersonic speeds decay with distance from the aircraft and the spread of the waves increases with distance from the source. The time variation of the shock wave as it appears to an observer on the ground is an N-shaped wave, figure 1. Theoretical treatments of this phenomenon and some experimental results[9-12] are found in the literature. The agreement between theory and experiment is good.

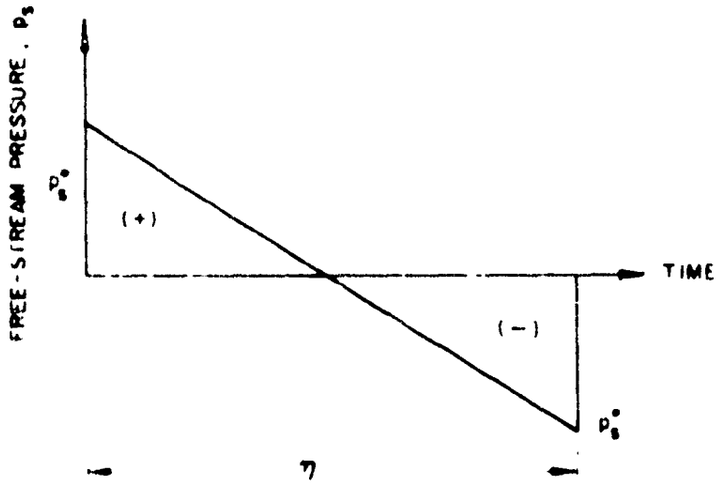

Figure 1. N-Shaped Pressure Wave

In this report the word "pressure" denotes overpressure (positive or negative), i.e., the difference between the actual free-stream pressure and undisturbed ambient pressure.

2. Effects of Temperature, Winds and Terrain

Temperature gradients in the atmosphere, winds, and reflections from terrain affect the propagation of the pressure of the shock wave. The speed of propagation of this pressure disturbance is a function of temperature. The increase of temperature with decrease in altitude will cause a higher velocity in the lower portions of the wave front which bends the shock front. Variations of wind velocity can also produce a curving of the shock front. For certain combinations of temperature gradients and winds, it is possible to either amplify the pressures in a local area on the ground by the "focusing" effects of the curved shock fronts or to deflect the shock waves so that they never reach the ground. A focusing effect or "cusp" is also produced by accelerated flight[4,5,6].

Terrain effects (reflections, shielding) can either amplify or attenuate the shock wave pressure[29]. Large hills, for example, tend to increase shock wave effects in some areas and decrease them in others. The increase or decrease depends upon the change in slope from the horizontal. Steep slopes produce an increase in pressures.

Some reductic in pressure occurs on the reverse slope of the hill.

A detailed consideration of the effects of temperature gradients, winds, and terrain upon free-stream pressure amplitudes is not practical since they are random occurrences. These factors would have to be examined in each particular situation However, in order to evaluate these effects for the purposes of this report, it wi l be assumed that a practical maximum amplification factor for aircraft generated shock wave pressures is o. the order of 2. This value is equivalent to that for a reflection of a sonic wave normal to a flat surface. It is possible, however, with the proper combination of ref.ection and cusps to obtain amplification factors which are much higher. For instance, a factor of 4 can be obtained for reflection in a convex corner[60].

3. Structurally Important Free-Stream Peak Pressures and Wave Durations

Shock wave free-stream peak pressure amplitudes near ground level (in the absence of amplification factors) are quite small except for cases of (1) low altitude flight, (2) high Mach number flight, and (3) accelerated flight. Some representative values[6] of peak free-stream pressure amplitudes are given in Table I below.

TABLE I

REPRESENTATIVE VALUES OF PEAK FREE-STREAM SHOCK WAVE PRESSURE AMPLITUDES

Flight Condition	Distance Normal to Aircraft Flight Path (Ft.)	Peak Pressure Amplitude (psi)
Steady Level Flight Mach Number, M = 1.01	1,000	0.073
	5,000	0.022
	10,000	0.016
	14,000	0.010
Steady Level Flight Mach Number, M = 3.5	1,000	0.162
	5,000	0.048
	10,000	0.028
	14,000	0.022

Flight Condition	Peak Pressure Amplitude At Ground (psi)
Accelerated flight through Mach 1 at 5,000 feet altitude	0.03 to 0.05

Most building codes require structures to be designed to resist wind loads of 30 lb./ft.^{2} = 0.208 psi. Assuming: (a) an amplification factor of 2 for effects of terrain, winds, temperature, etc., (b) a factor of 2 for reflection of the pressure wave by a building, (c) a factor of 2 for dynamic load effects, and (d) that these effects are cumulative, a total amplification factor of 2 x 2 x 2 = 8 is achieved. This gives a lower bound of peak free-stream pressure amplitudes, which is of interest from a structural failure point of view, equal to 0.208/8 or 0.026 psi.

Inspection of Table I reveals that steady level flight at altitudes at or below 5,000 and 10,000 feet respectively for the M = 1.01 and M = 1.5 conditions and the accelerated flight through Mach 1 at 5,000 feet are in the range where structural damage can be expected.

Supersonic flow theory[2,9] gives the following expression for the pressure jump across the bow shock wave:

$$p \simeq 0.53\, p_o (M^2 - 1)^{1/8} \frac{(d/l)}{(y/l)^{3/4}} \qquad (1)$$

Also, the distance between the bow and tail shock waves is given as:

$$D \simeq 1.82\, l\, M^2 \left[\frac{(d/l)\,(y/l)^{1/4}}{(M^2 - 1)^{3/8}} \right] \qquad (2)$$

where, d = maximum body diameter

D = distance between waves

l = body length

M = flight Mach number

p_o = free-stream static pressure

p = pressure jump across wave

y = distance from flight path

From equations (1) and (2) it can be determined that the quantity $p\, D^3/l^3$ is a constant for fixed values of free-stream Mach number, static pressure and body diameter to length ratio. Flight test data[9,10] and experiments with bullets and small shells[12] confirm this relationship.

The pressure peaks, $p = \mathring{p}_s$, of the N-shaped wave, figure 1, are produced by the bow and tail shock waves of the aircraft and the distance between them, D, is the product of flight speed, Ma, and the duration of the wave η .

Data[9] correlated with body length l = 45 feet and Mach number = 1.04 gave,

$$p\, D^3 \simeq 10^7$$

for p in units of lb./ft.^{2} and D in feet.

Taking $p = \mathring{p}_s = 30/8$ lb./ft.^{2} (low bound of structural damage) one has,

$D = \sqrt[3]{\frac{10^7}{30/8}} = 138$ feet as the space spread of the N-wave at this pressure level.

For sonic speed a = 1100 feet/second, the maximum duration of the sonic boom N-wave from the point of view of structural failure is estimated from:

$$\eta = D/Ma \qquad (3)$$

Therefore, $\eta_{max} = \frac{138}{1100 \times 1.04} \simeq \frac{1}{8}$ sec. for this aircraft and Mach number.

At higher pressures, the duration is reduced. An eightfold pressure increase will reduce the duration by one-half. The duration is directly proportional to the

length of the generating aircraft for fixed diameter to length ratio. For a given aircraft, the duration is a weak function of Mach number[9];

$$\eta \propto \frac{M}{(M^2-1)^{3/8}}$$

At M = 2.0, the duration computed above would be approximately 0.06 sec., the minimum at that pressure level. For M = 3, the duration changes to about 0.08 sec. For an aircraft such as the B-52, which has a length of approximately 152 feet, the duration for M = 1.04 would be approximately (152/45)(1/8) = 0.40 sec. Summarizing, for pressures ranging from 30/8 to 30 lbs./ft.^{2}, for airplanes ranging in length from 45 to 150 feet, and for Mach numbers between 1.04 and 3.0, the duration of the N-wave varies between 0.03 and 0.40 seconds.

TRANSFORMATION OF FREE-STREAM PRESSURE TO PRESSURE ON STRUCTURES

1. General

The pressure distribution on a structure subjected to a pressure wave is a function of the structure's shape and size and the free-stream pressure of the wave. The pressure on the structure differs from free-stream values due to the diffraction and reflection of the free-stream pressure wave as it passes over the body.

No experimental measurements of the pressure distributions on structures subjected to sonic boom pressure waves are available. Test information[13-15,18] concerning pressure loads on structures subjected to blast waves is available. Shock tube measurements[19-22] on scale models of structures have also been made.

The blast wave data (including weak conventional explosion information) were obtained mainly for overpressures greatly in excess of shock wave induced pressure and the pressure wave form, figure 2, differs from the N-shaped wave of figure 1. When the pressures from weak conventional explosion tests were of the order of shock wave pressure levels and the wave form was similar to the N-wave, only free-stream pressures were measured or the pressure at one point in the building was recorded. Shock tube data were also measured at high pressure levels and the pressure wave shapes were different from those caused by shock waves.

Procedures[23-30] for predicting the pressure distributions on buildings subjected to blast waves have been developed. These methods are based on a plane shock wave striking a rigid structure and on the Rankine-Huginoit[31,32] relations for normal shock waves. In addition, certain empirical characteristic times (function of the dimensions of the building and the sonic speed of the pressure wave) are employed to depict the pressure rise and decay on the structure. The blast wave procedure is supported by numerous tests[13-18,22,29] on structures subjected to atomic and conventional explosion shock waves and by shock tube studies[19-21] employing models of buildings.

A recent paper[59] has treated the diffraction of a plane step-function pressure disturbance by a two-dimensional rectangular barrier. The method is illustrated by determining the transient pressure distribution on a barrier whose height is equal to one half its length. The undisturbed pressure wave consists of a step function rise in pressure and the shock wave moves parallel to the height of the barrier. There is a sudden rise in pressure to twice the pressure disturbance amplitude when the disturbance hits the barrier. The pressure drops to the amplitude of the step function in a "decay" time of 3 face heights divided by the sonic velocity. (See Figure 2, part b.) These results are in exact agreement with blast wave theory[29].

The shock wave pressure loads presented in this section are based on the sim-

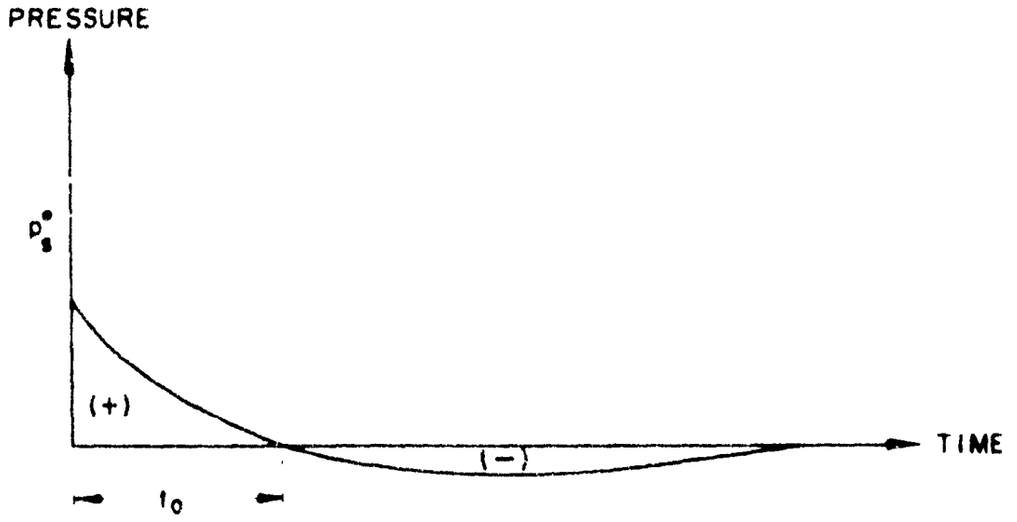

a) BLAST PRESSURE WAVE

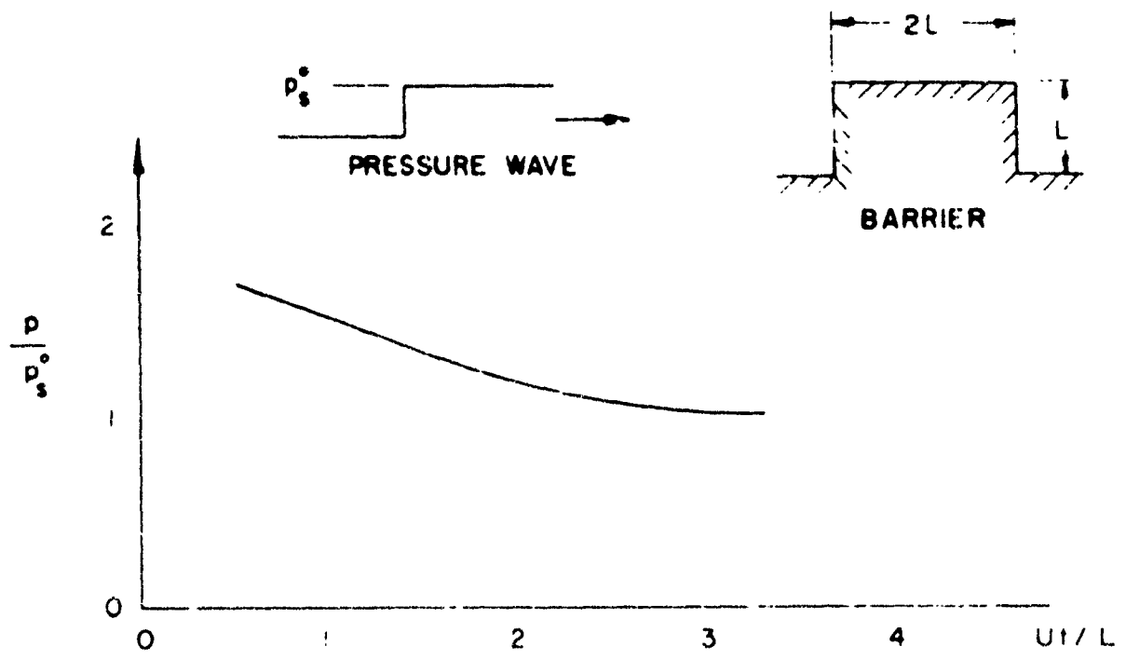

b) AVERAGE PRESSURE DISTRIBUTION ON FRONT FACE OF BARRIER
(DERIVED FROM FIG 3, REF 59)

FIG 2 BLAST PRESSURE WAVE & PRESSURE DISTRIBUTION ON A BARRIER SUBJECTED TO A SONIC PRESSURE PULSE

plified blast theory concepts of characteristic pressure decay, rise times and reflections from rigid walls. Blast wave theory has been modified to account for the difference in shock wave shape (two step discontinuities of the N-wave) and the lower pressure levels. The superposition principle, valid for sonic disturbances, is also employed. The bulk of the blast wave basic load data is taken from the latest compilations[29,30] of load information.

Extension of Ting's[59] analysis to the problem of an N-wave contacting a two-dimensional barrier of arbitrary dimensions was not attempted since this information has only recently become available. Although an analytic solution to a simplified problem is desirable as a guide in understanding a physical phenomenon, the simplified-theory and experimental approach used for blast waves appears more suitable for the determination of shock wave loads in view of (1) the complexities introduced by the many possible variations of the structure (including three-dimensional effects), and (2) the complexities brought about by consideration of nonnormal incidence, whose solution by Ting's method may not converge as rapidly as for normal incidence.

Test results for structures subjected to shock wave loads are urgently needed to check the following assumptions:

1) The characteristic pressure rise and decay times are identical to those known to exist for blast waves and shock tube experiments.

2) The step changes in pressure at the beginning and at the end of the N-wave can be treated identically.

3) The time-constant for decay to free-stream pressure is the same for normal and nonnormal incidence to a vertical plane, when the trace of the shock front on the ground is parallel to the vertical plane.

The pressures considered here are average pressures over a complete surface. For whole buildings or large structural elements of buildings such as walls and roofs, the average load (average pressure times the area) is significant compared to local loads in producing failure. In some cases, local loads (local pressure times a small area) can be significant. An example of this is given by windows. Average local pressure acting on the window area should be taken into account where possible in predicting failure pressures for these elements.

2. Closed Buildings - Normal Incidence

A qualitative picture of the diffraction of a pressure wave moving over a closed structure is given below. The concepts follow conventional simplified blast theory.

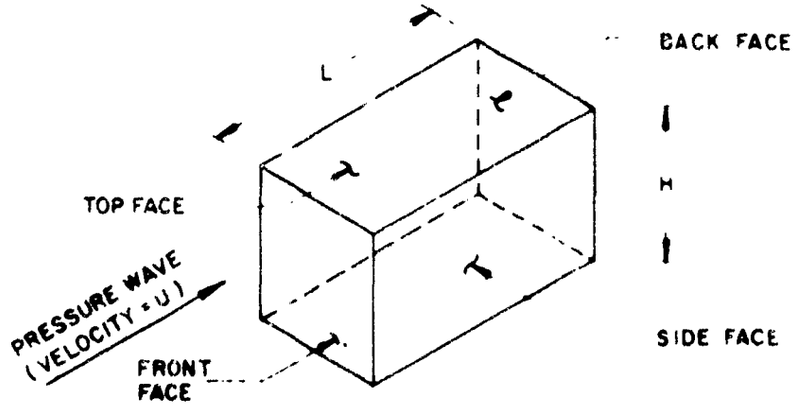

Figure 3. Closed Block - Normal Incidence of Pressure Wave

Consider the structure in Figure 3. When the pressure wave strikes the front face at normal incidence, the pressure rises instantaneously to the reflected pressure[29], $p_r = 2p_s \left(\frac{7p_o + 4p_s}{7p_o + p_s}\right)$. For shock wave pressure levels, the free stream overpressure p_s is much smaller than the ambient pressure p_o and $p_r \dashrightarrow 2p_s$ (the sonic theory result).

The reflected pressure on the front face decays in a time τ to the stagnation pressure because of the rarefaction waves travelling from the corners of the front face to the center. The stagnation pressure p' is given by, $p' = p_s + p_D = p_s + C_D q$ (sum of the free-stream pressure and drag pressure). The drag coefficient C_D for the front face is the order of unity and the dynamic pressure[29] $q = \frac{5}{2}\left(\frac{p_s^2}{7p_o + p_s}\right)$. For sonic waves, $(p_s/p_o) \ll 1$ and the drag pressure may be neglected since it is much smaller than the free-stream pressure p_s. The stagnation pressure p' is then the free-stream pressure p_s.

The decay time τ is approximately that required for a rarefaction wave to travel from the edges of the front face to the center of this face and back to the edges. Experiments[29] indicate that τ can be represented approximately by, $\tau = 3S/U$. The quantity S is a characteristic building dimension (height H or half width B/2, whichever is smaller) and U = shock velocity $= a\left(1 + \frac{6p_s}{7p_o}\right)^{1/2}$. For sonic waves, $p_s/p_o \ll 1$ and U is given by the sonic speed a.

The pressures on the sides and top faces build up to the free-stream pressure p_s (drag pressure neglected) when the wave front reaches particular points on these faces.

The pressure wave reaches the back face after a time delay L/U and diffracts around the edges, traveling down the back surface. The pressure on the back face then changes from zero to free-stream values after a build up time interval t_b. The quantity t_b is given approximately by $t_b = 4S/U$.

Blast wave procedure for prediction of the pressure distribution on a structure is based on a free-stream pressure wave with one step discontinuity. Shock wave free-stream N-waves have two step discontinuities in pressure. In order to apply blast wave theory to estimate the pressure distribution on a structure subjected to a free-stream N-wave, the N-wave is decomposed into two components (each having only one step discontinuity) In addition, each free-stream component is multiplied by a function δ. The δ function represents the decay or rise of pressure with time on particular faces of the building. In this manner, the effect of the second N-wave step discontinuity (negative pressure peak) may be taken into account within the framework of blast wave theory.

a. Average Outside Front Face Pressure

The free-stream pressure of Figure 1 is decomposed into two components as indicated in Figure 4(a). Each step discontinuity in the free-stream N-wave will produce a reflected pressure of twice the free-stream pressure upon striking the front face and decay in a time $\tau = 3S/U$ to free-stream pressure. The δ functions which represent this decay for the two step discontinuities are indicated in Figures 4(b) and 4(c) for $\tau < \eta$. For simplicity, a linear decay has been assumed.

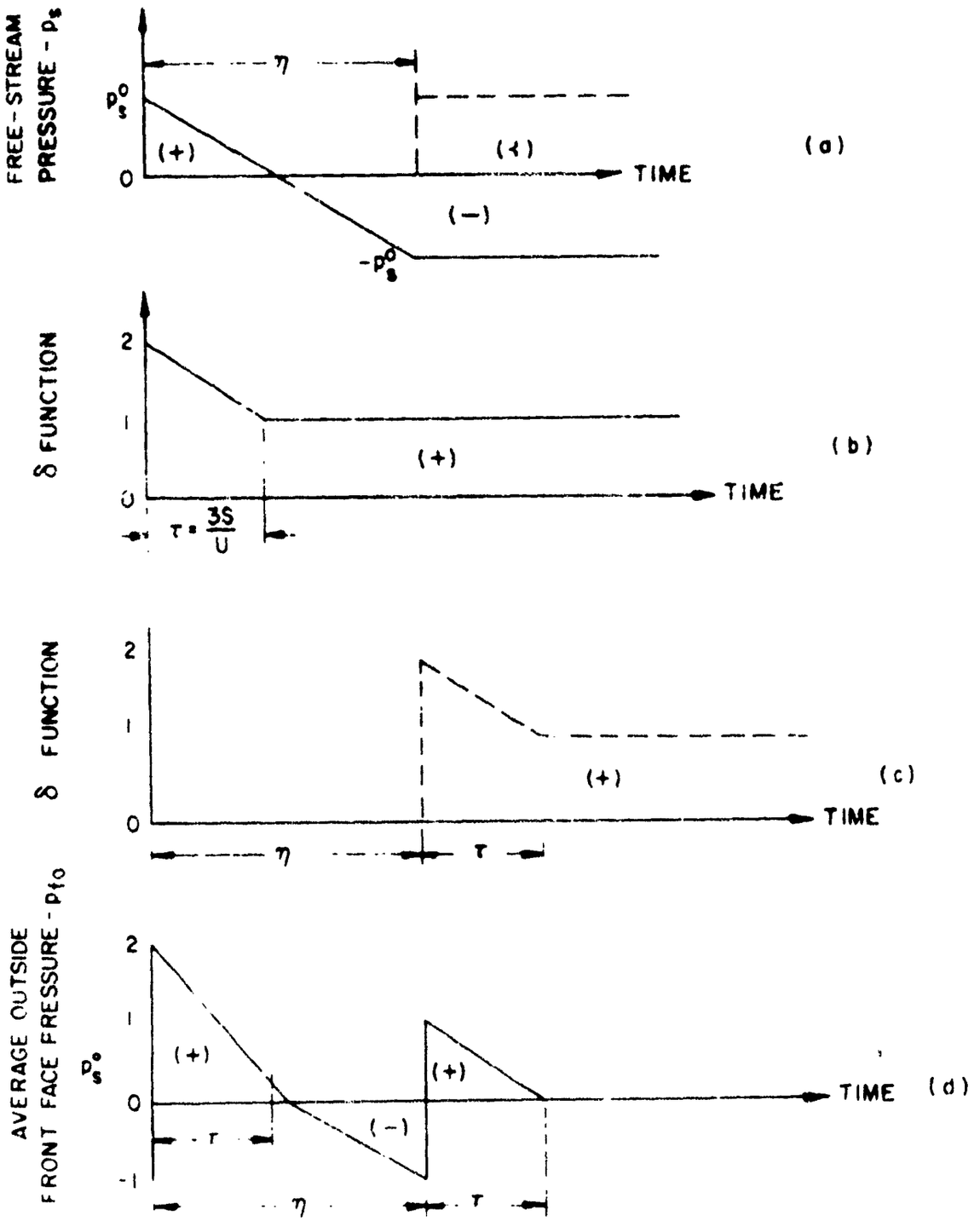

FIGURE 4 AVERAGE OUTSIDE FRONT FACE PRESSURE, p_{fo} FOR DECAY TIME $\tau <$ N-WAVE DURATION, η

The average outside front face pressure p_{fo} is given on Figure 4(d). It was obtained by:

(1) Multiplying the free-stream pressure component for the first step discontinuity, solid line of Figure 4(a), by its δ function, Figure 4(b).

(2) Multiplying the free-stream pressure component for the second step discontinuity, dashed line of Figure 4(a), by its δ function, Figure 4(c).

(3) Superposing items 1 and 2 (superposition is valid for sonic waves).

Figure 4(d) actually should be curved in some regions since the multiplication of the free-stream linear pressure distribution by the sloped portions of the δ function produces a curve. Only critical points on Figure 4(d) were located, and for simplicity a linear variation between these points assumed.

The average outside front face pressure p_{fo}, shown on Figure 5(d), is determined in a similar manner for the case of decay time τ > wave duration η .

Table II gives characteristic building dimensions S corresponding to values of decay times τ for the front face. The N-wave velocity U has been taken as 1100 feet/second.

TABLE II

CHARACTERISTIC BUILDING DIMENSION S FOR VALUES OF DECAY TIME τ

τ (sec.)	$S = \frac{U\tau}{3}$ (ft.)	Remarks
0.05	18.5	Residential size structure
0.10	37	Moderately large structure
0.20	74	Large structure

S = Building height or half width, whichever is smaller

N-wave durations, η , of importance from a structural failure p nt of view are primarily in the range of 0.03 to 0.40 seconds (see page 6). The critical building type is the residential dwelling (see Section 3). Since the τ for residential structures is given as 0.05 seconds in Table II and $\eta_{min.}$ of interest is 0.03 seconds, $\tau > \eta$ is not a situation of frequent interest.

b. Average Outside Top and Side Pressures

The pressures on the top and sides are free-stream pressures p_s. To obtain the load on the top and sides as a function of time, we trace the variation in pressure on a face element of the structure and sum up over the loaded face area. Figure 6 shows the pressure variations on the structure of length L. Time coordinate t' has been converted to a distance coordinate X = Ut. The pressure wave is considered stationary and the structure moving with a velocity U. Figure 6(a) applies when $t \leq L/U$ and Figure 6(b) is valid for $t \leq \eta$.

The load is equal to the shaded area under the pressure-distance curve times

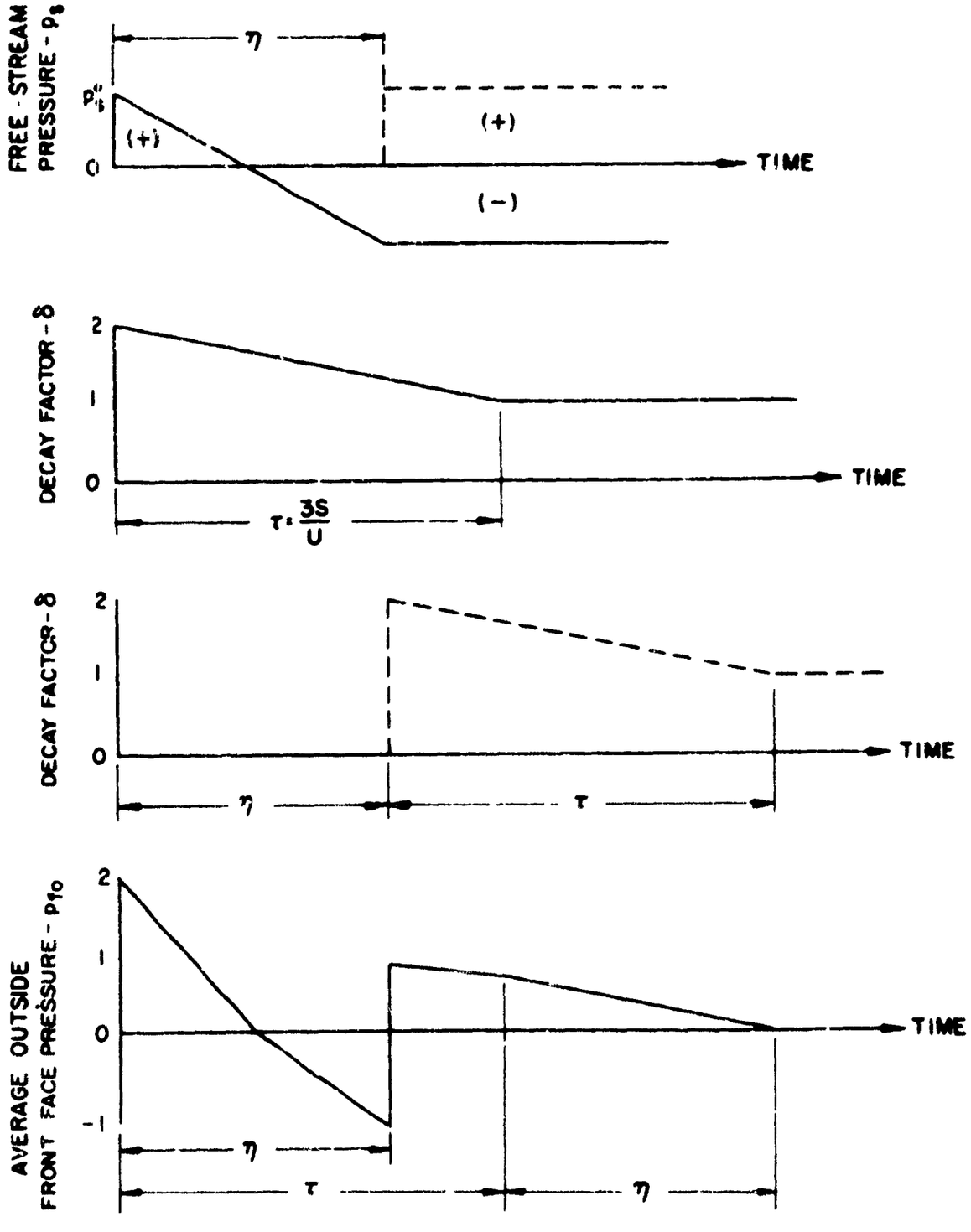

FIGURE 5 AVERAGE OUTSIDE FRONT FAC. PRESSURE, p_{fo} FOR DECAY TIME, $\tau >$ N-WAVE DURATION, η

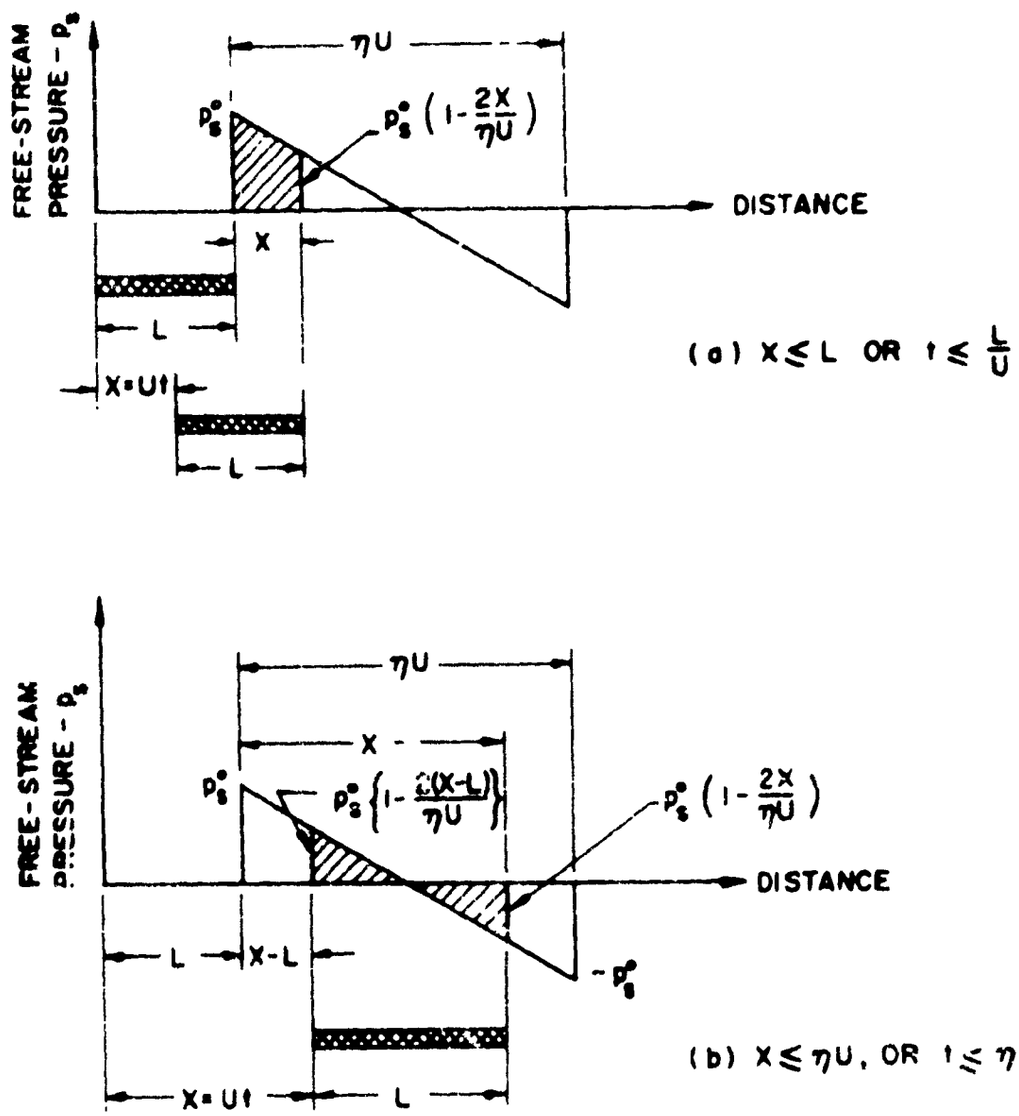

p_s° = MAXIMUM FREE-STREAM PRESSURE
η = DURATION OF FREE-STREAM PRESSURE WAVE
L = BUILDING LENGTH
U = VELOCITY OF FREE-STREAM PRESSURE WAVE
t = TIME

FIGURE 6 TOP AND SIDE PRESSURE VARIATION — CLOSED BUILDING

the top face width B or side face height H. For Figure 6(a) the area under the curve is

$$\frac{X}{2}\left\{\dot{p}_s + \dot{p}_s\left(1 - \frac{2X}{\eta U}\right)\right\} = \dot{p}_s \times \left(1 - \frac{X}{\eta U}\right)$$

Since $X = Ut$ and the average pressure equals the total load divided by the face area BL or HL, we find the average outside top and side pressure as,

$$p_{to}/\dot{p}_s = \frac{t}{t_L}\left(1 - \frac{t}{\eta}\right) \qquad 0 \leq t \leq \frac{L}{U} \tag{4}$$

with, $t_L = L/U$.

Similarly for Figure 6(b),

$$p_{to}/\dot{p}_s = \left(1 + \frac{t_L}{\eta} - \frac{2t}{\eta}\right) \qquad \frac{L}{U} \leq t \leq \eta \tag{5}$$

For $\eta \leq t \leq \eta + \frac{L}{U}$, the average outside top and side pressure is the negative of equation (4) from anti-symmetry considerations. At values of time, $t > \eta + \frac{L}{U}$, the pressure is zero.

Lengths of roof beams and rafters very generally between 15 and 25 feet. Taking a range of wave duration η between 0.05 and 0.10 seconds, the parameter $tL/\eta = L/U\,\eta$ varies between about 0.20 to 0.50 with wave velocity U taken as 1100 feet/second (sonic speed).

Figure 7 shows the average outside top and side pressure variation. For comparison, a sine curve with the same peak amplitude and a period of $t_L + \eta$ is also indicated. It is seen that the sine curve represents the pressure distribution reasonably well for the range of t_L/η from 0.20 to 0.50.

c. Average Outside Back Face Pressure

The back face is not loaded until the pressure wave arrives at the time, $t = L/U$. Time, t, is measured from the instant the wave strikes the front face. The pressure then builds up linearly with time to time-delayed free-stream pressure at the back face, $p_s\,(t - L/U)$ at time, $t = L/U + 4S/U$.

Figure 8(a) shows the time-delayed free-stream pressure $p_s\,(t - L/U)$ broken up into its two components. The δ functions for each component are indicated in Figures 8(b) and 8(c). The average outside back face pressure, p_{bo}, given in Figure 8(d), is obtained by multiplying the time-delayed free-stream pressure components by their respective δ functions and superposing. The curved regions of p_{bo} have again been replaced by straight lines for simplicity as in the case of the front face (see page 11).

The pressure shown in Figure 8 is based on $\frac{4S}{U} < \eta$. The pressure distribution for $\frac{4S}{U} > \eta$ is obtained in a similar manner.

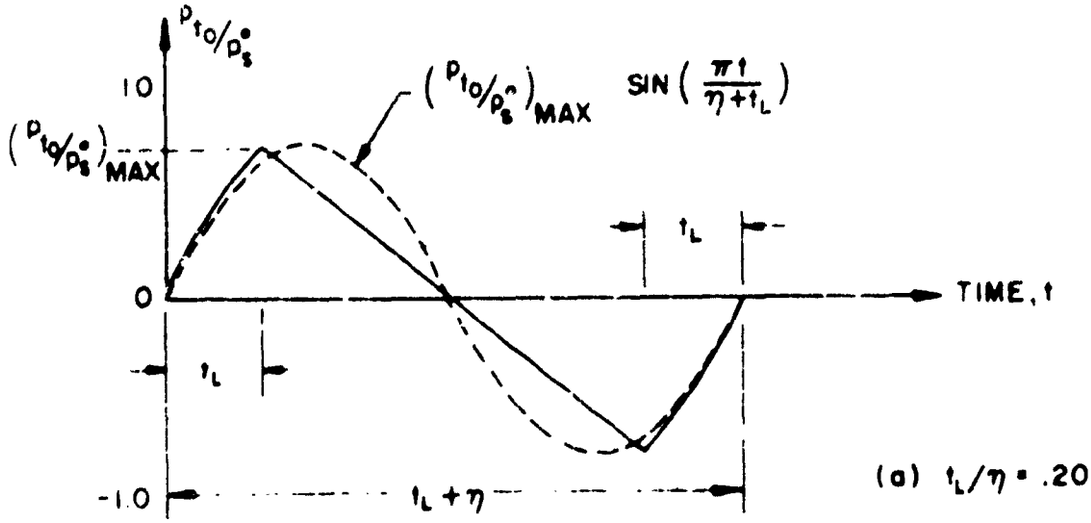

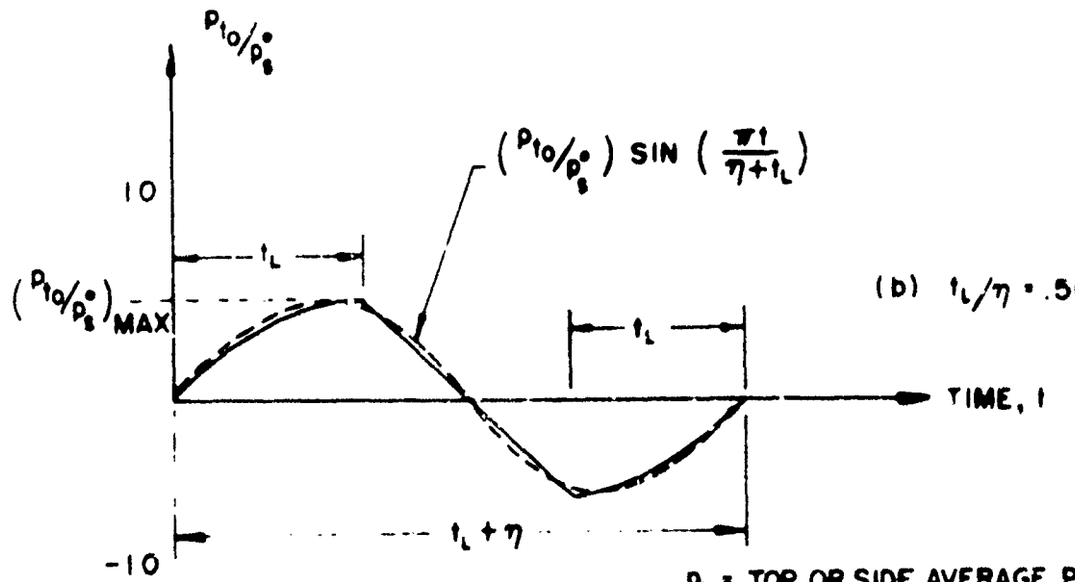

p_{to} = TOP OR SIDE AVERAGE PRESSURE
p_s^* = MAXIMUM FREE-STREAM PRESSURE
η = DURATION OF FREE-STREAM PRESSURE WAVE
t = TIME
$t_L = L/U$
L = LENGTH OF BUILDING
U = VELOCITY OF FREE-STREAM PRESSURE

FIGURE 7 COMPARISON OF OUTSIDE TOP AND SIDE AVERAGE PRESSURE WITH SINUSOIDAL PRESSURE VARIATION - CLOSED BUILDING

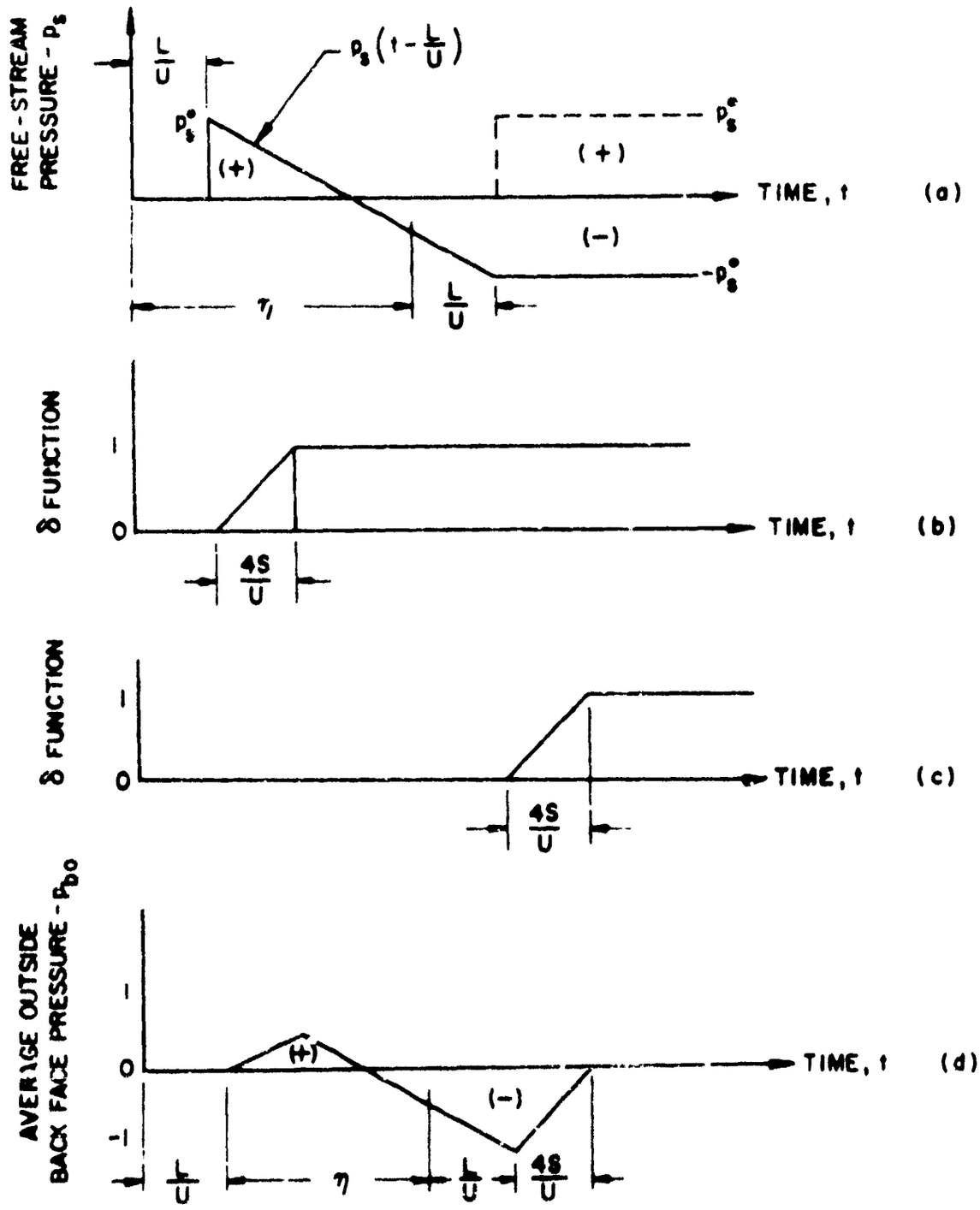

FIGURE 8 AVERAGE OUTSIDE BACK FACE PRESSURE p_{bo} -- CLOSED BUILDING

d. Net Average Translational Pressure

The net average translational pressure, p_t, is defined as the vector sum of the front and back face average pressures. The net average translation pressure times the face area yields the average translational force tending to shear the building.

Figure 9 shows a typical net average translational pressure distribution for a closed building. The data employed were:

Building length, L = 40 Ft.

Building height, H = 24 Ft.

Building width, B = 28 Ft.

Wave duration, η = 0.10 seconds

Free-stream pressure peak amplitude, $\dot{p}_s$ = 1 unit

The building size is representative of residential structures. The average front and back face pressures, p_{fo} and p_{bo}, shown on Figure 9(a) were computed utilizing the procedures discussed in the preceding sections. The net average translational pressure, p_t, given in Figure 9(c) results from the superposition of p_{fo} and p_{bo}. The total duration of p_t is $\eta + \frac{L + 4B}{U}$.

3. Closed Buildings - Nonnormal Incidence

When a pressure wave contacts a closed building at nonnormal angle of incidence, the pressure distribution on the structure is altered from that produced by normal incidence of the pressure wave.

Figure 10(a) illustrates nonnormal incidence in a plane parallel to the horizontal plane of the ground and Figure 10(b) shows nonnormal incidence in a plane perpendicular to the horizontal plane of ground. The angles of incidence θ and β vary between 0 and $\pi/2$.

Experimental data and load calculation procedures[21,30] for vertical front blast waves are available for nonnormal incidence for faces 1 through 4, Figure 10(a), but no data is available for roof loads. The case of nonnormal incidence in side view, Figure 10(b), is not considered in blast wave theory and no information is available.

Nonnormal incidence of the wave front trace in plan view is not as critical as normal incidence except for face 2, Figure 10(a), whose average pressure is increased because of reflection effects. However, in most cases, it is conservative to check a structure for normal incidence in two directions, or to assume normal incidence in a direction which produces the highest translational load (pressure wave normal to largest area face). Loadings for nonnormal incidence in a horizontal plane are discussed here for sake of completeness and for application to vertical plane nonnormal incidence.

Nonnormal incidence in side view, Figure 10(b), is complex because of the interaction of the pressure wave with the two wall boundaries (the ground and the vertical building wall) which intersect in the convex corner at 0.

a. Nonnormal Incidence as Seen in Plan View

The qualitative effects compared to normal incidence are as follows:

(1) The effects of reflected pressure are shared by faces 1 and 2, Figure

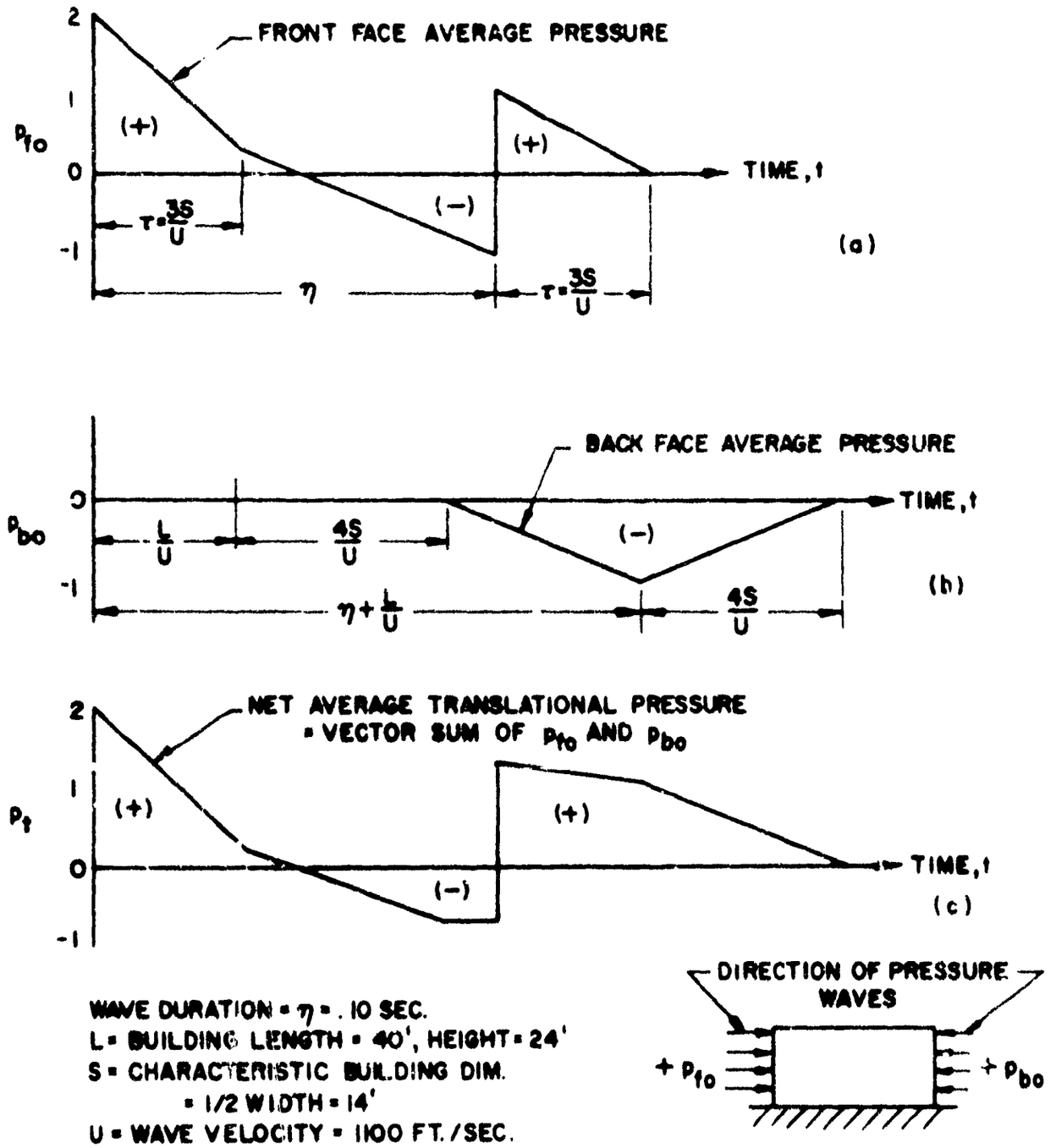

FIGURE 9 TYPICAL NET TRANSLATIONAL PRESSURE ON A CLOSED BUILDING

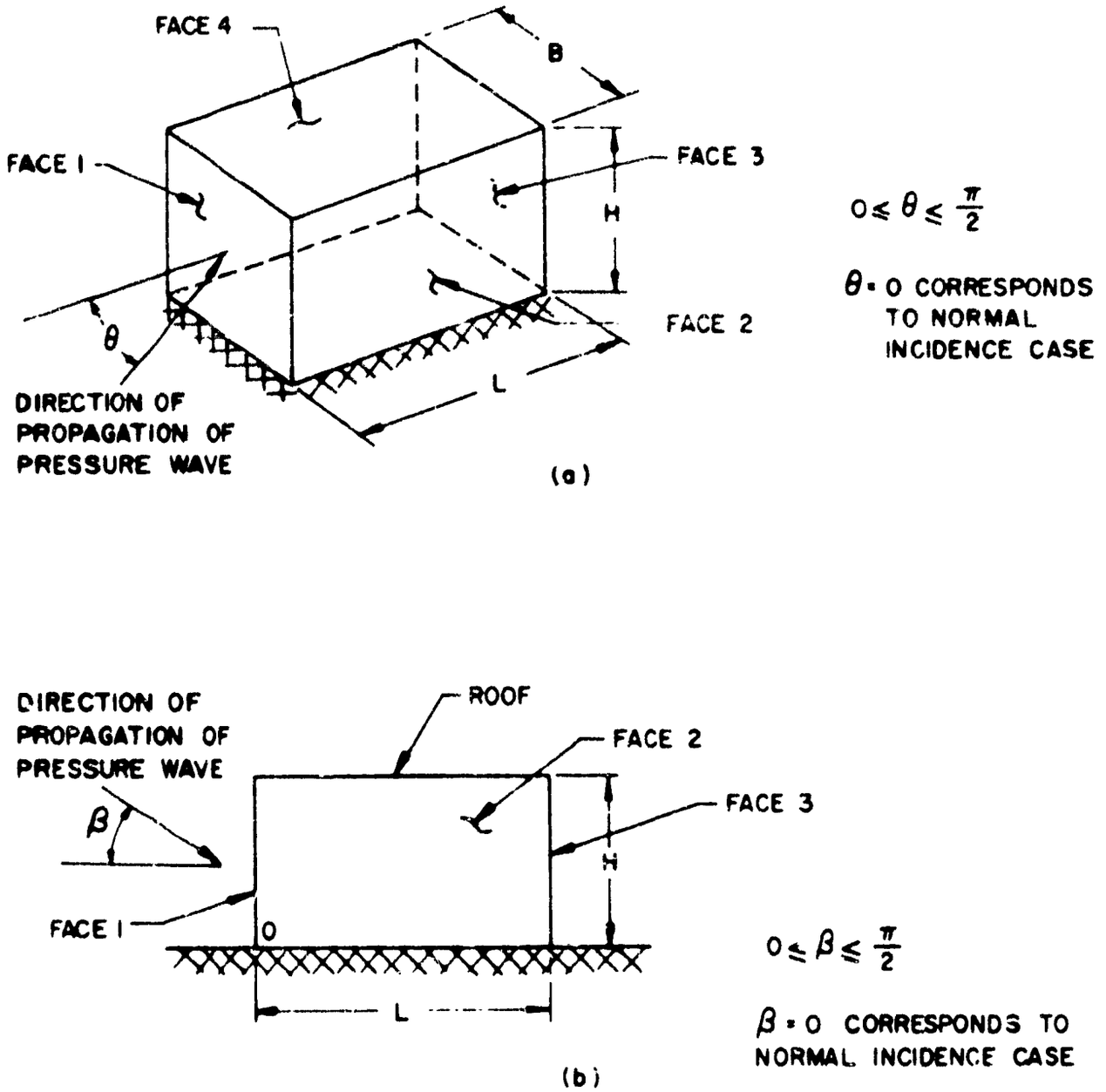

FIGURE 10 NONNORMAL INCIDENCE OF SHOCK WAVE ON A CLOSED BUILDING

10(a). The peak average pressure on face 1 is less than twice the maximum free-stream pressure (the result for normal incidence of sonic waves). The peak average pressure on face 2 is increased over its free-stream value for normal incidence due to reflection effects. The rise to peak pressure on face 1 requires a finite rise time in contrast to the zero rise time for the normal incidence case.

(2) Different characteristic times (functions of angle of incidence θ, building dimensions, and pressure wave velocity U depict the pressure rise and decay.

(3) The pressures on faces 3 and 4, Figure 10(a), are similar to the normal incidence case for the back and side faces respectively, except for different decay and build-up times.

These concepts are applied to estimate the average pressures on the four vertical faces and the net average translational pressures in the directions parallel and normal to the vertical faces, see Figure 10(a).

Blast wave procedures have been somewhat simplified and modified to be consistent with the limiting cases ($\theta = 0$ and $\theta = \pi/2$, corresponding to normal incidence or side on pressure) and to account for the N-shaped shock wave.

(1) Average Outside Pressure, Face 1

Figure 11 (d) gives the average outside pressure on face 1 for decay time $\tau_2 <$ wave duration η. It was constructed employing the same procedures used in Figure 4 for the normal incidence case, except that different characteristic times and δ functions are used. The average pressure for $\tau_2 > \eta$ is constructed in a similar manner.

(2) Average Outside Pressure, Face 2

This case is similar to that of face 1, Figure 11(d), but the characteristic times and maximum values of the δ function are changed. For face 2, we set $\tau_1 = \tau'_1 = \frac{L \cos\theta}{U}$, $\tau_2 = \tau'_2 = \tau'_1 + \frac{3S \sin\theta}{U}$ and the δ functions have maximum values of $(1 + \frac{2\theta}{\pi})$ instead of $2(1 - \frac{\theta}{\pi})$.

(3) Average Outside Pressure, Face 3

The average outside pressure on face 3 is shown in figure 12(d). It is similar to Figure 8 except characteristic times $t_1 = \frac{L \cos\theta}{U}$ and $t_b = \frac{B \sin\theta}{U} + \frac{4S \cos\theta}{U}(1 - \frac{2\theta}{\pi}) + \frac{L \cos\theta}{U}$ replace the normal incidence values $\frac{L}{U}$ and $\frac{4S}{U} + \frac{L}{U}$.

(4) Average Outside Pressure, Face 4

This case is similar to that of face 3, Figure 12 (d) except different characteristic times are employed. For face 4 we set $t_1 = t'_1 = \frac{B \sin\theta}{U}$, $t_b = t'_b = \frac{B \sin\theta + L \cos\theta}{U} + \frac{2\theta}{\pi}(\frac{4S \sin\theta}{U})$.

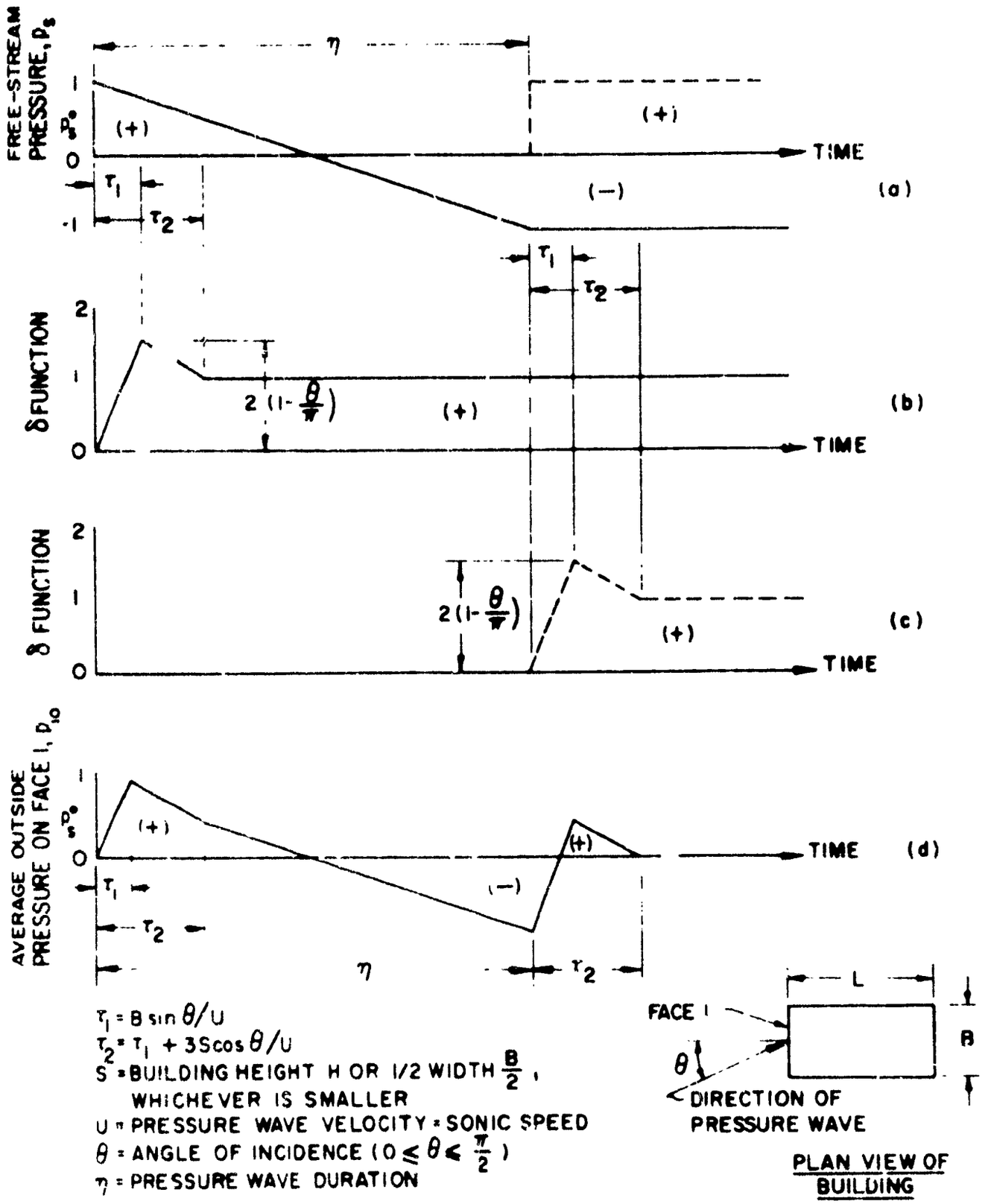

FIGURE II AVERAGE OUTSIDE PRESSURE ON FACE 1, DECAY TIME τ, < WAVE DURATION η, NONNORMAL INCIDENCE, CLOSED BUILDING

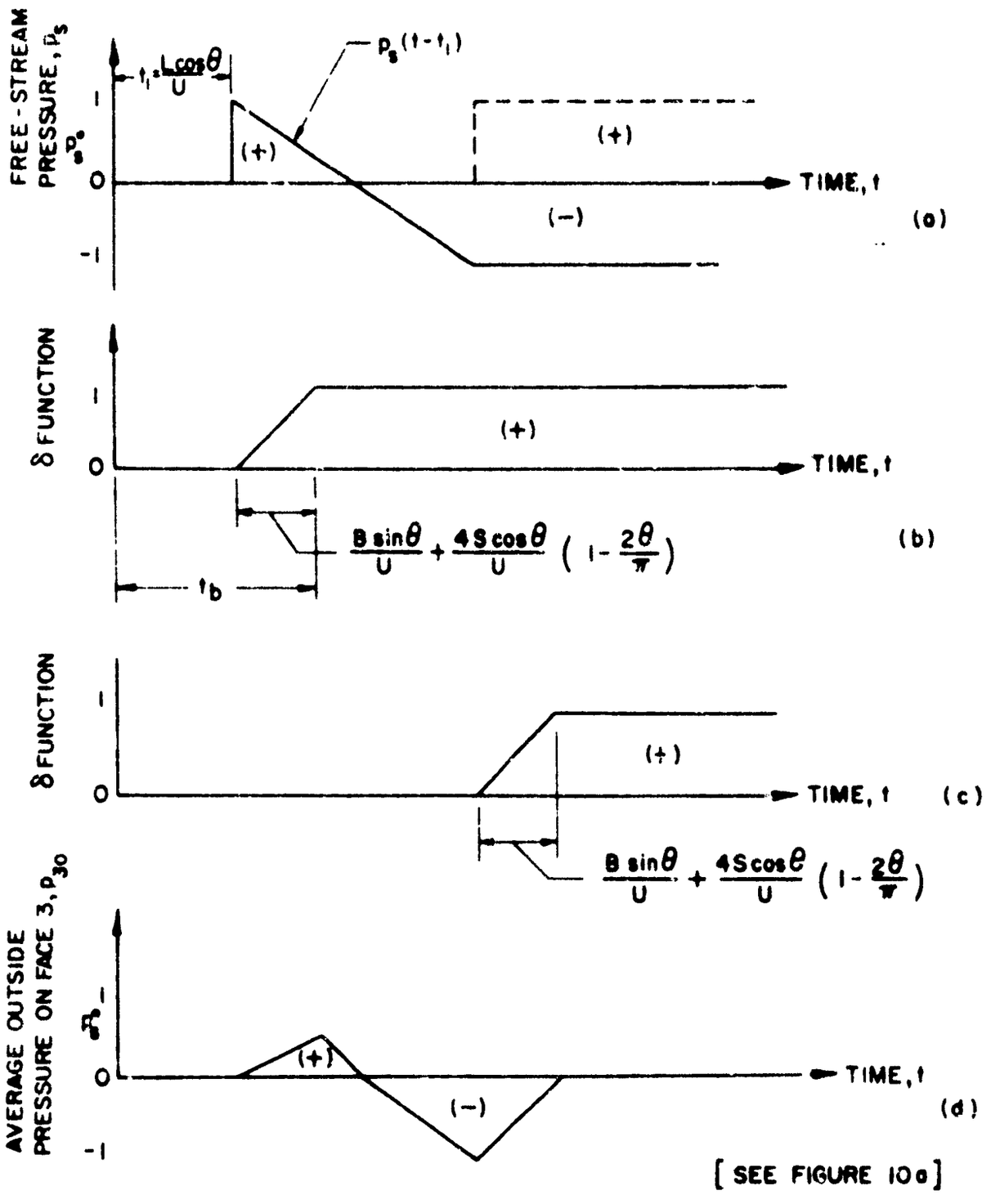

FIGURE 12 AVERAGE OUTSIDE PRESSURE ON FACE 3, NONNORMAL INCIDENCE IN A HORIZONTAL PLANE - CLOSED BUILDING

(5) Average Net Translational Pressure

The average net translational pressure in the two principal directions (normal and parallel to face 1), figure 10(a), are obtained as the vector sum of the pressures on faces 1 and 3 and 2 and 4, respectively

(6) Roof Pressures

For flat roofs, the procedure for estimating the average roof pressure for normal incidence is recommended as a first approximation.

b. Nonnormal Incidence as Seen in a Side View

Pressures as high as four times free-stream pressure are produced on the front vertical wall, Figure 10(b), by nonnormal incidence in side view. Increases in roof pressure over those produced by normal incidence also occur.

These results are obtained from physical considerations concerning the reflection of moving pressure waves. Consider the four pressure wave fronts 1 to 4 (assumed plane) moving with a wave velocity U = wave velocity, as shown on Figure 13. The waves are inclined at an angle β with the vertical and the direction of movement is indicated by the arrows. The wave thickness is η U, with η the duration of the pressure wave, and p_s the free-stream pressure of the wave.

Figure 13 indicates the wave positions at time, t = 0, the instant the incident wave 4 contacts the building at a. Waves a2 and d1 are reflected waves. The other waves are mirror images of these waves, employed to maintain symmetry about eacg and hdbf. A plane of symmetry corresponds to a wall boundary since there is zero flow normal to it. Additional waves required to maintain other building boundaries will not be considered since we are primarily interested in the vertical wall ao.

The shaded areas, ae, bf, cg, dh, correspond to regions where the incident and reflected sonic waves have come together, thus doubling the pressure p_s.

At a time, $t = t_1$, the waves 1, 2, 3, and 4 have moved together a distance Ut_1, Figure 14. The primed letters indicating the new position. A disturbance from the building corner (rarefaction wave) has propagated from a. Its influence is restricted to the circle of radius Ut_1 as indicated. The pressure distribution inside the circle of radius Ut_1 is difficult to describe precisely. It will be assumed to be free-stream pressure p_s. The area of doubled pressure produced by the incident and reflected waves coming together on the vertical wall is then seen to be restricted to the shaded conical region. The vertical wall is loaded only in the region aa' (free-stream pressure p_s inside the circular region and twice free-stream pressure in the conical region). The average pressure on the full vertical wall is less than $2p_s$ and may even be less than p_s depending on the ratio of $Ut_1/\sin\beta$ to wall height H. The vertical distance $Ut_1/\sin\beta$ is greater than the distance the waves moved Ut_1. Point a' can therefore be considered as propagating supersonically with a velocity $\frac{U}{\sin\beta}$. Point d' can also be considered as propagating supersonically with a velocity $\frac{U}{\cos\beta}$.

In Figure 15, the waves 1 and 2 and 3 and 4 have come together at time t_2, with the cones meeting. The new positions of the points is shown by the double primes. The shaded area indicates the region of doubled pressure. The time t_2 is

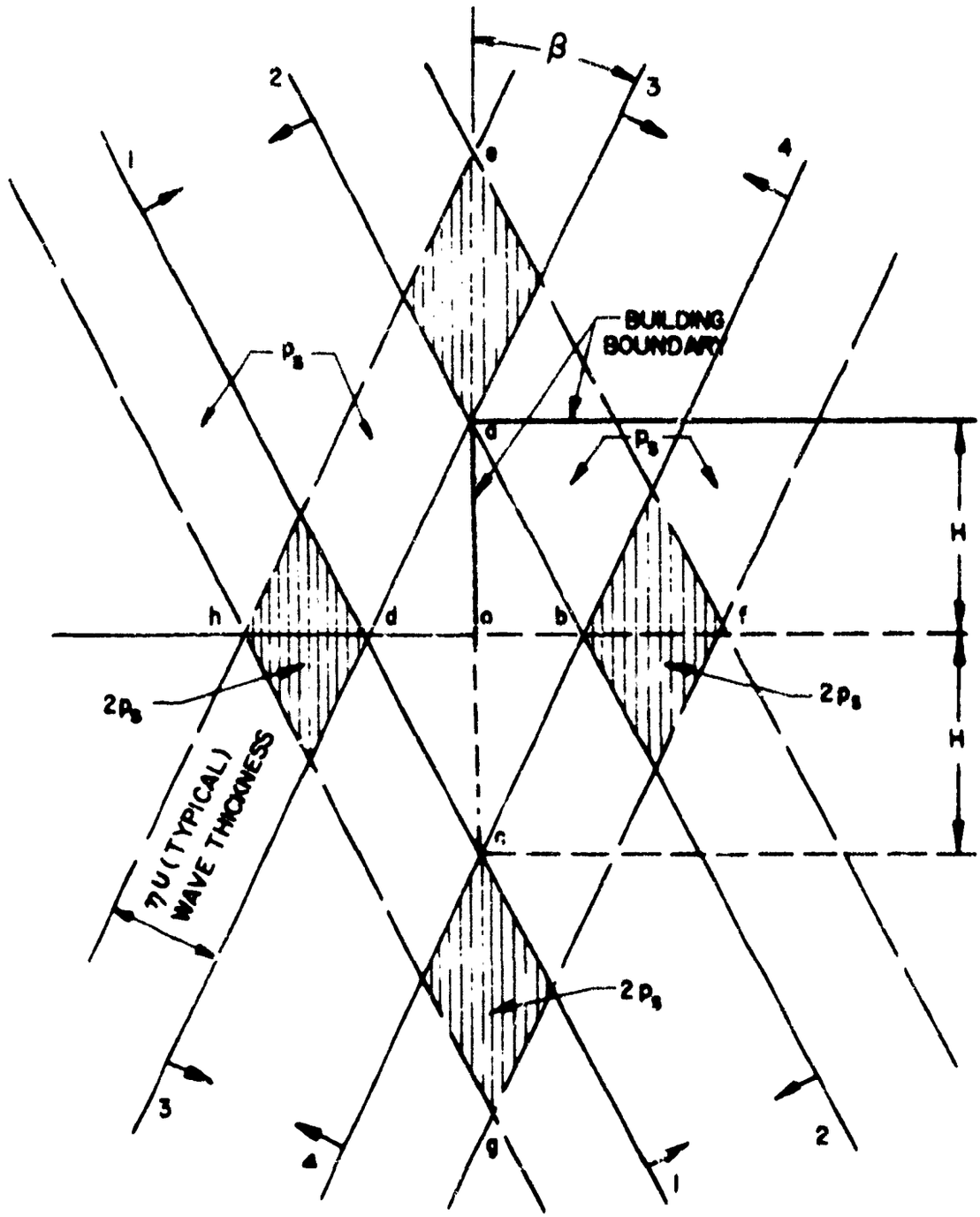

FIGURE 13 NONNORMAL INCIDENCE IN A VERTICAL PLANE

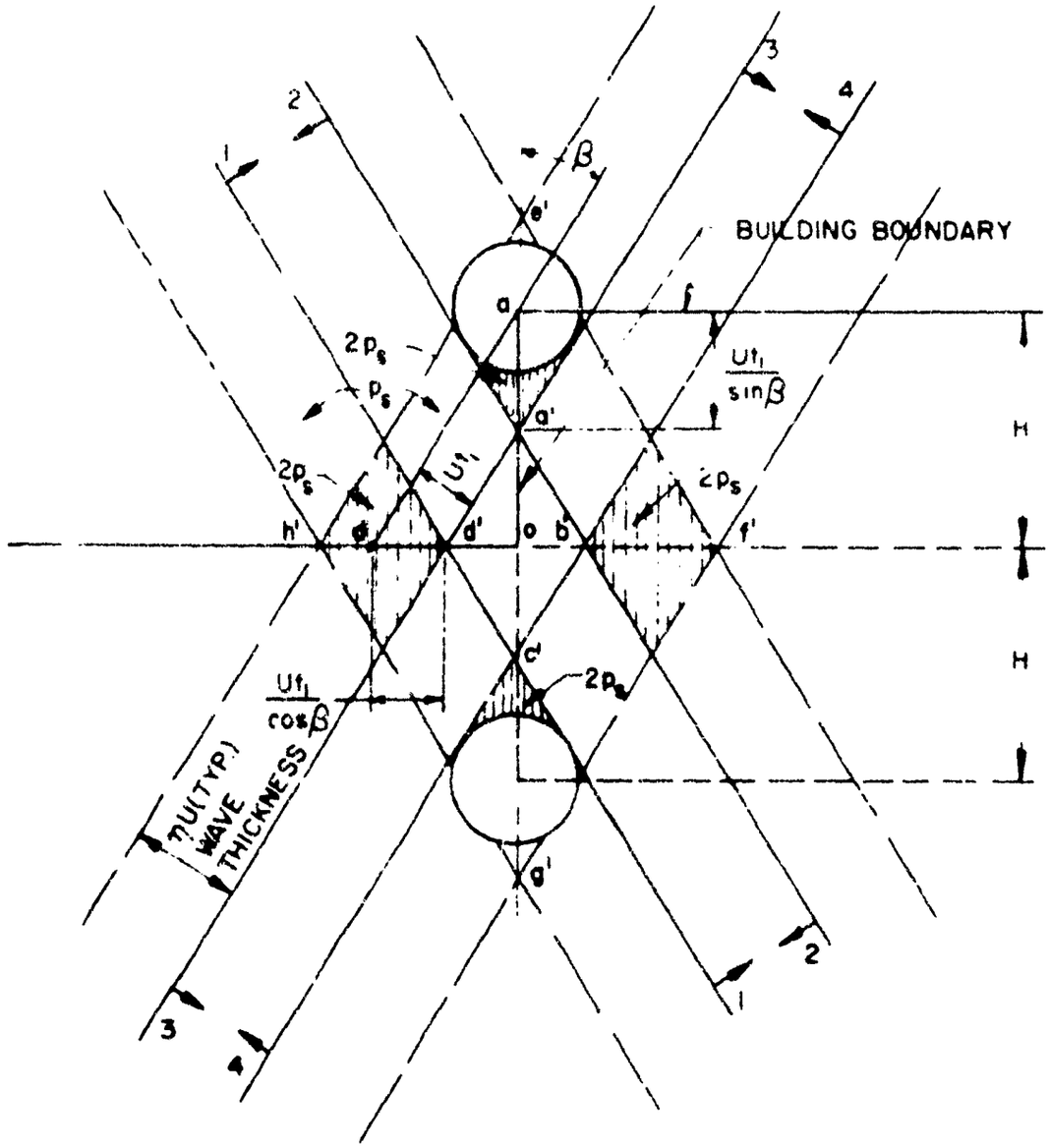

FIGURE 14 NONNORMAL INCIDENCE IN A VERTICAL PLANE ($t = t_1$)

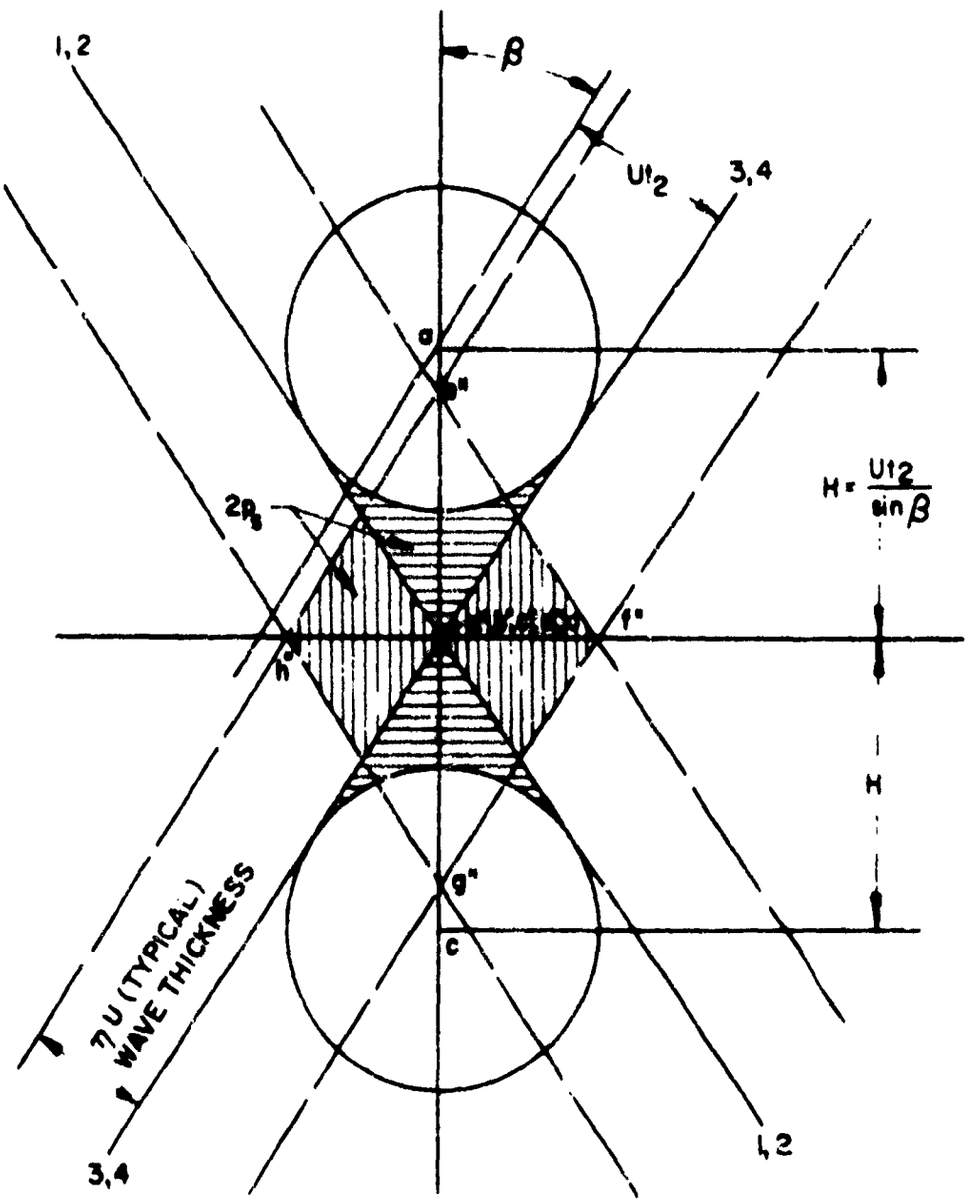

FIGURE 15 NONNORMAL INCIDENCE IN A VERTICAL PLANE ($t = t_2$)

given by, $t_2 = \frac{H \sin \beta}{U}$. The whole vertical wall is loaded (the circular region at pressure p_s and the cone region at $2p_s$) with the average pressure given by $p_s (2 - \sin \beta)$. The average pressure on the vertical wall varies between $2p_s$ for normal incidence ($\beta = 0$) and p_s for the side on case ($\beta = \frac{\pi}{2}$).

In Figure 16 at $t = t_3$, the waves 1 to 4 have passed over each other. The pressure in the doubly cross hatched area is $4p_s$ since all four waves have come together in this region. The pressure in the other shaded region is $2p_s$ (only two waves have come together here). The vertical wall ao is fully loaded, with pressure p_s within the circular region, pressure $4p_s$ in the region c'''o, and $2p_s$ over the remaining region.

The height oc''' is $(\frac{Ut_3}{\sin \beta} - H)$ and the average pressure on the vertical wall is given by,

$$\frac{p_s Ut_3}{H \sin \beta} (2 - \sin \beta) \qquad \text{for} \qquad \sin \beta \leq \frac{Ut_3}{H} \leq \frac{2 \sin \beta}{1 + \sin \beta}, \quad \beta \neq o$$

and

$$p_s (4 - \frac{3Ut_3}{H}) \qquad \text{for} \qquad \frac{2 \sin \beta}{1 + \sin \beta} \leq \frac{Ut_3}{H} \leq 1, \quad \beta \neq o$$

For β a small angle, the maximum average pressure on the vertical wall approaches $4p_s$ when the cone and circle of Figure 16 intersect $(\frac{Ut_3}{H} = \frac{2 \sin \beta}{1 + \sin \beta})$.

The above formulas are not valid at $\beta = 0$ for $\frac{Ut_3}{H} = \frac{2 \sin \beta}{1 + \sin \beta}$ since the cone apex is not infinity and the circle has zero radius. Moreover, the four waves at an angle β with the vertical, Figure 13, become (at $\beta = 0$) two waves parallel to the vertical building face in order to maintain it as a plane of symmetry. The whole front vertical wall is then at an average pressure of $2p_s$ at time $t = 0$ (the normal incidence result). For practical purposes, however, the average pressure on the front vertical wall can be considered $\simeq 4p_s$ for small angles β.

After the time, $t_3 = \frac{H}{U}$, when the circle of radius Ut_3, figure 16, has reached the convex corner at o, the problem cannot be described further in terms of the simple mechanism postulated. A decay to free-stream pressure p_s at times $\geq \frac{H}{U}$ is assumed.

It has been tacitly assumed in the foregoing discussion that the building width is infinite. For finite building width B, the use of an equivalent building dimension is necessary. In addition, blast wave experiments indicate a decay time to essentially free-stream pressure for normal incidence of about 3H/U. In order to be consistent with blast wave tests and take the finite building width into account, it will be assumed that the height H is replaced by $H' = \frac{3B}{2}$ or 3H, whichever is

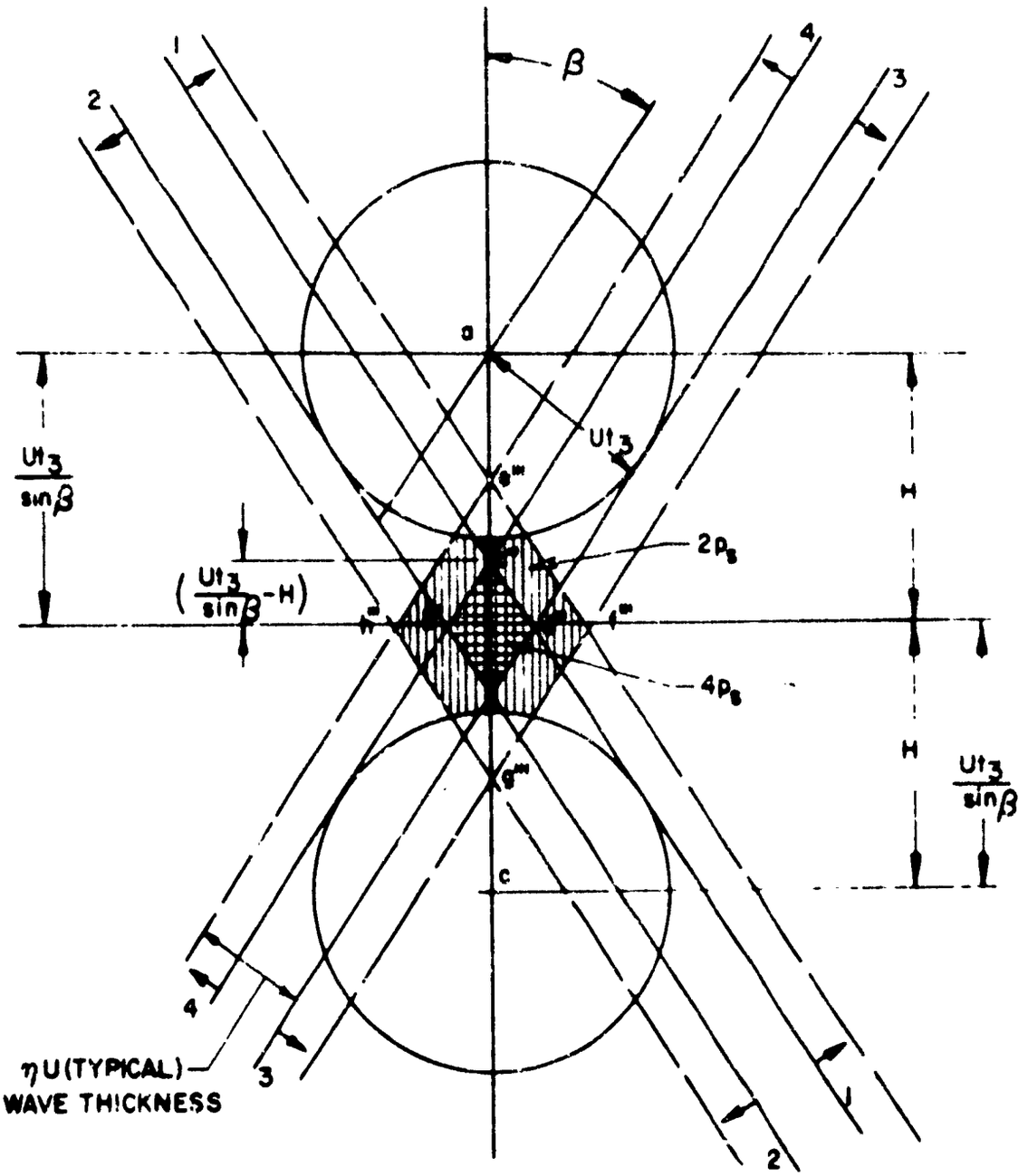

FIGURE 16 NONNORMAL INCIDENCE IN A VERTICAL PLANE ($t = t_3$)

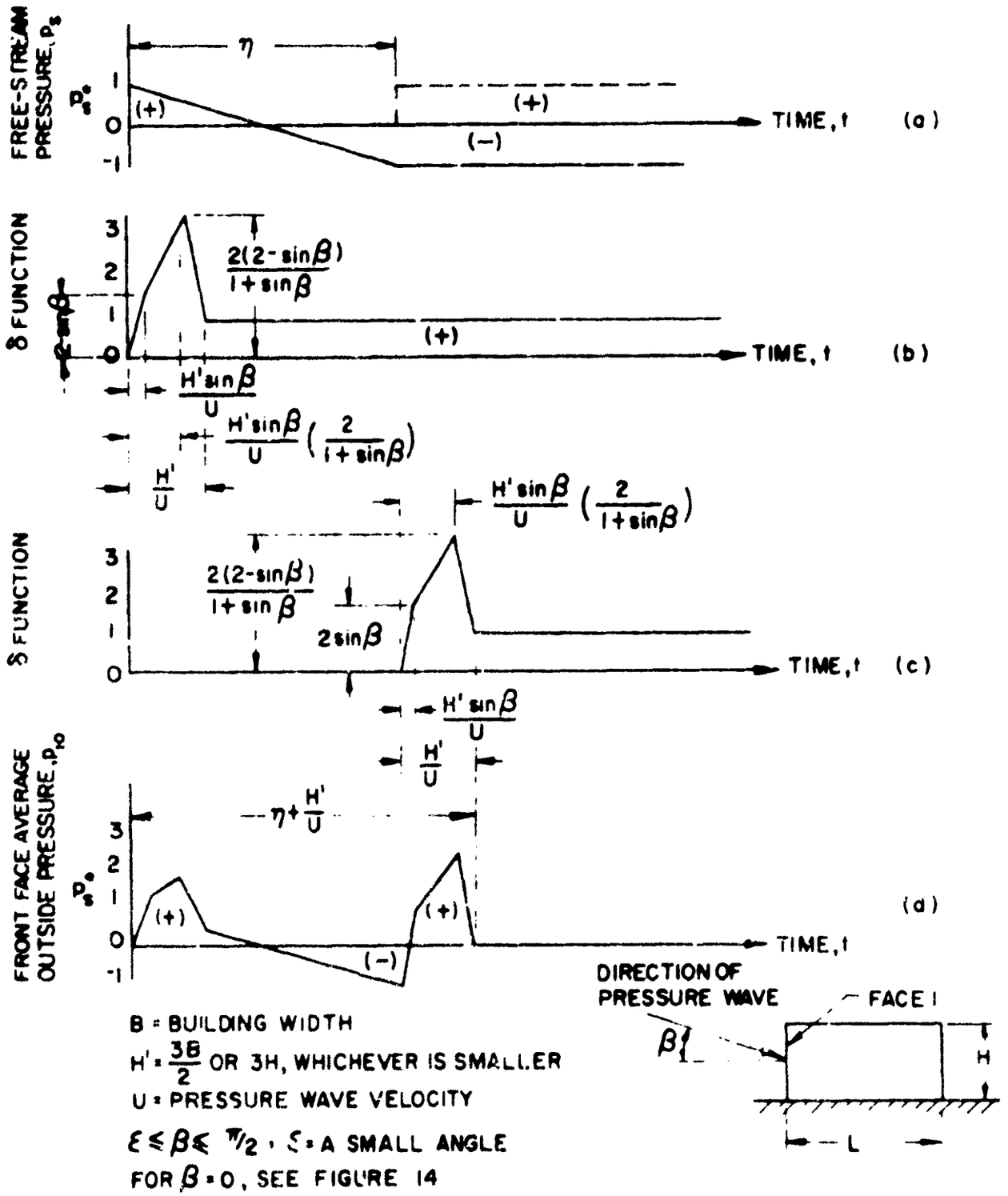

FIGURE 17 AVERAGE OUTSIDE PRESSURE ON FACE I, NONNORMAL INCIDENCE IN A VERTICAL PLANE - CLOSED BUILDING

smaller.

The average outside pressure p_{10} on face 1, Figure 17(b), for nonnormal incidence in a vertical plane, is indicated in Figure 17(d). It was obtained in a manner similar to Figure 4 except different δ functions are employed.

For flat roofs, the average pressure corresponds to that for face 2, Figure 10(a) (nonnormal incidence in a horizontal plane).

The behavior of the rear wall, face 3 of Figure 10(b), will be taken as being similar to that on face 3 for normal incidence in a horizontal plane (Figure 10(a)).

The net translational pressure for nonnormal incidence in a vertical plane for a building with a flat roof is the vector sum of the pressures on faces 1 and 3 (front and back faces) Figure 10(b).

For side walls, face 2 of Figure 10(b), the procedure used for estimation of side wall pressures for the normal incidence case is recommended for estimation of the average pressure.

4. Closed Buildings - Shielding Effects

Figure 18 shows two structures, I and II, situated one directly behind the other. The separation distance between them is d. The pressure wave first contacts structure I, is defracted and reflected by it, and then passes over building II. The pressure distributions on structures I and II differ from those obtained if only one structure (in the absence of the other) were subjected to the pressure wave. The upstream structure (I) shields the downstream structure (II) from the full effect of the pressure wave. Structure I is thus called the shielding structure and structure II, the shielded structure.

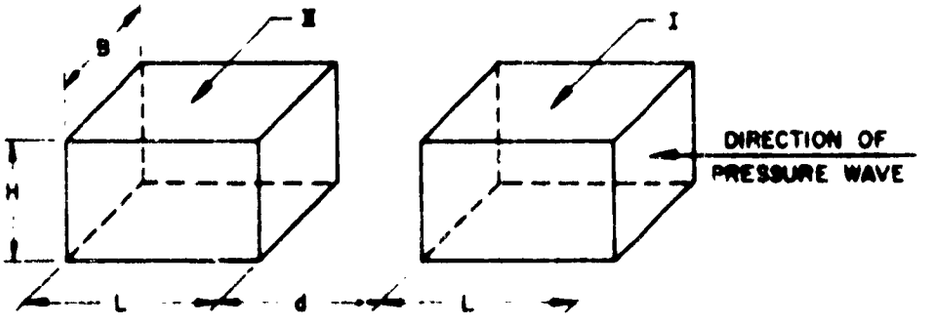

Figure 18. Shielding of Structures

Experiments[14,15] and blast wave procedures[30] indicate that the pressures on the back face of the shielding structure are reduced and the net translational pressure on the shielded structure is also reduced. The magnitude of the shielding effect is a function of the ratios d/S and B/S, where d is the separation distance, S the characteristic building dimension (height or half width, whichever is smaller), and B is the building width.

The reduction in back face pressure on the shielding structure is small and decreases as B/S decreases, being negligible for $B/S \leq 3$. The shielding structure can therefore reasonably be treated as if it were isolated and the procedures discussed in previous sections applied in order to estimate the building pressures.

The effects on the shielded structure are of sufficient magnitude so that they cannot be ignored. Data[30] available at present are for relatively high overpressures and are valid for normal incidence and identical building geometries. The information only applies to the first shielded structure placed directly behind the shielding structure. Some experimental results[15] for nonnormal incidence effects on self-shielding of building wings are also available.

The effect of shielding on the shielded structure is to reduce the peak reflected pressure on the front face to $2\mu_s$ where $0 \leq \mu_s \leq 1$. A plot[30] of μ_s versus the ratio of separation distance to characteristic building dimension d/S is given on Figure 19. The pressures on the other faces are unchanged from their values estimated on the basis of no shielding.

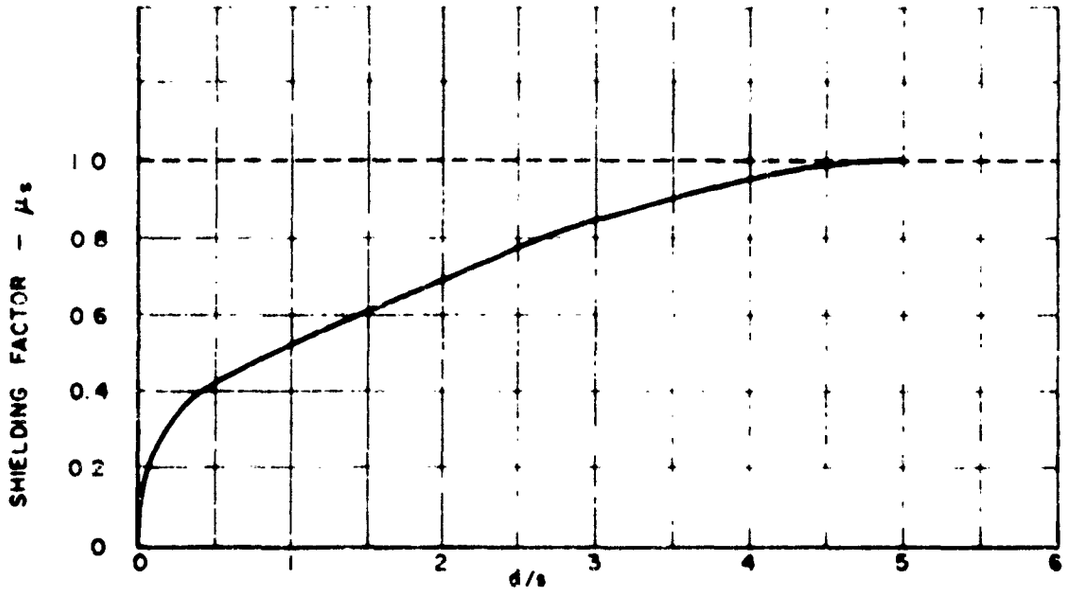

Figure 19. Shielding Factor - μ_s

The procedures used for unshielded structures discussed in the preceding sections (for normal incidence) may be used to predict pressures on the shielded structure except that the δ function, Figures 4 and 5, for the front face now has a maximum value of $2\mu_s$ instead of 2.

5. Closed Buildings - Interference Effects

When structures are adjacent to each other and subjected to a free-stream pressure wave as indicated in Figure 20, the diffraction of the free-stream wave by each structure has an effect on the other structures. This effect is known as interference. The primary result of interference is to increase the loads on each structure due to an increase in the characteristic building dimension from S (no interference effects) to S'.

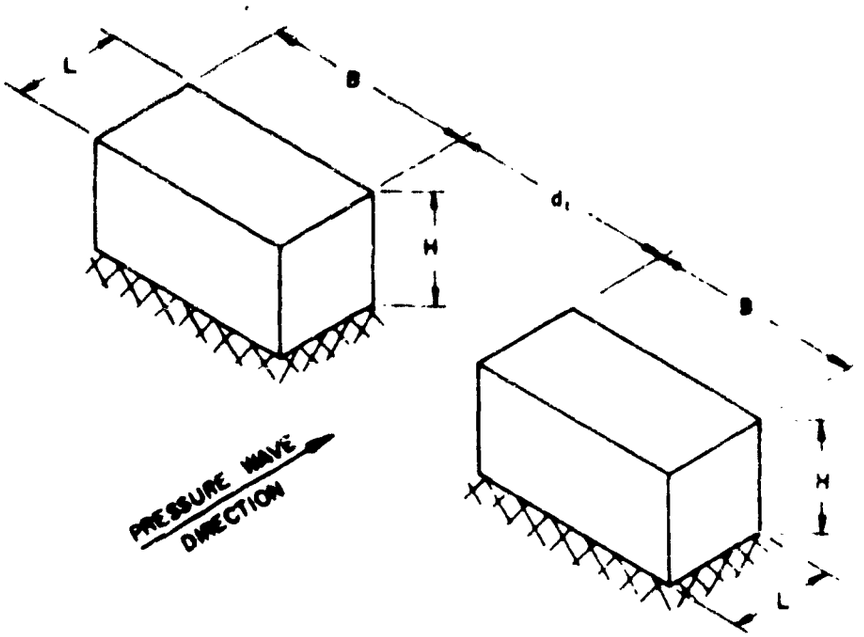

Figure 20. Interference of Structures

Table III gives values of effective characteristic building dimension S' employed in blast wave procedures[30]. No data are available for roof loads.

TABLE III

EFFECTIVE CHARACTERISTIC BUILDING DIMENSION S' (INTERFERENCE EFFECT)

Spacing to Width Ratio	Height to Width Ratio	S'/H
	$\frac{H}{B} \leq \frac{1}{2}$	$\frac{S'}{H} = 1$
$\frac{d_1}{B} \leq 2$	$\frac{1}{2} \leq \frac{H}{B} \leq \frac{N}{2}$	$\frac{S'}{H} = 1 + \frac{d_1}{4H}\left(1 - \frac{2H}{B}\right)$
	$\frac{H}{B} > \frac{N}{2}$	$\frac{S'}{H} = \frac{N}{2}\frac{B}{H} + \frac{d_1}{4H}(1-N)$
$\frac{d_1}{B} > 2$		$\frac{S'}{H} = \frac{S}{H}$ (no interference case)

N = number of buildings in a row perpendicular to the direction of propagation of the pressure wave.

The pressures for the case of interference may be estimated employing the procedures discussed for non-interference except replace S by S'. Roof and side face loads will not be affected.

6. Closed Building - Sloped Roofs

Figure 21 indicates the normal incidence case for sloped roofs. For roof slopes, $\alpha \leq 5°$, the roof is considered flat and the procedures previously discussed for flat roofs with normal incidence apply. The upper limit on α is taken as 45°.

To compute the outside normal force on roof elements 1 and 2, Figure 21 (b) and (c), we follow the passage of the free-stream pressure wave over the roof similar to that employed in Figure 6, taking the difference in geometry and direction of the pressure into account. Roof element 2 is not loaded until the N-wave front has reached the roof ridge. This occurs at a time $L/2U$.

The results of this procedure are given on Figure 22. The resultant vertical and horizontal forces and vertical and horizontal pressures are found by superposing Figure 22(a) and (b) as follows:

Net Vertical Force F_V (positive downward)

$$F_V = \cos\alpha \left\{ F(t)_{N1} + F(t)_{N2} \right\} \tag{6}$$

Net Vertical Pressure P_V (positive downward) (7)

$$P_V = \frac{F_V}{BL}$$

Net Horizontal Force F_H (positive in direction of pressure wave)

$$F_H = \sin\alpha \left\{ F(t)_{N1} - F(t)_{N2} \right\} \tag{8}$$

Net Horizontal Pressure P_H (positive in direction of pressure wave)

$$P_H = \frac{F_H}{BH_R} \tag{9}$$

with,

B = Roof width)
L = Roof Total Length) --- See Figure 21
H_R = Roof Height)

α = arctan $2H_R/L$

If the direction of the pressure wave is oriented at 90° to the direction shown on Figure 21, the outside roof pressure is treated in the same manner as flat roofs for normal incidence. The vertical roof area is considered as part of the front and rear face areas and is taken into account in computing the net translational force. The use of a characteristic front and rear face dimension of $B = H + H_R/2$ or $\frac{L}{2}$, whichever is smaller, is recommended.

For nonnormal incidence in a vertical plane, roof elements 1 and 2 are considered to behave essentially as faces 2 and 3 of Figure 10(a).

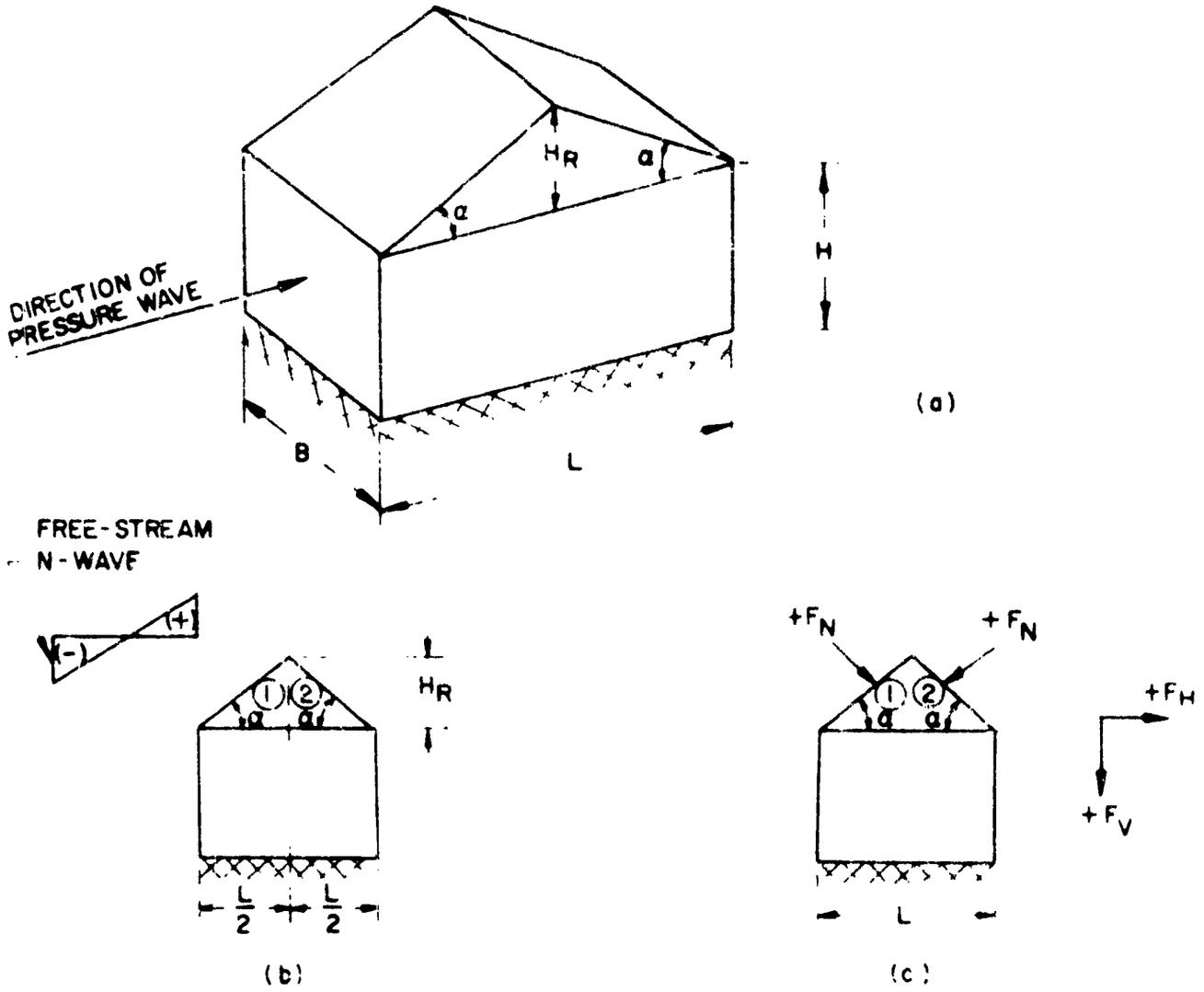

FIGURE 21 SLOPED ROOFS, NORMAL INCIDENCE - CLOSED BUILDING

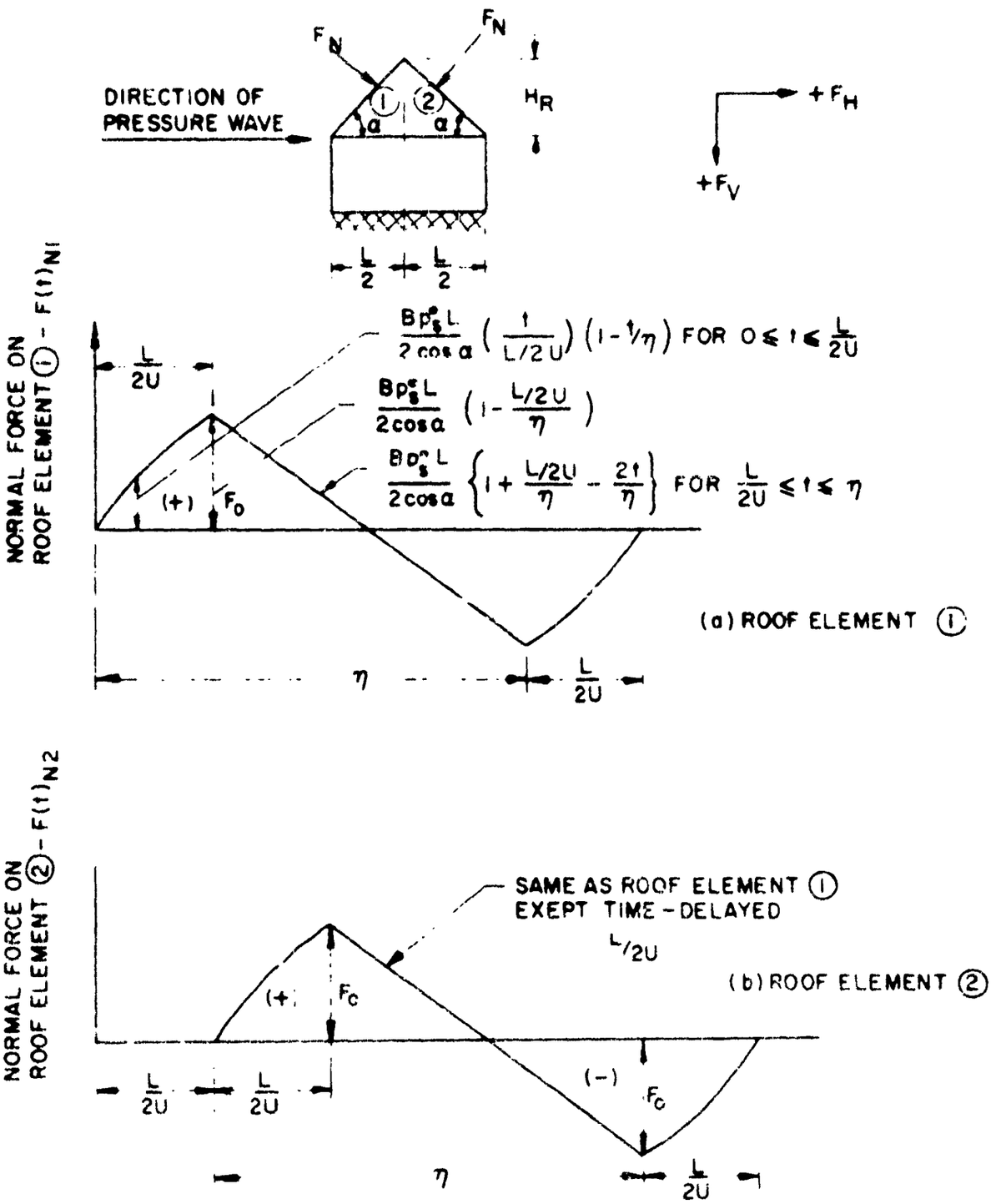

FIGURE 22 OUTSIDE NORMAL FORCES ON SLOPED ROOF ELEMENTS, CLOSED BUILDING, NORMAL INCIDENCE

7. Partially Open Buildings - Normal Incidence

When a building with openings is subject to a pressure wave, pressure loads exist on the inside as well as on the outside of the structure. The resultant pressures on structural elements of buildings with openings can differ significantly from the resultant pressures acting on corresponding structural elements of closed buildings.

If the open area of the building is small, it behaves essentially as a closed building. On the other hand, if the open area of the building is large, it behaves primarily as a drag type structure. Drag type structures, such as poles, open frameworks, etc., are subjected mainly to pressure loads resulting from aerodynamic drag. These structures are not important in our application since, for aircraft generated shock wave pressure levels, the drag pressure is much smaller than the free-stream pressure.

A building is considered closed if the front and back walls have less than 30% of openings or window area[29] ($\Lambda < .30$). If the percentage of openings or window area is greater than 70%, the building is assumed to be a drag structure. A partially open building then has window area or openings in the front and back wall in the range of $.30 \leq \Lambda \leq .70$.

The gross effects of openings on the pressure distribution on buildings[29,30] are:

(1) The outside building pressures are similar to those for closed buildings except that the characteristic building dimension s changes to s", where s" is the average distance which rarefaction waves must travel on the front face to reduce reflected pressure to stagnation pressure. Figure 23 gives a typical illustration. Additional data is found in the literature[30].

(2) The pressures on the inside surface of the structure approach free-stream values and are affected by internal reflections.

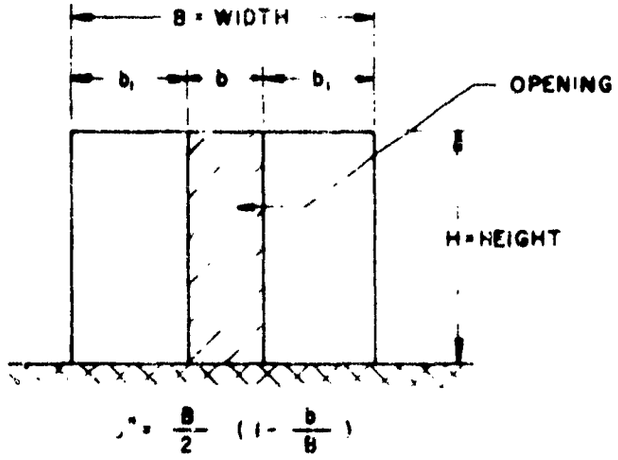

Figure 23. Characteristic Building Dimension S" For a Typical Opening - Open Building

For the purpose of estimating inside pressure on building surfaces, we consider the idealized problem of a structure with no internal partitions subjected to normal incidence of a shock wave. Only one reflection is considered on an internal surface. It is also assumed that rapid free-stream pressure wave fluctuations are attenuated by diffusion.

a. Average Back Face Inside Pressure

The inside back face (at a distance L from the front face) is unloaded until the free-stream pressure wave (with velocity U) arrives at a time, $t = L/U$, measured from the instant the wave contacts the front face. The free-stream pressure wave that arrived at time L/U has been attenuated by diffusion effects. Extrapolating blast wave data[29] to low pressure levels, the attenuation factor is taken as the open area ratio Λ. The pressure of the wave arriving at the back face is then $\Lambda\ p_s\ (t - \frac{L}{U})$. This attenuated pressure wave $\Lambda\ p_s\ (t - \frac{L}{U})$ is then doubled by reflection from the back face. The back face pressure $2\ \Lambda\ p_s\ (t - \frac{L}{U})$ then decays to the time-delayed free-stream pressure $p_s\ (t - \frac{L}{U})$ in a time interval $4(1 - \Lambda)\frac{L}{U}$.

Figure 24(d) gives the average inside pressure on the back face. It is constructed in a manner similar to Figure 8 except different characteristic times and δ functions are employed to depict the diffusion, reflection and decay of the pressure.

b. Average Front Face Inside Pressure

The inside front face average pressure rises from zero at time, $t = 0$, to free stream pressure $p_s(t)$ in a build up time t_b. The build up time is approximated[29,30] as $\frac{2L}{U}$. At time, $t = \frac{2L}{U}$, the pressure wave (originally at the front face at time $t = 0$) which was attenuated by the factor Λ and reflected from the back face, has reached the front face again. This attenuated pressure wave, $\Lambda\ p_s\ (t - \frac{2L}{U})$, is reflected from the front face, increasing the front face average pressure by $2\ \Lambda\ p_s(t - \frac{2L}{U})$. The average front face pressure then decays to free-stream pressure $p_s(t - \frac{2L}{U})$ in a time interval $4(1 - \Lambda)\ \frac{L}{U}$.

Figure 25 (d) gives the average inside front face pressure p_{fi}. It is constructed similar to Figure 24(d) except that a time delay $\frac{2L}{U}$ is employed and the pressure builds up from zero to free-stream pressure $p_s(t)$ at $t = \frac{2L}{U}$ before being increased by reflection from the time-delayed attenuated wave.

c. Average Side Face and Roof Inside Pressure

The average side face and roof inside pressure (considered as the pressure at $\frac{L}{2}$, middle of the faces) rises from zero at time $t = 0$, to the time-delayed free-stream pressure $p_s(t - \frac{L}{2U})$ in a time $(3 - 4\ \Lambda)\ \frac{L}{U}$. It is assumed that the pressure decays to zero in a time interval $4(1 - \Lambda)\ \frac{L}{U}$ after the negative peak of the N-wave reaches the middle of the faces. Figure 26(b) shows the average inside side face and roof pressure.

d. Net Average Translational Pressure

The net average translational pressure is obtained as the vector sum of the inside and outside pressures acting on the front and rear faces (and inside and out-

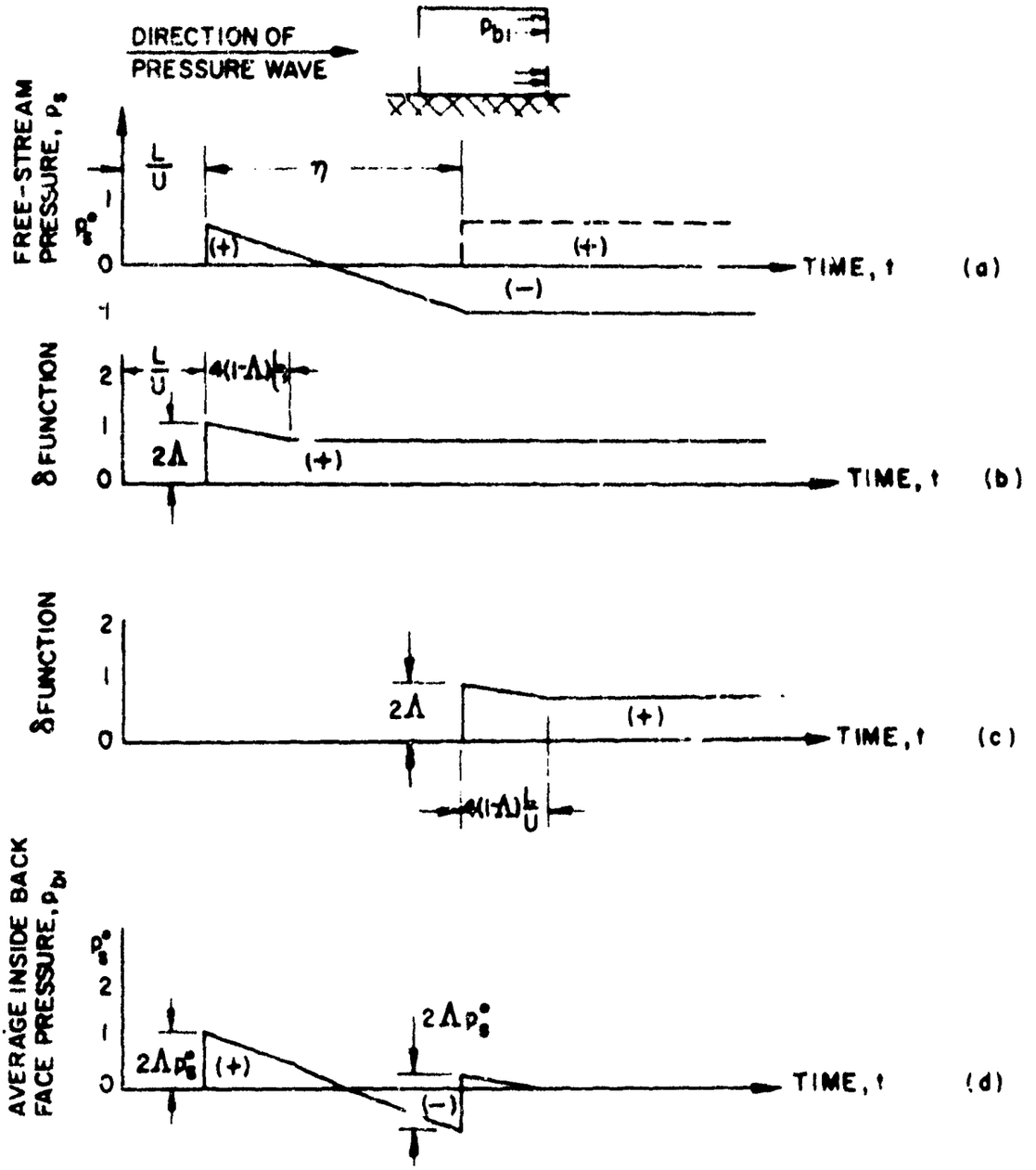

FIGURE 24 AVERAGE INSIDE BACK FACE PRESSURE PARTIALLY OPEN BUILDING- NORMAL INCIDENCE

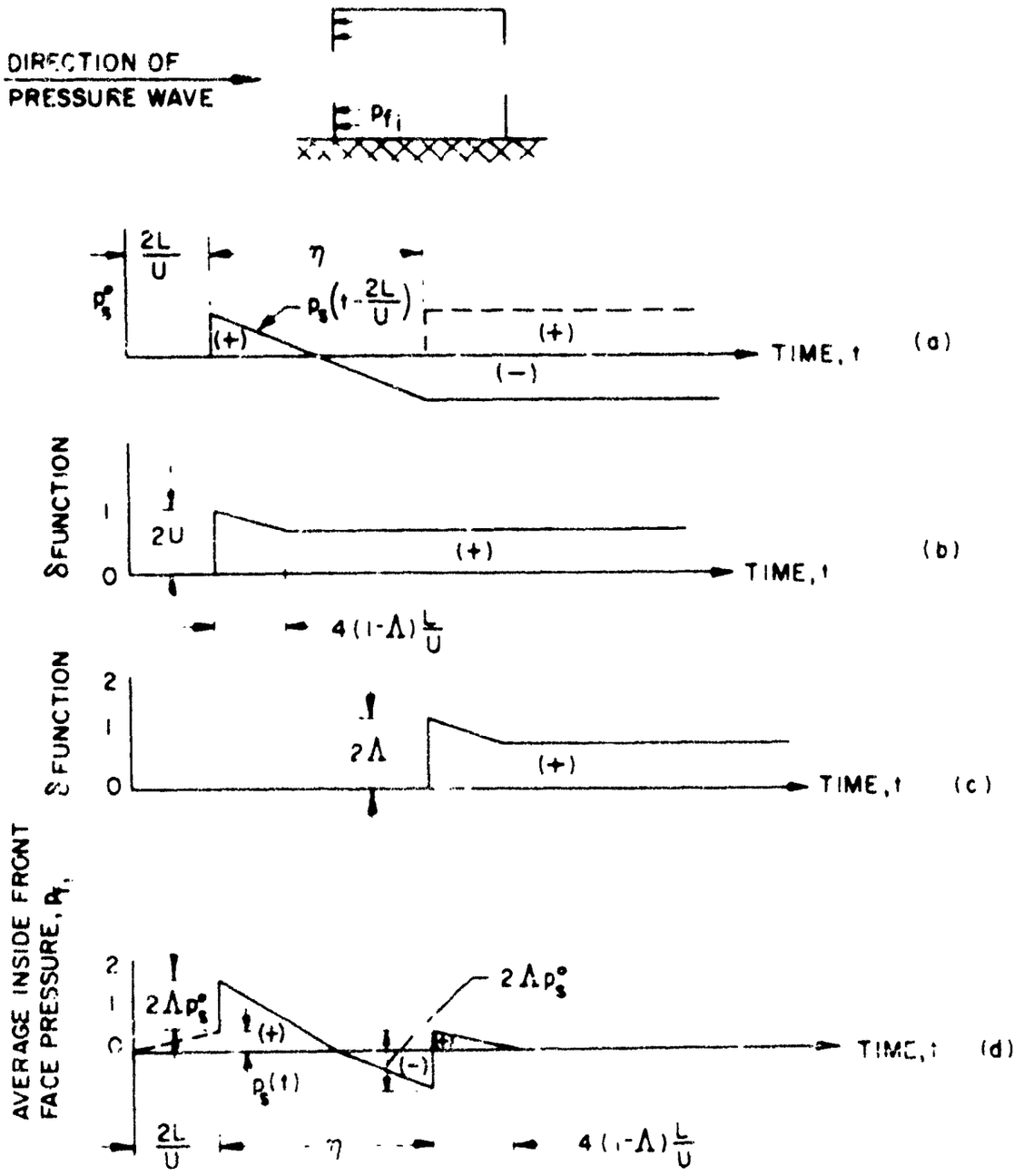

FIGURE 25 AVERAGE INSIDE FRONT FACE PRESSURE PARTIALLY OPEN BUILDING - NORMAL INCIDENCE

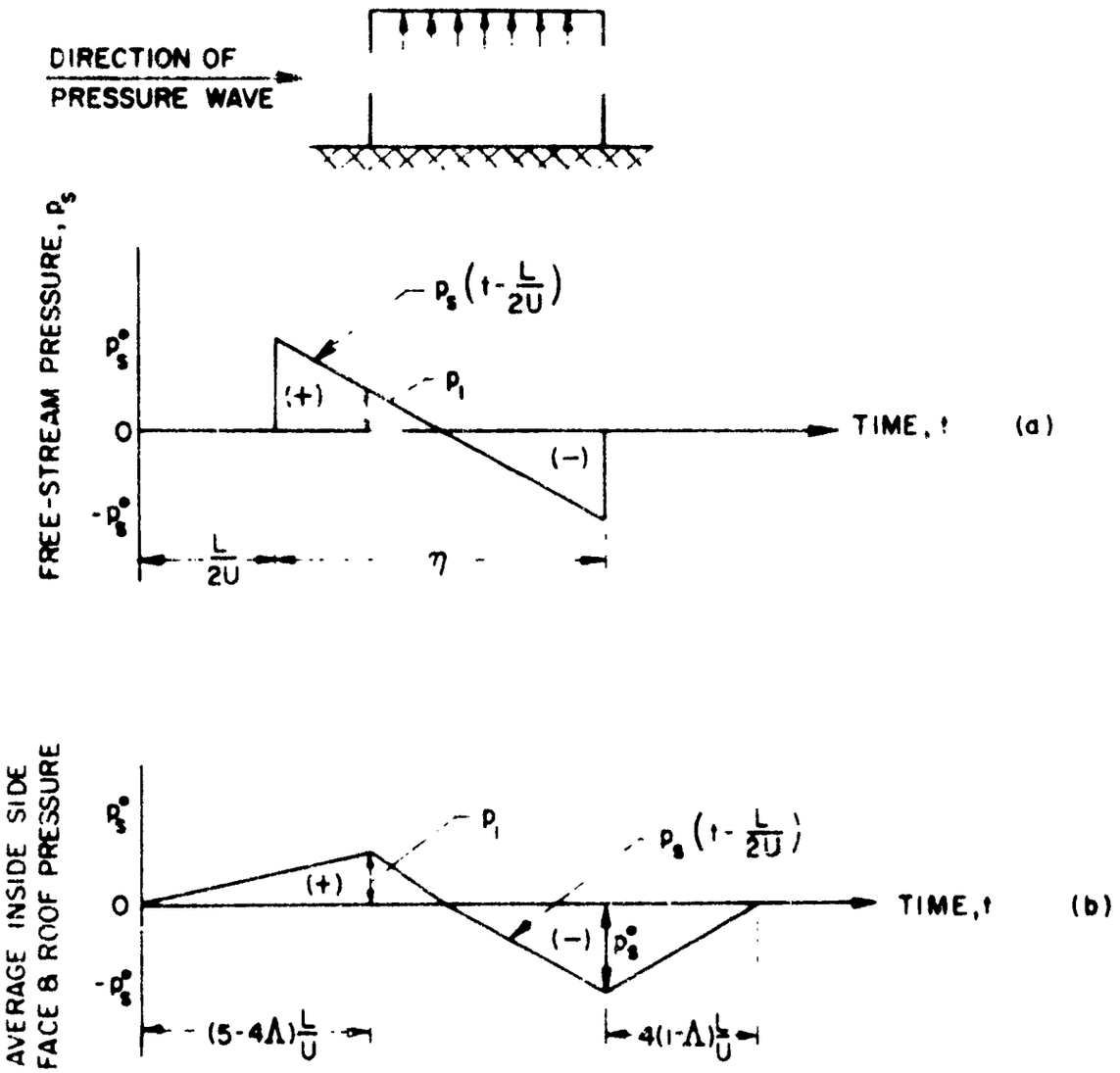

FIGURE 26 AVERAGE INSIDE ROOF AND SIDE FACE PRESSURE PARTIALLY OPEN BUILDING - NORMAL INCIDENCE

side horizontal roof pressure, if the roof is sloped). The total load on any face is the product of the average pressure and the closed face area.

SECTION 3

FUNDAMENTAL VIBRATION AND STRUCTURAL CONCEPTS

STATIC EFFECTS

When studying dynamic effects it is useful to compare the dynamically induced stresses or deflections with the stresses and deflections which would have resulted if the maximum dynamic external load had been gradually applied and maintained. The latter deflections and stresses are referred to as the "static deflection shape" and the "static stresses", respectively. Formulas for the maximum static stresses in beams and panels with various edge supports and with an applied pressure p are given in Table IV.

NORMAL MODES OF VIBRATION

Suppose an elastic structure is deflected from its position at rest. When the structure is released, if all points on the body move through displacements which are in phase and sinusoidal with respect to time, the original deflected shape (described as a function of position on the undeformed structure) is called a "normal mode of vibration" and the frequency is called the "corresponding natural frequency". These normal modes and natural frequencies are "classical[47,48]", useful in the exact solution of vibration problems, and suggestive in formulating approximate solutions. Table V shows the effect of the method of support on the mode shape and natural frequency of beams and plates[43,48]. The double subscript notation a_{ij} for the square plates indicates that the mode shape consists of a shape similar to the i^{th} beam normal mode in the x direction multiplied by a shape similar to the j^{th} beam normal mode in the y direction, where the x and y directions are parallel to the edges of the plate.

STATIC PARTICIPATION FACTORS

The static displacement of an elastic structure can be described in terms of a sum of the normal modes adjusted to appropriate amplitudes (see equation (33), Appendix II). If one now examines the contribution of each mode to the maximum static stress and divides each contribution by the maximum static stress, the resulting terms are the "static participation factors[49]" contributed by each mode. The evaluation procedure for the participation factors is similar to that for Fourier Series coefficients, and is given in Appendix II. Table V gives participation factors for several beams and plates, subjected to uniformly distributed normal load or pressure.

There are several points of interest in Table V. For beams and plates whose ends are both simply supported or both clamped, the "anti-symmetric", even numbered, modes have zero participation factor. This is to be expected because uniform pressure is symmetric and will not induce anti-symmetric modes. For the beam with one end clamped and the other simply supported the even numbered modes are <u>nearly</u> anti-symmetrical; hence, their contribution is small but not zero. The next point of interest is that uniform pressure induces mostly the first mode; hence, the participation factor is near unity for all the first modes. For simply supported beams and plates, the participation factors in the first mode are 1.03 and 1.12, respectively, and the remainder of the participation factors oscillate in sign. For members with clamped ends, the participation factor in the first mode is .89 and the remainder of the participation factors are positive. Since by definition, the participation factors add up to unity, the sum of absolute values of participation functions exceeds unity whenever the signs alternate. The ratio of the second to first symmetric mode frequencies lie between 5 and 9.

TABLE IV

STRESS AND DEFLECTIONS

a, b, L	DIMENSIONS, INCHES
c	DISTANCE FROM CENTROID TO OUTER FIBER, INCHES
E	YOUNG'S MODULUS, POUNDS PER SQUARE INCH
G	SHEAR MODULUS, POUNDS PER SQUARE INCH
I	MOMENT OF INERTIA OF CROSS SECTION, INCH^4
P	UNIT PRESSURE, POUNDS PER SQUARE INCH
p	TOTAL LOADS, POUNDS
q	SHEAR FLOW, POUNDS PER INCH
s	STRESS, POUNDS PER SQUARE INCH
t	THICKNESS, INCHES
v	DISPLACEMENT, INCHES
α	b/a
ν	POISSON'S RATIO, TAKEN AS .3
x	POINT OF MAXIMUM STRESS
□	POINT OF MAXIMUM DISPLACEMENT

STRUCTURE AND LOADING	MAX. STRESS, s	MAX. DEFLECTION, v
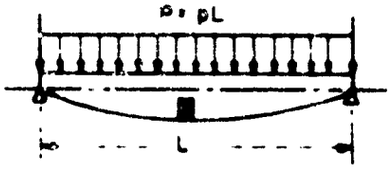 BEAM END SUPPORTS, UNIFORM LOAD.	$\frac{PLc}{8I}$	$\frac{5}{384}\frac{PL^3}{EI}$
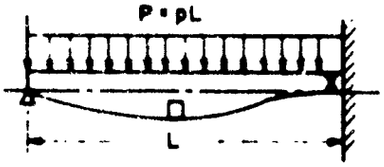 BEAM ONE END FIXED, ONE END SUPPORTED. UNIFORM LOAD	$\frac{PLc}{8I}$	$.0054\frac{PL^3}{EI}$
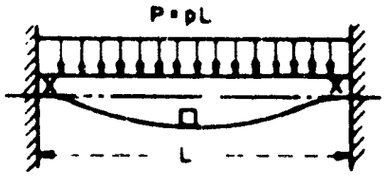 BEAM BOTH ENDS FIXED. UNIFORM LOAD	$\frac{PLc}{12I}$	$\frac{1}{384}\frac{PL^3}{EI}$
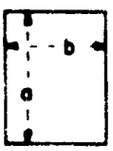 $\frac{b}{a} = \alpha$ PLATE. ALL EDGES SUPPORTED. UNIFORM LOAD OVER ENTIRE SURFACE	$\frac{.75\,pb^2}{t^2(1+1.61\alpha^3)}$	$\frac{.1422\,pb^4}{Et^3(1+2.21\alpha^3)}$
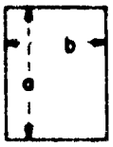 $\frac{b}{a} = \alpha$ PLATE ALL EDGES FIXED. UNIFORM LOAD OVER ENTIRE SURFACE.	$\frac{.5\,pb^2}{t^2(1+.623\alpha)}$	$\frac{.0284\,pb^4}{Et^3(1+1.056\alpha^5)}$
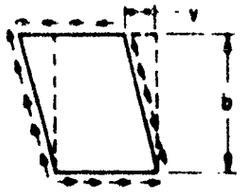 PLATE RACKING LOAD, q POUNDS PER INCH	$\frac{q}{t}$	$\frac{bq}{Gt} = K(bq)$

TABLE V

NATURAL FREQUENCIES AND PARTICIPATION FACTORS

$$\omega_n = a_n \sqrt{\frac{EI}{ML^3}} \quad \text{, (BEAM OF UNIFORM CROSS-SECTION)}$$

$$= a_n \sqrt{\frac{(D_L)}{ML^3}} \quad \text{. (SQUARE PLATE OF UNIFORM THICKNESS)}$$

ω_n = NATURAL FREQUENCY IN RADIANS/SECOND

EI OR DL = BENDING STIFFNESS OF BEAM OR FULL WIDTH OF SQUARE PLATE

M = TOTAL UNIFORMLY DISTRIBUTED MASS OF BEAM OR PLATE

L = SPAN OF BEAM AND LENGTH OF EDGE OF SQUARE PANEL

PF = PARTICIPATION FACTOR, OR FRACTIONAL CONTRIBUTION OF THIS MODE TO THE MAXIMUM STATIC STRESS DUE TO UNIFORM PRESSURE ON TOP SURFACE

 a_1 a_2 a_3 SIMPLY-SUPPORTED BEAM	$a_1 = 9.87$ $a_2 = 39.5$ $a_3 = 88.9$ $a_4 = 158$ $a_5 = 247$ $\sum_{j=1}^{\infty} \lvert(PF)_j\rvert = 1.10$	$(PF)_1 = 1.053$ $(PF)_2 = 0$ $(PF)_3 = -.038$ $(PF)_4 = 0$ $(PF)_5 = +.008$
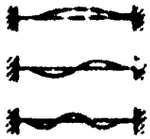 a_1 a_2 a_3 CLAMPED-CLAMPED BEAM	$a_1 = 22.4$ $a_2 = 61.7$ $a_3 = 121.0$ $a_4 = 200$ $a_5 = 298$	$(PF)_1 = .891$ $(PF)_2 = 0$ $(PF)_3 = .072$ $(PF)_4 = 0$ $(PF)_5 = .019$
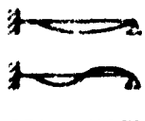 a_1 a_2 CLAMPED-HINGED BEAM	$a_1 = 15.4$ $a_2 = 50$ $a_3 = 104$ $a_4 = 178$ $a_5 = 272$	$(PF)_1 = .893$ $(PF)_2 = .026$ $(PF)_3 = .051$ $(PF)_4 = .004$ $(PF)_5 = .001$
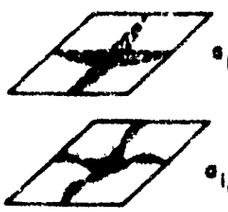 $a_{1,1}$ $a_{1,3}$ & $a_{3,1}$ SIMPLY SUPPORTED SQUARE PLATE	$a_{1,1} = 19.75$ $a_{3,1} = a_{1,3} = 98.7$ $a_{5,1} = a_{1,5} = 257$ $a_{7,1} = a_{1,7} = 493$ $a_{3,3} = 177.6$ $a_{5,3} = a_{3,5} = 335.5$	$(PF)_{1,1} = 1.115$ $(PF)_{1,3} = -.1485$ $(PF)_{1,5} = +.0362$ $(PF)_{1,7} = -.0127$ $(PF)_{3,3} = .0138$ $(PF)_{3,5} = -.0087$
 $a_{1,1}$ CLAMPED SQUARE PLATE	$a_{1,1} = 28.0$ (APPROX.) $\sum_{j=1,1}^{\infty} \lvert(PF)_j\rvert = 1.367$	

1. Modal Dynamic Response Functions

It is known that the dynamic response of any structure can be described as the sum of products of the form:

(normal mode shape) (corresponding dynamic response function).

When the shape of load-distribution is spacewise constant*, the sum takes the form:

$$\sum_{j=1}^{\infty} \left\{ \begin{array}{l} \text{contribution of the } j^{\text{th}} \\ \text{mode to the static} \\ \text{deflection} \end{array} \right\} \times \left\{ \begin{array}{l} j^{\text{th}} \text{ dynamic} \\ \text{response} \\ \text{function} \end{array} \right\}$$

Consequently,

$$\left\{ \begin{array}{l} \text{Critical} \\ \text{Dynamic} \\ \text{Stress} \end{array} \right\} = \sum_{j=1}^{\infty} \left\{ \begin{array}{l} \text{Maximum} \\ \text{Static} \\ \text{Stress} \end{array} \right\} \times \left\{ \begin{array}{l} j^{\text{th}} \text{ partici-} \\ \text{pation} \\ \text{factor} \end{array} \right\} \times \left\{ \begin{array}{l} j^{\text{th}} \text{ dynamic} \\ \text{response} \\ \text{function} \end{array} \right\}$$

The attractiveness of this procedure lies in the simplicity of the dynamic response functions. They are the solutions of the following differential equation:

$$\frac{1}{\omega_j^2} \frac{d^2 f_j}{dt^2} + f_j = \frac{F - F(t)}{F_{max.}} \tag{10}$$

$$\text{with} \quad f_j(o) = \frac{df_j}{dt}(o) = 0 \tag{11}$$

where ω_j is the natural frequency of the j^{th} mode, radians/second

f_j is the dynamic response function for the j^{th} mode, non-dimensional

t is time, seconds

F is proportional to the load applied to the structure as a function of time

F_{max} is the maximum value of F

As one changes modes ω_j changes; this will change the form of f_j but $F(t)/F_{max}$ is variant.

2. Modal Amplification Factor

Each $f_j(t)$ has a maximum value, A_j, which depends on the shape of the forcing function, $F(t)/F_{max}$, and the natural frequency considered. A_j is the j^{th} modal amplification factor. One can plot the value of A_j vs. $\omega_j t_F$ where t_F is

---

*For procedure if load shape is not constant with time, see Appendix II.

a characteristic time associated with F(t), such as the duration of the load.

a. Special Cases

(1) $(\omega_j t_F) < \frac{\pi}{8}$

In this situation, the body acquires a velocity but substantially zero displacement during the loading time, t_F. If this fact is used in the differential equation, one obtains:

$$A_j = \omega_j \int_0^{t_F} \frac{F(t)}{F_{max.}} dt \leq \omega_j t_F \qquad (12)$$

(2) $(\omega_j t_F) > \pi$, $F(t)/F_{max}$ rises as a step, and decays slowly

In this situation, it is well known that the amplification factor is two. This is so because the body has a steady state response of unity and finds itself at zero velocity depressed to zero displacement or to minus unity below steady state. It then vibrates to plus unity above steady state or to two, absolute, which it reaches at zero velocity.

b. Modal Amplification Factor for N-Shaped Pressure Vs. Time Relation

Figure 31 gives the modal amplification factor for an N-shaped pulse. This pulse shape corresponds to that for the parameter $\tau/\eta \to \infty$ (Figure 28). These results were obtained analytically.

c. Response for An Arbitrary $F(t)/F_{max}$ Relation

The solution of equations (10), (11) gives the response. Analytic, analog computer and graphical procedures are employed. Figures (27) through (30) show the wiring diagrams and typical forcing functions and responses for the analog computer technique. The graphical method, described in Appendix II, uses phase plane theory[52]. In this procedure, the actual $F(t)/F_{max}$ curve is replaced by a step-shaped function of identical area during each step. The recommended non-dimensional duration of each step is $\omega(\Delta t) = \pi/3$ or less, where ω is the natural frequency considered. When applied, as an illustration, to an N-shaped wave of duration equal to one natural period, and when only six steps were used, the approximate amplification factor was 1.965 compared to the exact value of 2.00.

DYNAMIC STRESS AMPLIFICATION FACTOR

On page 46, a formula was given for the critical dynamic stress as a function of time in terms of the maximum static stress and a sum of products of participation factors and corresponding modal response functions (of time). "A", the dynamic amplification factor, is the ratio of the maximum value of the critical dynamic stress to the maximum static stress.

1. Upper Limit on Dynamic Amplification Factor

It is easier (and not overly conservative) to obtain an upper limit on A, or A_L than it is to obtain A. Thus, if one assumes that modes contribute their maxima simultaneously:

$$A_L = \sum_{j=1}^{\infty} \left| (PF)_j A_j \right| \qquad (12)$$

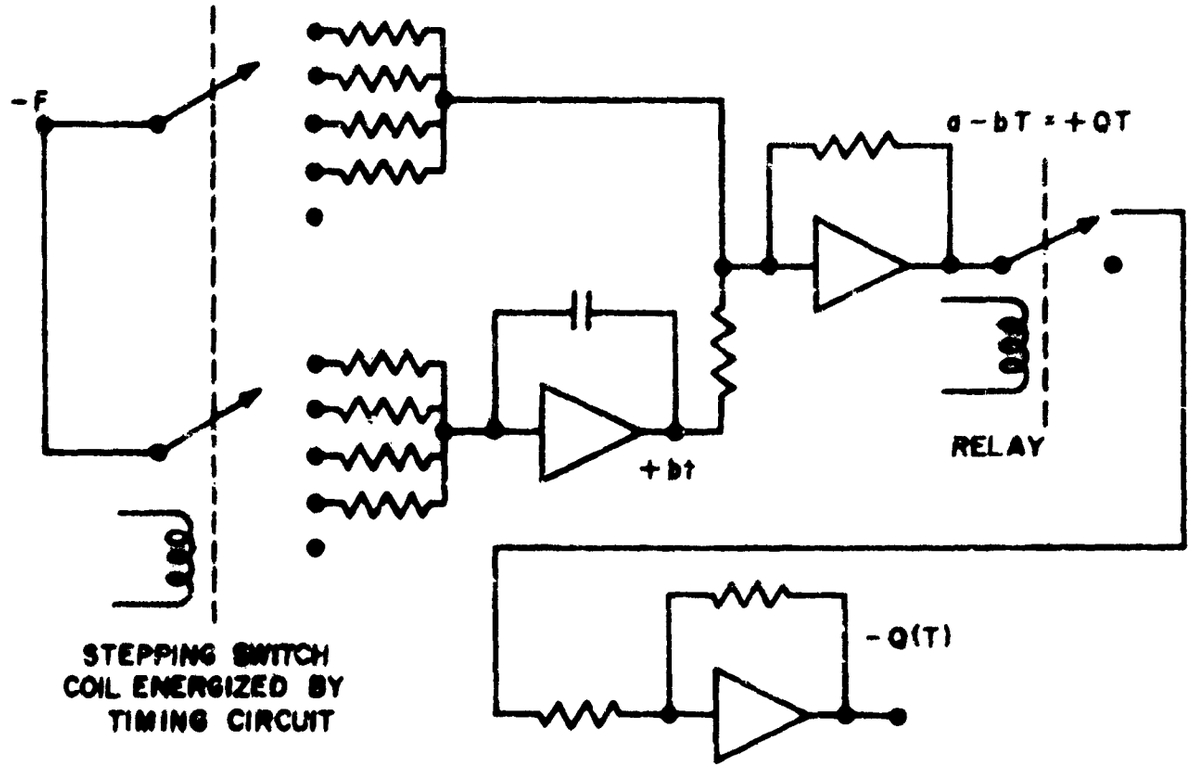

GENERATING THE FORCING FUNCTION

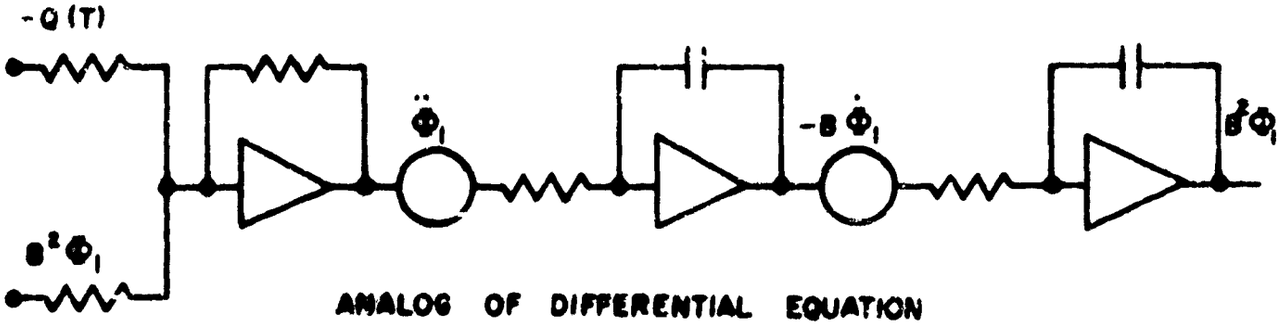

ANALOG OF DIFFERENTIAL EQUATION

SYMBOLS:

AMPLIFIER

COEFFICIENT SETTING POTENTIOMETER

FIGURE 27 ANALOG WIRING DIAGRAM

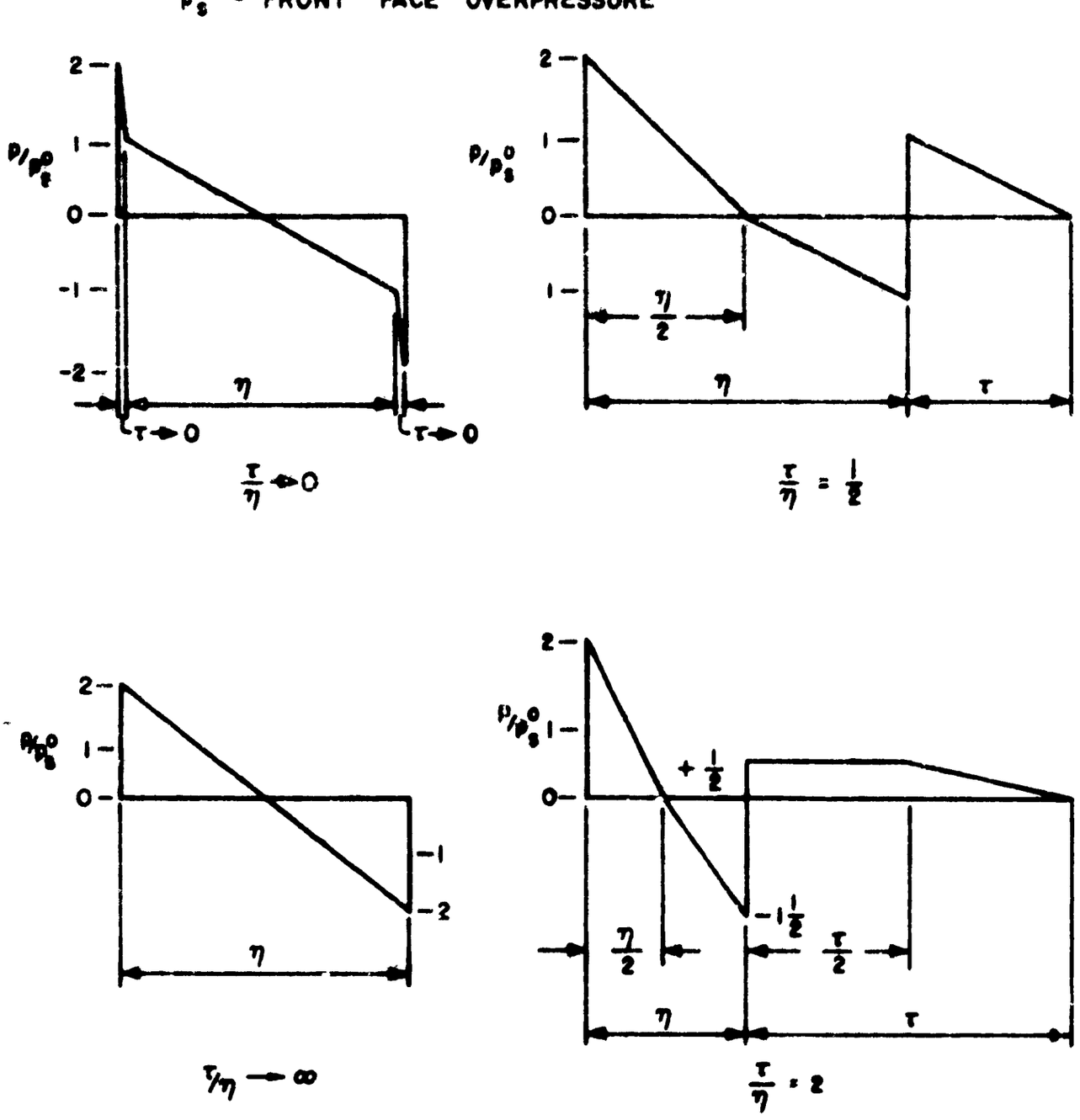

FIGURE 28 SHOCK WAVE LOADS FOR $\frac{\tau}{\eta} = 0, \frac{1}{2}, 2 \& \infty$

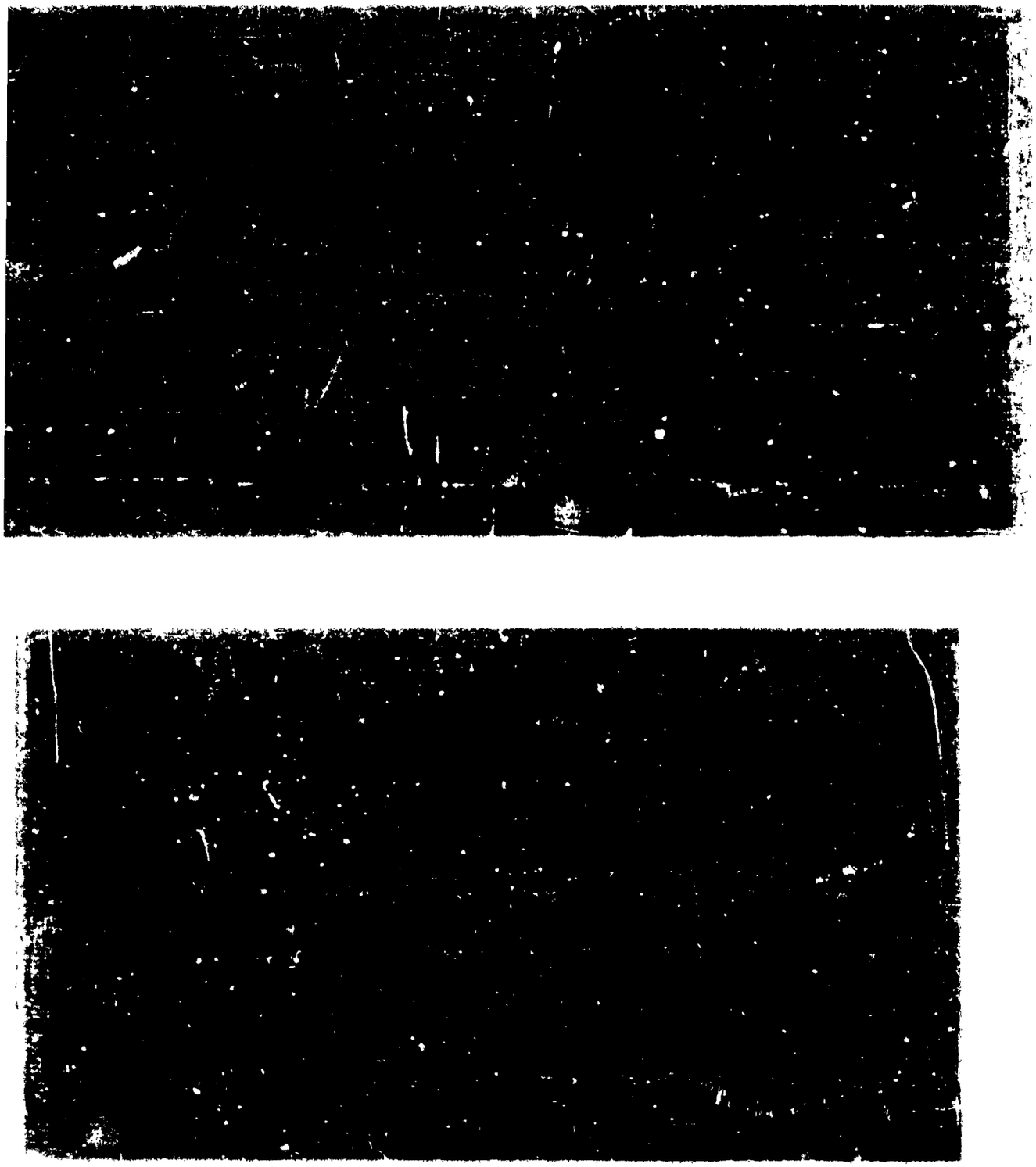

FIGURE 29 TYPICAL ANALOG COMPUTER SOLUTIONS (WITH N-WAVE FORCING FUNCTION)

FIGURE 30 TYPICAL ANALOG COMPUTER SOLUTION
[WITH MODIFIED N-WAVE FORCING FUNCTIONS]

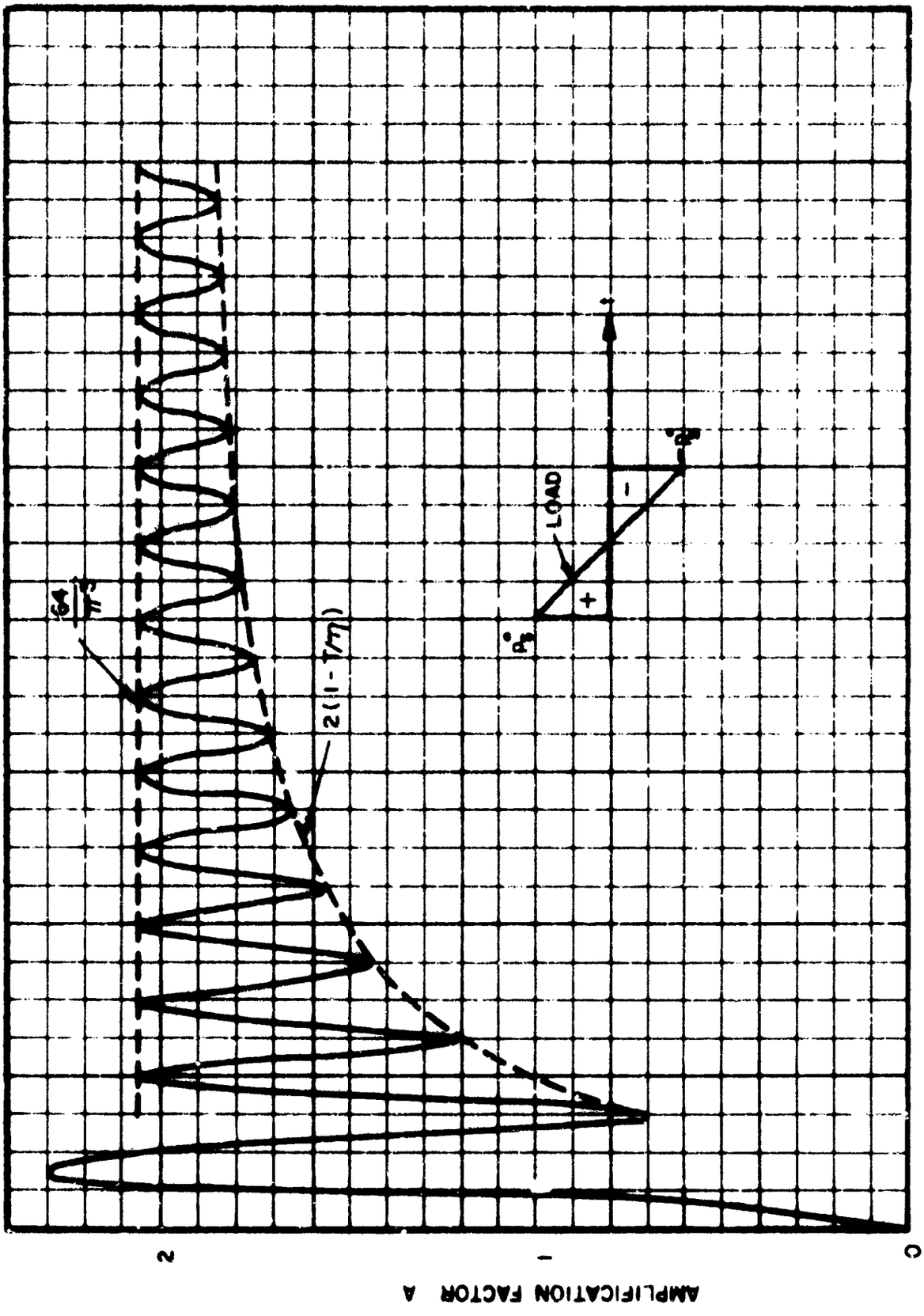

FIGURE 31 AMPLIFICATION FACTOR FOR N-SHAPED PULSE

But, it can be shown that for all the problems considered in Table V it is conservative to use:

$$A_L = (A_1 M) \sum_{j=1}^{m} (PF)_j \tag{13}$$

where M^* is a factor designed to exagerate the contributions due to A_j for the higher modes.

$$M = M\left(\frac{\omega_1}{\omega_{cr}}\right) \tag{14}$$

$$= 1 \quad \text{if} \quad \frac{\omega_1}{\omega_{cr}} > 1$$

$$= 1 + \frac{.225\ (1 - \frac{\omega_1}{\omega_{cr}})}{1.225\ (\frac{\omega_1}{\omega_{cr}})} \qquad 1 \geq \frac{\omega_1}{\omega_{cr}} \geq \frac{1}{9}$$

ω_{cr} is the radian frequency at which A_1 is a maximum. M is seen to vary from 2.5 to 1.0 in Figure 32. $(A_1 M)$ can be thought of as an equivalent first mode amplification factor while $\sum_{j=1}^{m} (PF)_j$ is the equivalent first mode participation factor, both of which take into account higher modes.

---

*See Appendix II.

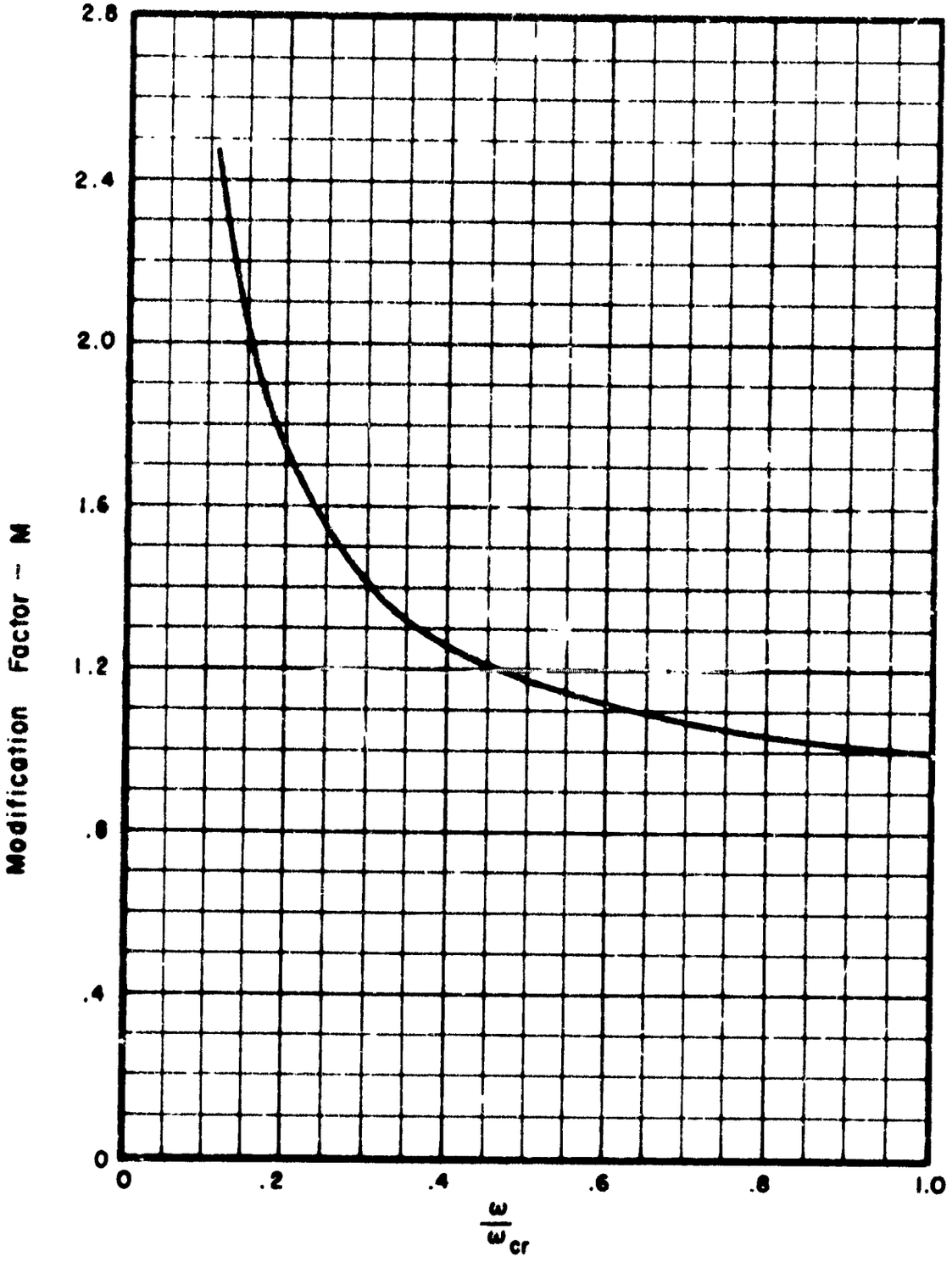

Figure 32 Modification Factor, M vs $\frac{\omega}{\omega_{cr}}$

SECTION 4

DYNAMIC EFFECTS PRODUCED BY SHOCK WAVE LOADS

GENERAL

In this report, we have followed precise vibration theory to establish suitable factors so that one need only know the lowest natural frequency to estimate the dynamic amplification factor due to uniform pressure varying with time. The amplification factor for the first mode is sometimes not large enough, if higher modes are important. It has been found that two factors will correct this deficiency. One is labeled the "C" factor on the accompanying graphs; it is the sum of the absolute values of the participation factors. The second factor is the "M" factor which accounts for the greater attenuation of the first mode than of the higher modes. The unmodified graphs are also given in the event there are no higher modes.

GRAPHS

Figures 33-35 are generally self explanatory. They give the amplification factors for various load-time relations which appear in normal incidence of the N-wave. The single period of a sine wave is an approximation to roof-load, under normal incidence. It is interesting that the maximum amplification factor is highest for this condition of loading.

For load-time relations for which amplification factors are not available, a simple quick graphical construction is available in the Appendix, page 109.

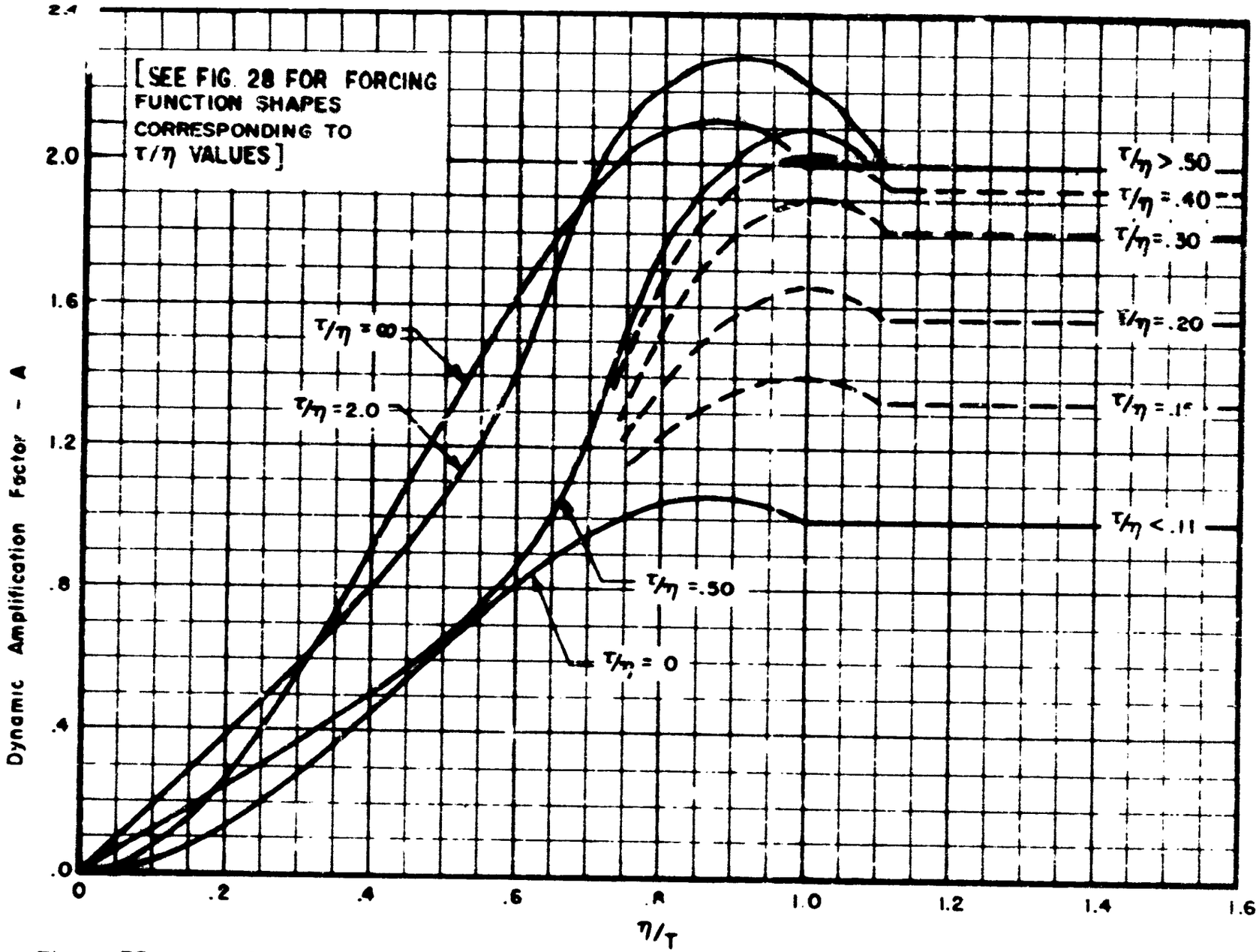

Figure 33 Amplification Factor vs. Loading Time in Number of Natural Period (η/T)

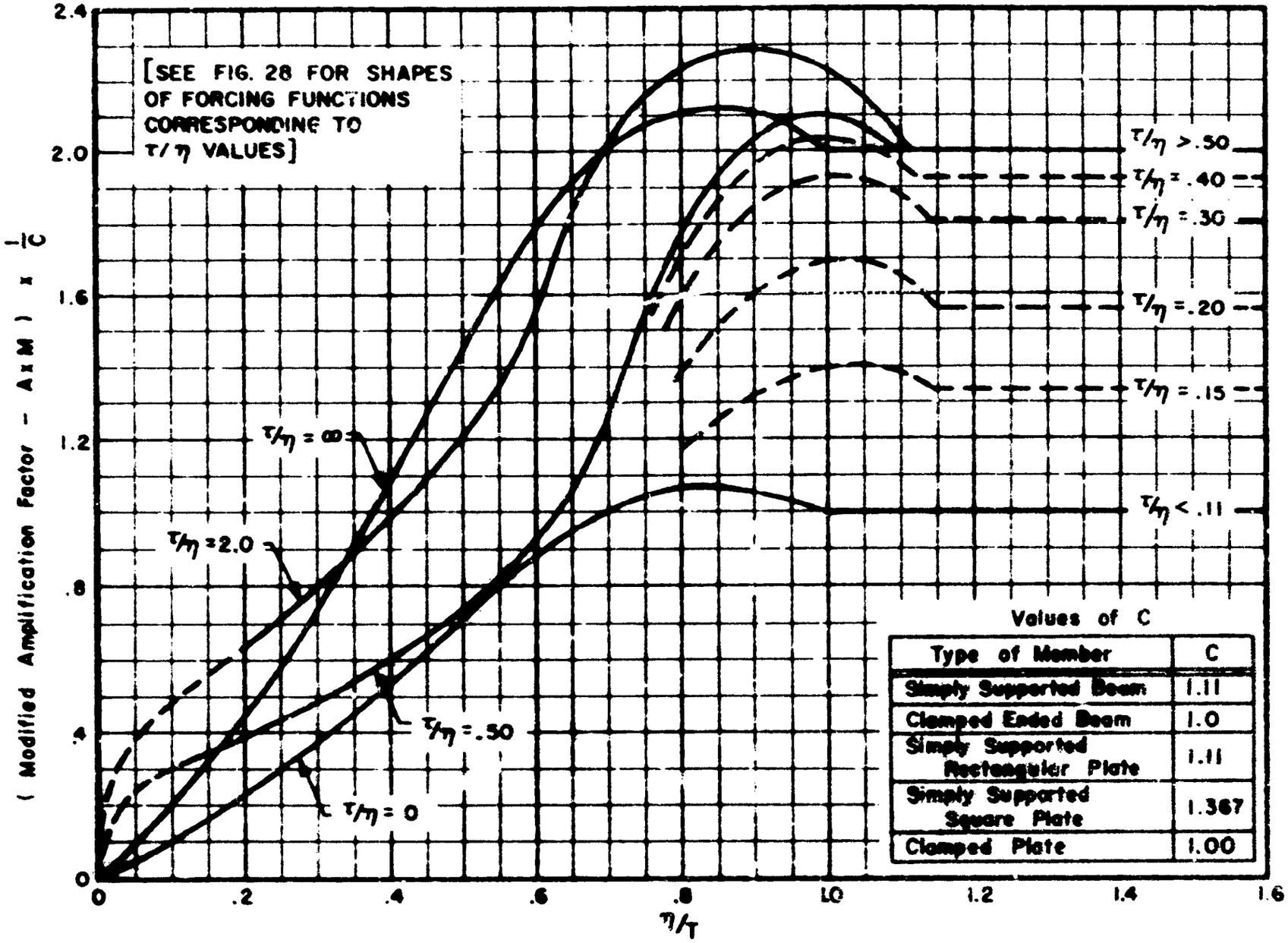

Figure 34 Modified Amplification Factor vs. Loading Time in Number of Natural Periods (η/T)

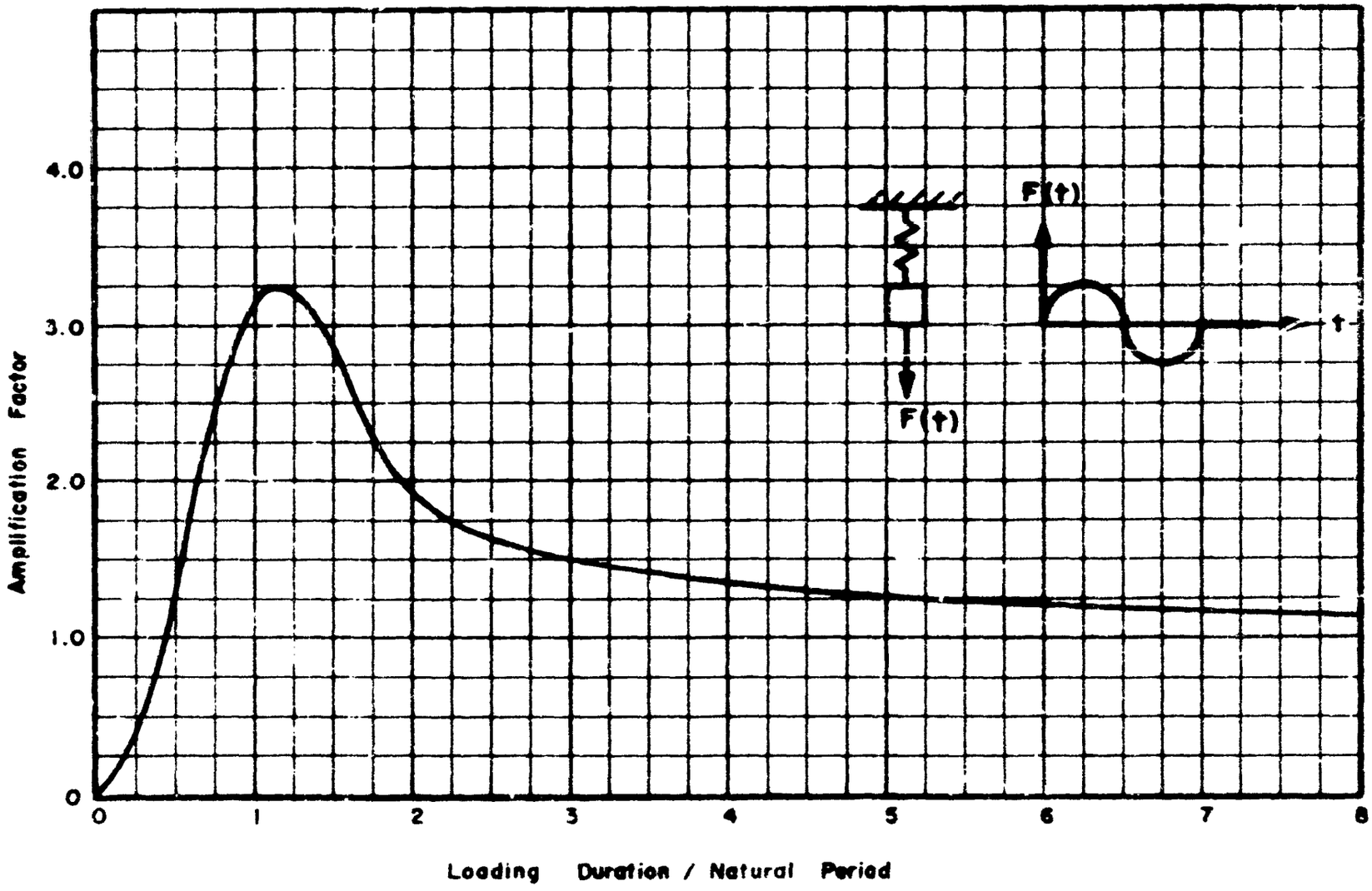

Figure 35 Amplification Factor For A Sinusodial Pulse

SECTION 5

CRITICAL STRUCTURES AND STRUCTURAL ELEMENTS

In Section 2, Table I, it has been shown that shock wave free-stream peak pressures are at most the order of .10 psi. Atomic and conventional explosive blast data[17,29,44] indicate that the only structural elements which fail at pressure levels five to fifteen times greater than the peak shock wave pressures are glass and plaster. In addition, most shock wave damage reports[45,46] concern glass and plaster damage. Theoretical estimates based on test data[37-39] also indicate that glass and plaster are critical structural elements.

Shock wave loads produce failure of brittle structural elements. Failure occurs before any plastic deformation can take place. In addition, the more ductile materials, such as steel and reinforced concrete, which may undergo large plastic deformation before failure, are stressed well below their yield points. Structural response is therefore governed by elastic behavior.

Glass windows are found in all classes of structures. Glass fails in tension produced by bending stresses. The bending stresses are proportional to $(\text{span/thickness})^2$. Store fronts are critical since large span/thickness ratios are common.

Most structures are designed according to building codes. For major structures these codes specify in detail design loads, allowable stresses and material properties. Factors of safety on failure of 4 or more are not uncommon.

Residential structures, on the other hand, are not subject to such rigid specifications and many factors which affect the strength of the house are left to the discretion of the builder. As a rule, no load or stress analysis is made on a house. Small structures such as sheds, wood frame garages, barns, etc., can be included in this category.

A study of various buildings indicated that walls of residential structures, particularly those with door and window openings, are normally critical in shear and in some cases bending action governs. In residential structures all the horizontal loads imposed on the house are transmitted to the foundation by shear in the walls. In larger structures, the shear loads are normally carried by columns or diagonal framing. The shearing and bending rigidity of residential type wall construction is smaller than that of other structures.

The emphasis, therefore, of this study is concerned with glass and plaster wall structural elements and residential type structures.

SECTION 6

APPLICATIONS TO GLASS WINDOWS

GENERAL

Glass is an elastic structural material. Like metals, its strength depends on its chemical composition and on its heat treatment. Ordinary window glass is annealed to remove internal residual stresses, while tempered plate glass has up to 4-1/2 times the strength of annealed glass. Glass is weakest in tension and all cracks are normal to the direction of maximum tension. Contact with water or alcohol reduces its strength. When dry, glass is 20% stronger than when wet. Its strength is also affected by the duration of loading. When it is loaded for several hours its strength is 50% of that for a one second loading time. The rate of pressure loading also has an effect on the strength of glass. Tests[37] on single strength glass panels 14" x 19" showed a breaking pressure of about 1.5 psi for a zero rate of pressure rise. At a pressure rise of 300 psi/sec., the breaking strength rose to about 4.5 psi. This represents an increase in dynamic strength of three times the static strength.

Cracks originate at a weak point such as a scratch or imperfection in the glass. Window glass is polished to a smooth surface. Since impurities cannot be avoided, glass is graded into different qualities described in United States Government Specifications[33].

DESIGN STANDARDS

The design of windows and window sash has been left to the discretion of the manufacturers and builders who have had many years of experience in this field. Building codes and engineering handbooks do not go into the details of designing the stiles, rails and dividing bars of a window sash. The building code of the City of New York, however, specifies that glazing shall be designed for a pressure of 30 lbs./ft.^{2} in either direction, and also gives a schedule of maximum areas of window panes for various thicknesses of glass (see Figure 36).

In order to standardize dimensions of windows, commercial organizations have adopted voluntary standards. For windows with wood frames, standards have been published by the United States Department of Commerce[34]. The Aluminum Window Manufacturers Association publishes its own standards[35] and offers a seal of approval to those meeting them.

DEFINITIONS

Following are definitions of terms that will be used in the discussion of windows:

Light - section of window enclosed by framing

Muntin - any short or light framing member, either vertical or horizontal

Rail - cross, or horizontal, outside framing member of a window sash

Check rail - meeting rail sufficiently thicker than the window to fill the opening between the top and bottom sash of a double hung window

Stile - the vertical outside framing member of a window sash

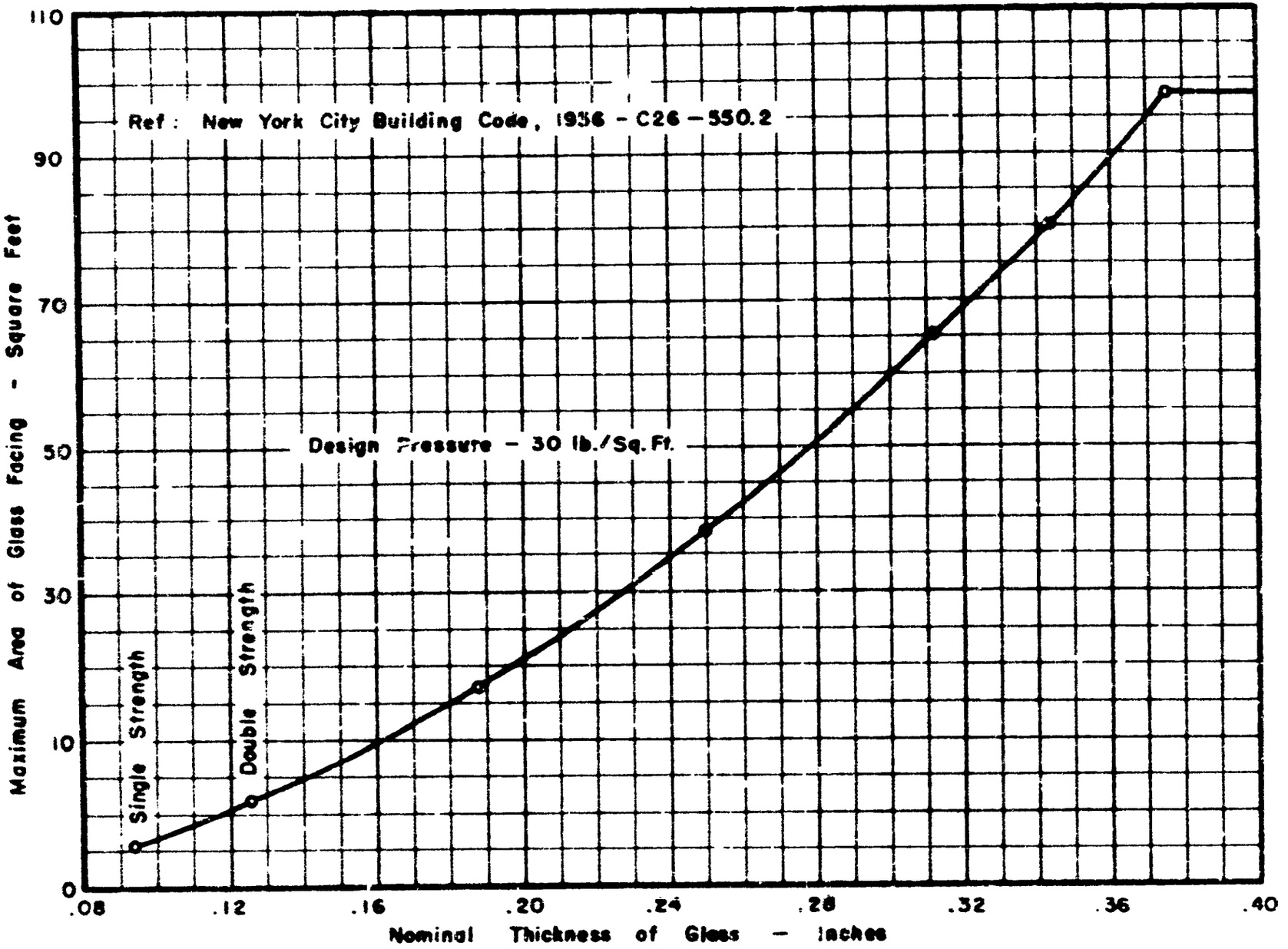

Figure 36 Maximum Area Of Glass Facing vs. Nominal Thickness Of Glass

Sash - single assembly of stiles and rails made into a frame for holding glass, with or without dividing bars

APPLICATION OF THEORY

A simple rational approach to the design of window sash is suggested by the National Academy of Sciences[36]. Drawing 45° lines from the corners of a window pane divides the area into triangular and trapezoidal sections. From statics, the loads and stresses on each stile, rail or dividing bar can be found. Window panes are analysed as rectangular plates, uniformly loaded and simply supported or clamped on all edges.

Figures 37 through 45 present curves, based on the above method of analysis, from which the breaking pressures for typical sizes of wooden rails and stiles can be determined. These curves are plotted for a wide range of window sizes and types.

Figures 46 through 49 present graphs for the computation of failure pressures for glass window panels of varying thicknesses, sizes and types. Graphs for the determination of natural frequencies of glass panels are presented in Figures 50 through 52.

CALCULATED RESULTS

Using the above mentioned data, free-stream shock wave pressures that produce failure can be determined for window panes from the following:

$$\dot{P}_s \text{ critical} = \frac{3P_u}{(2)(A \times M)} \qquad (15)$$

where P_u is the static failure pressure of the window element under investigation - psi

$A \times M$ is the modified dynamic amplification factor (Fig. 34) for $\tau/\eta \longrightarrow \infty$

The factor 3 in the numerator represents the increase in static strength due to a rapidly rising pressure load.

The factor 2 in the denominator is the maximum incident overpressure for normal incidence (Fig. 4).

Table VI presents critical free-stream shock wave pressures for glass panels of various sizes and thicknesses. The data in this table have been computed for a free-stream pressure wave duration, η , equal to .10 seconds and for normal incidence of the wave on the panes. The effect of the increase in strength due to rapid loading has been included by use of the factor 3 as shown in Equation (15). For non-normal incidence, the values of $\dot{P}_s$ critical could be reduced by a factor as large as 2. (See Section 2.)

EXPERIMENTAL RESULTS

A number of different glazing materials for use as window panes were tested at the Aberdeen Proving Ground[38]. The results of these tests on a 16" square glass pane 1/8" thick (double strength), gave a minimum free-stream or incident breaking pressure of 0.75 psi. Using the method described in this report for a 16" square, double strength, clamped-end glass pane, the predicted free-stream failure pressure would also be 0.75 psi.

A number of tests were conducted at Aberdeen Proving Ground[17], to investigate

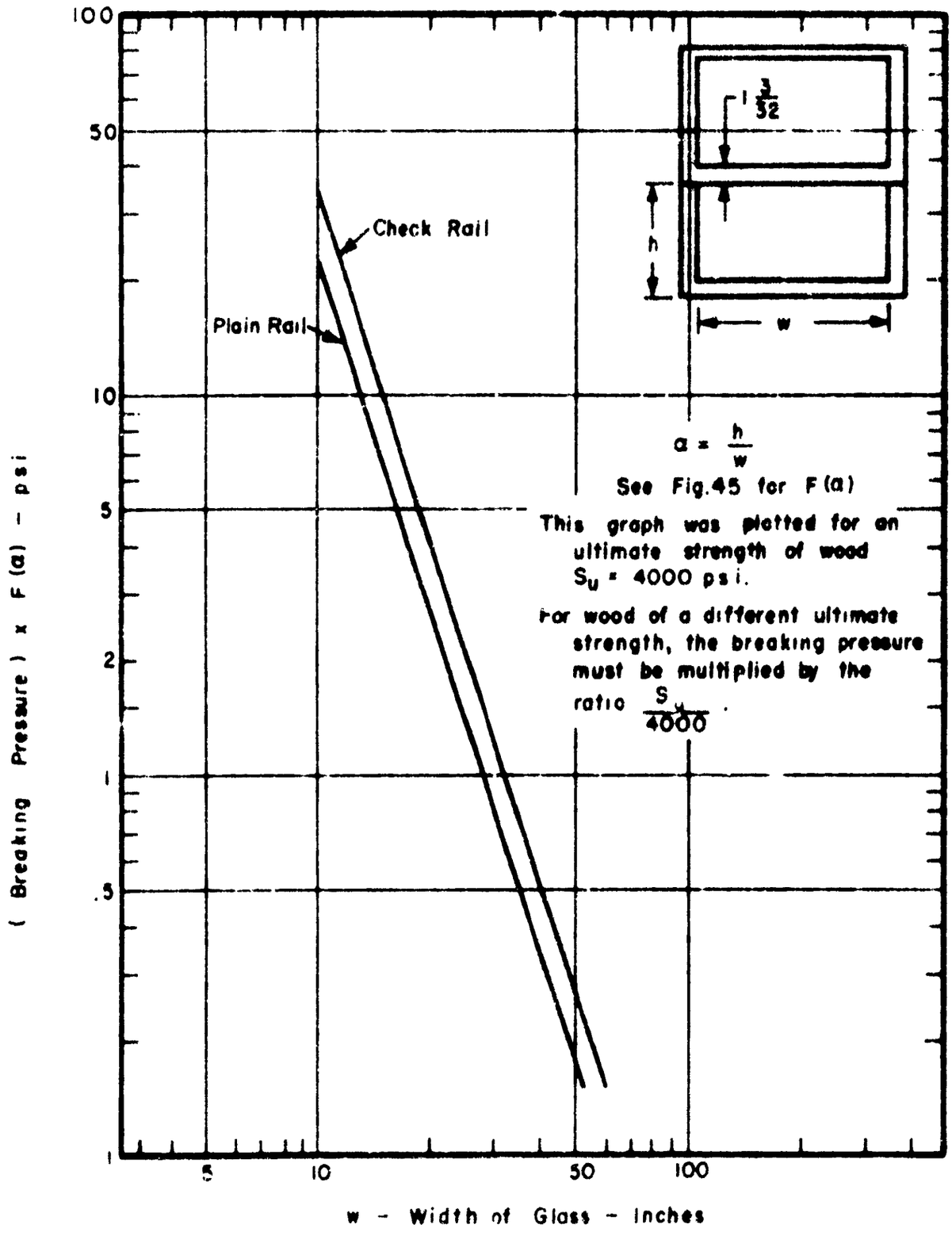

Figure 37 Breaking Pressure For Middle Rail
Wooden Windows — Two Lights

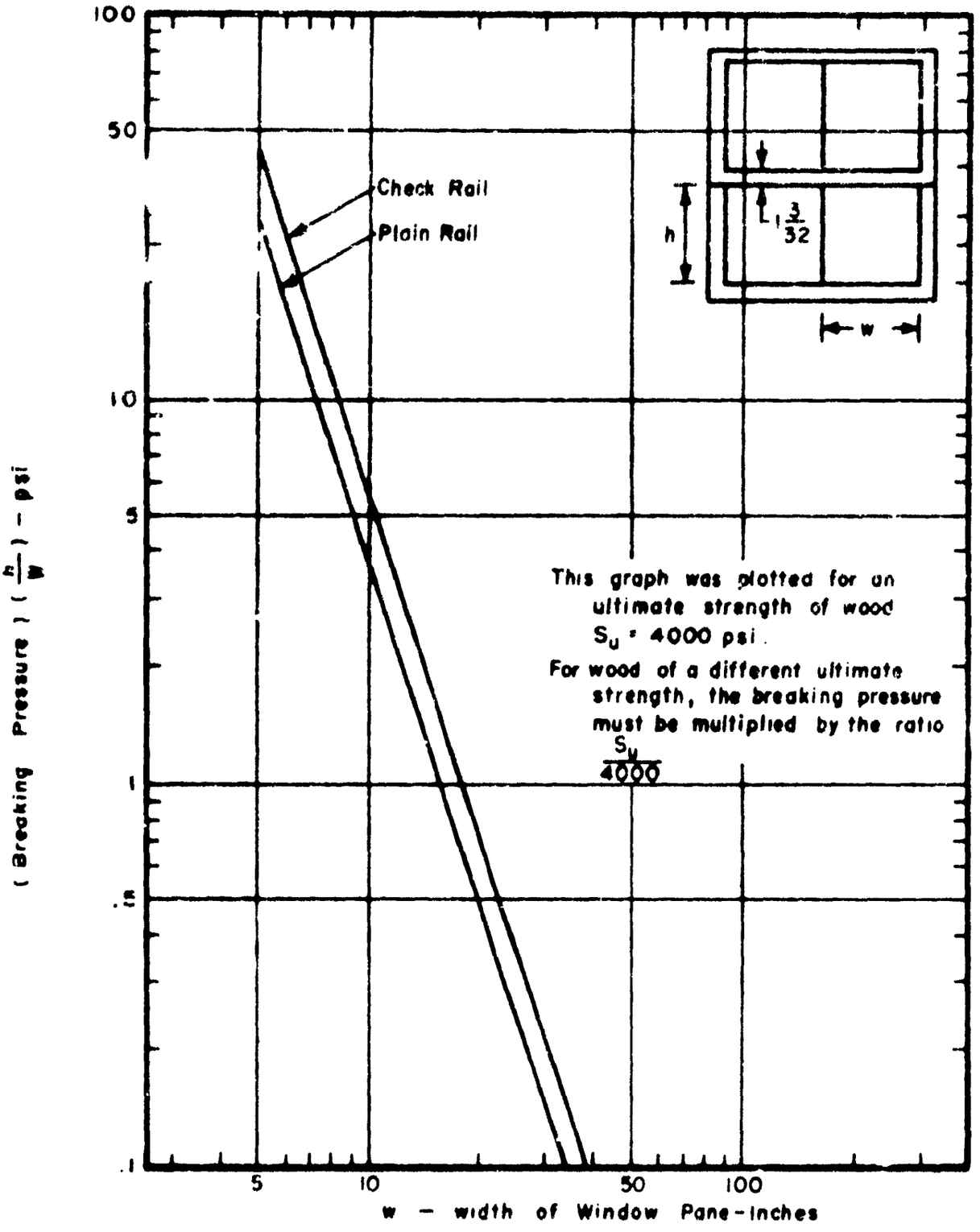

Figure 38 Breaking Pressure For Middle Rails
Wooden Windows - Four Lights

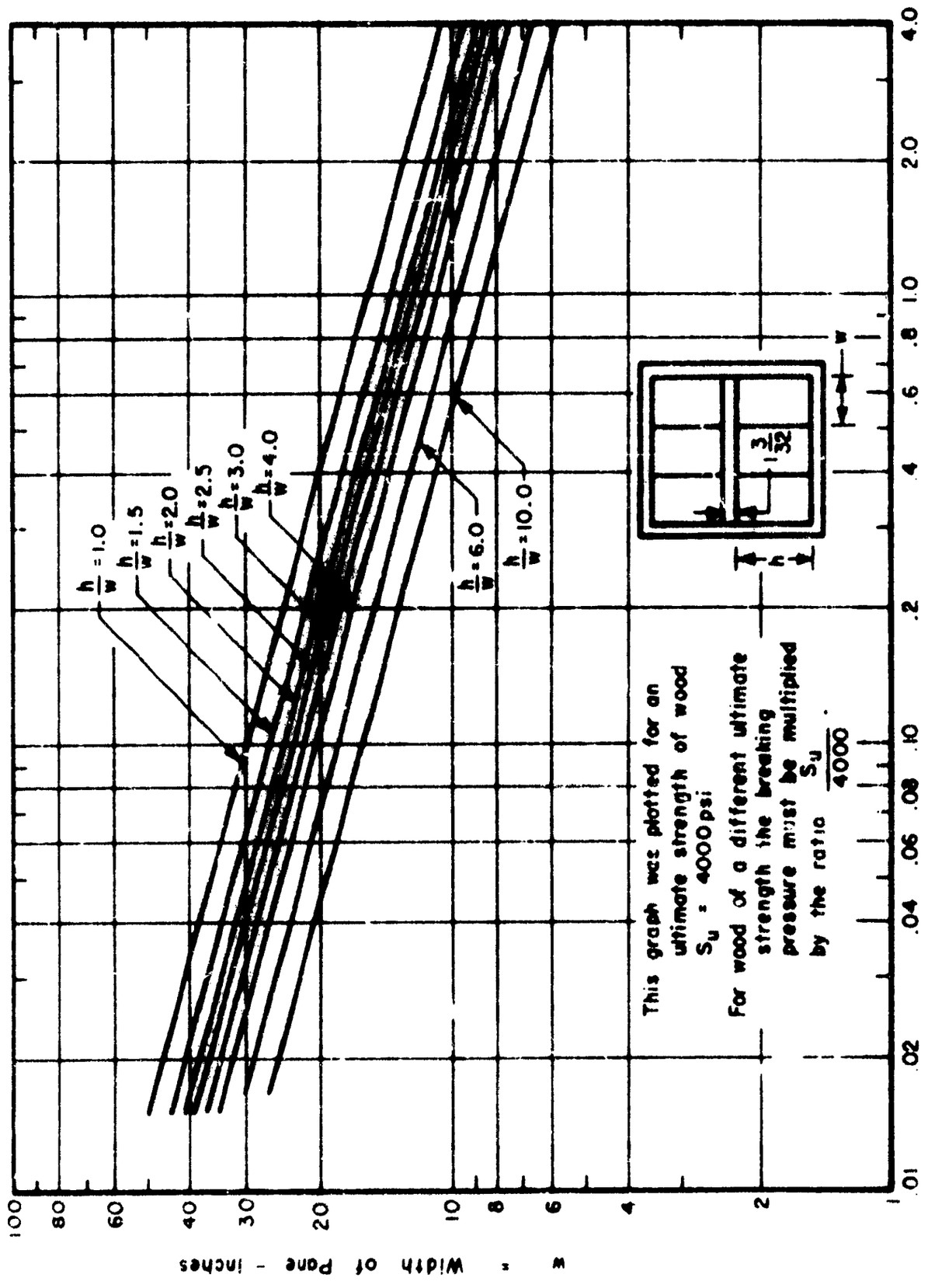

Figure 39 Breaking Pressure For Horizontal Rail Wooden Check Rail Windows - Six Lights

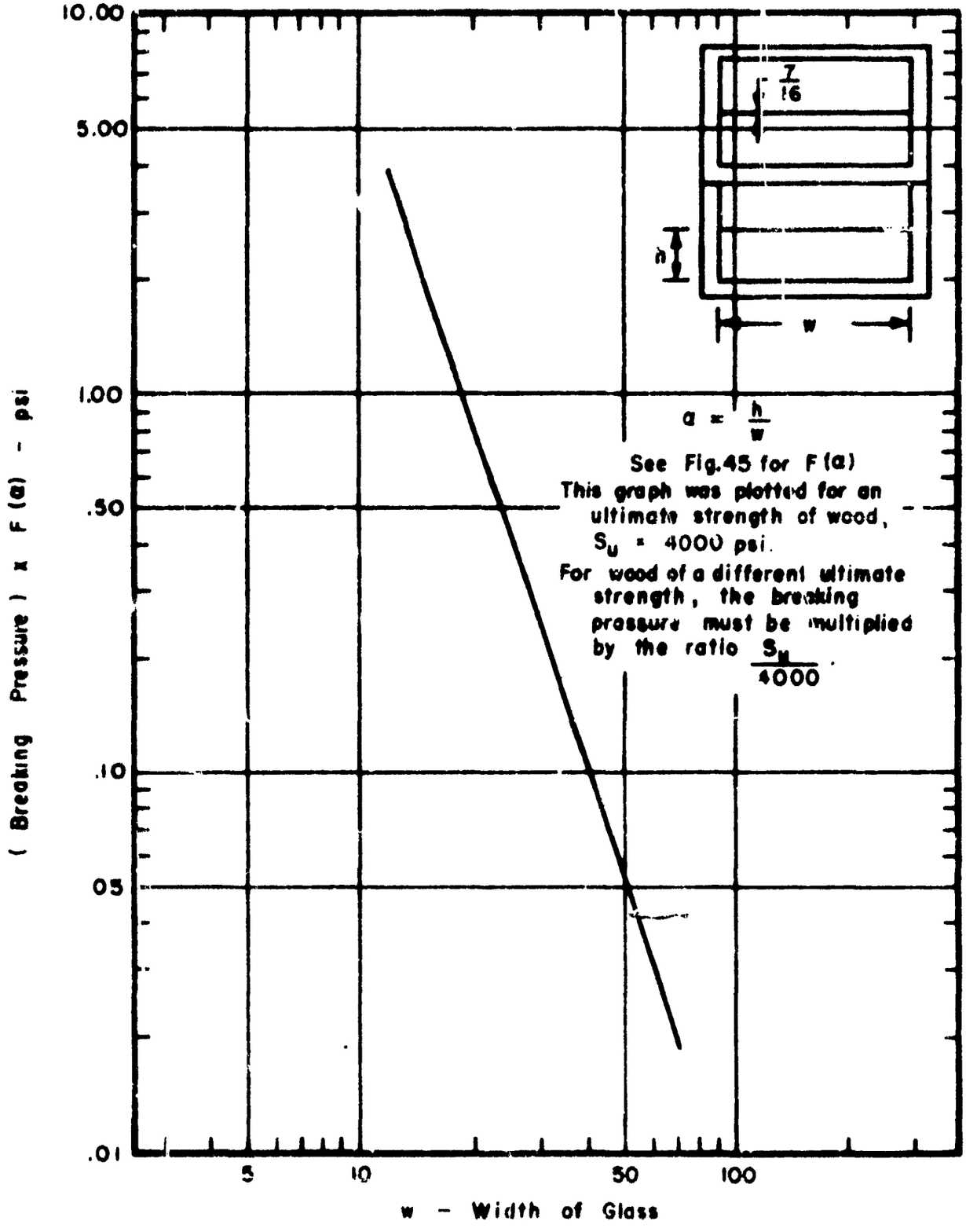

Figure 40 Breaking Pressure For Horizontal Bar Wooden Check Rail Windows - Four Lights

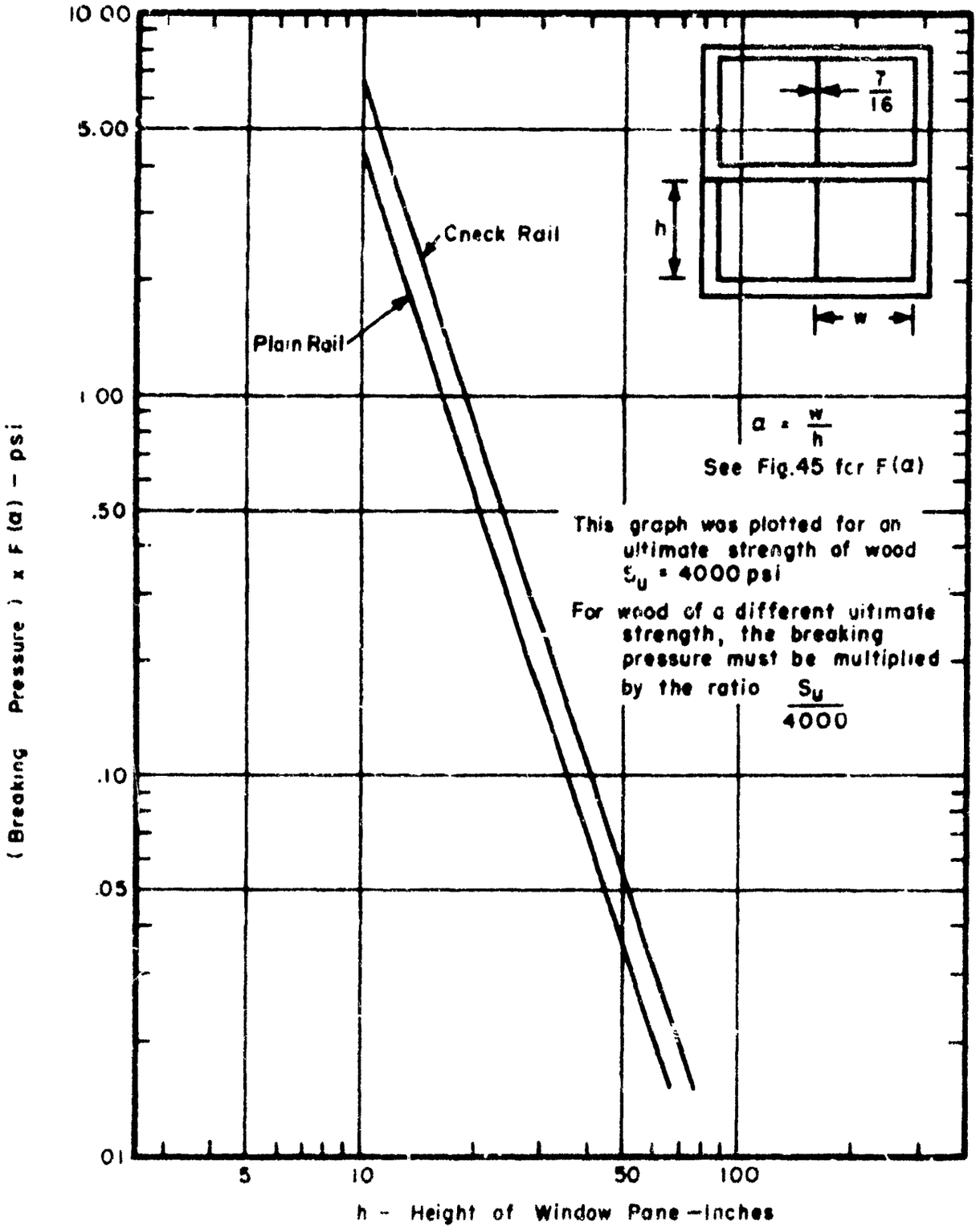

Figure 41 Breaking Pressure For Vertical Bar Wooden Windows – Four Lights

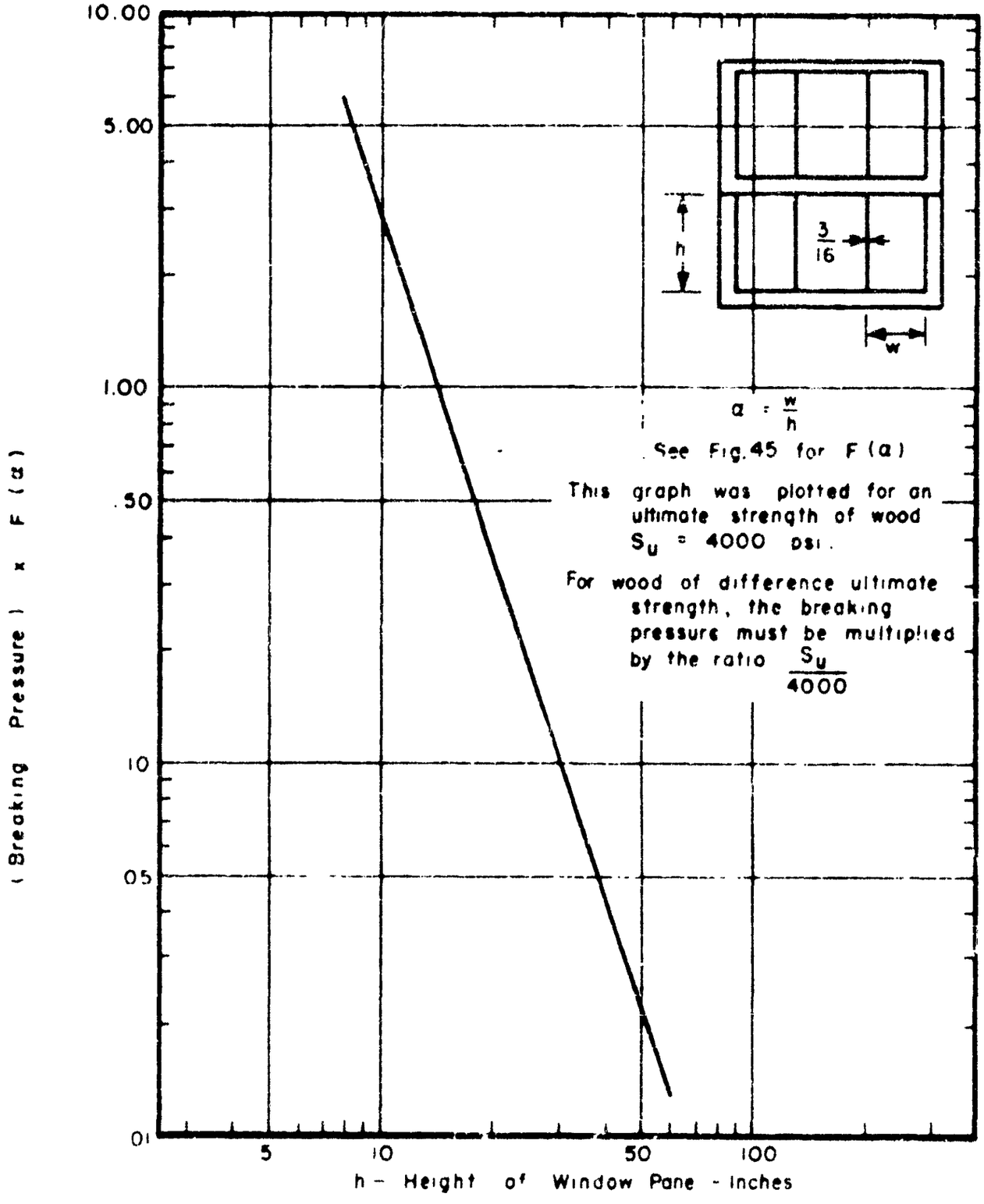

Figure 42 Breaking Pressure For Vertical Bar Wooden Check Rail Windows-Six Lights

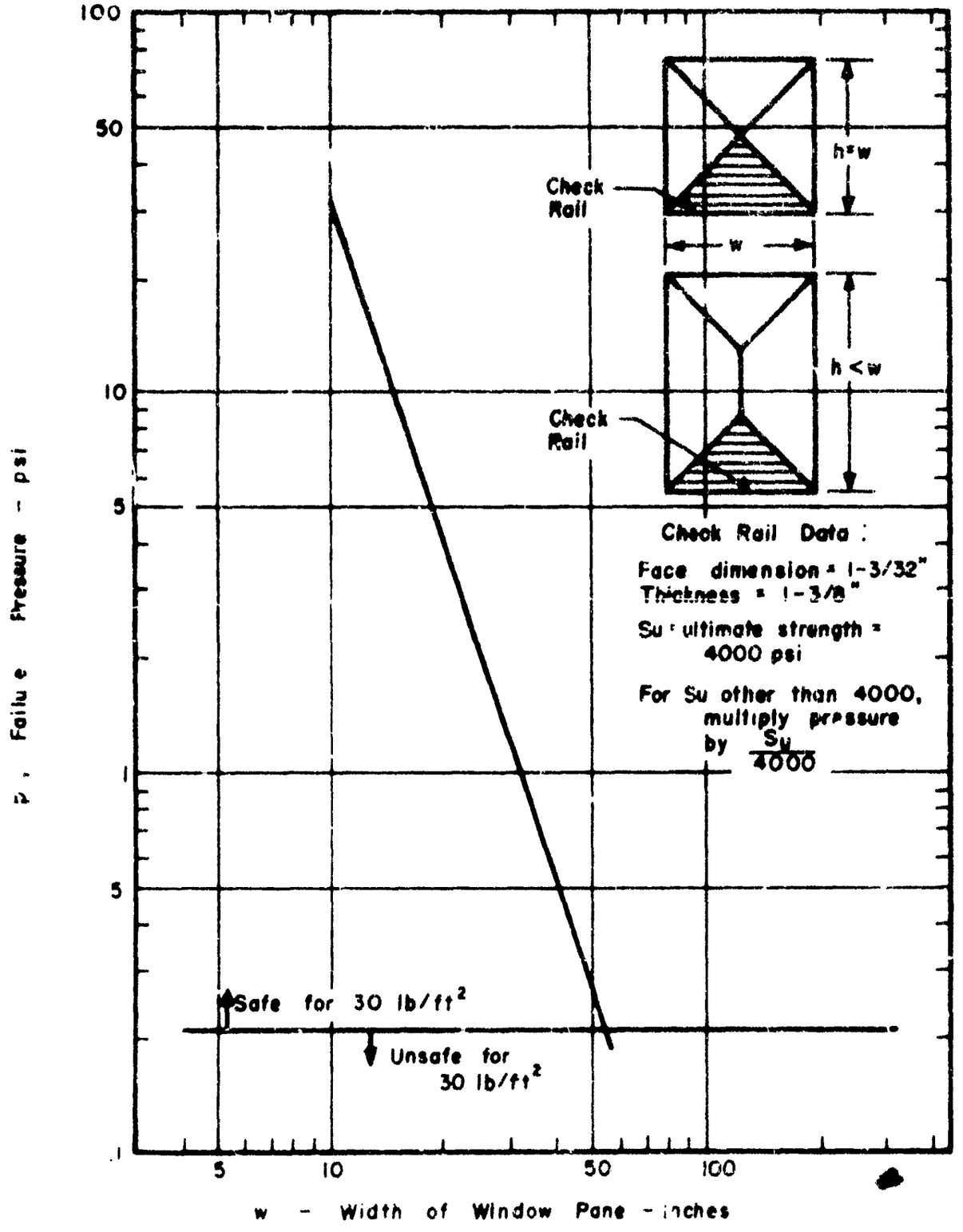

Figure 43 Breaking Strength of Wooden Check Rail With Triangular Load

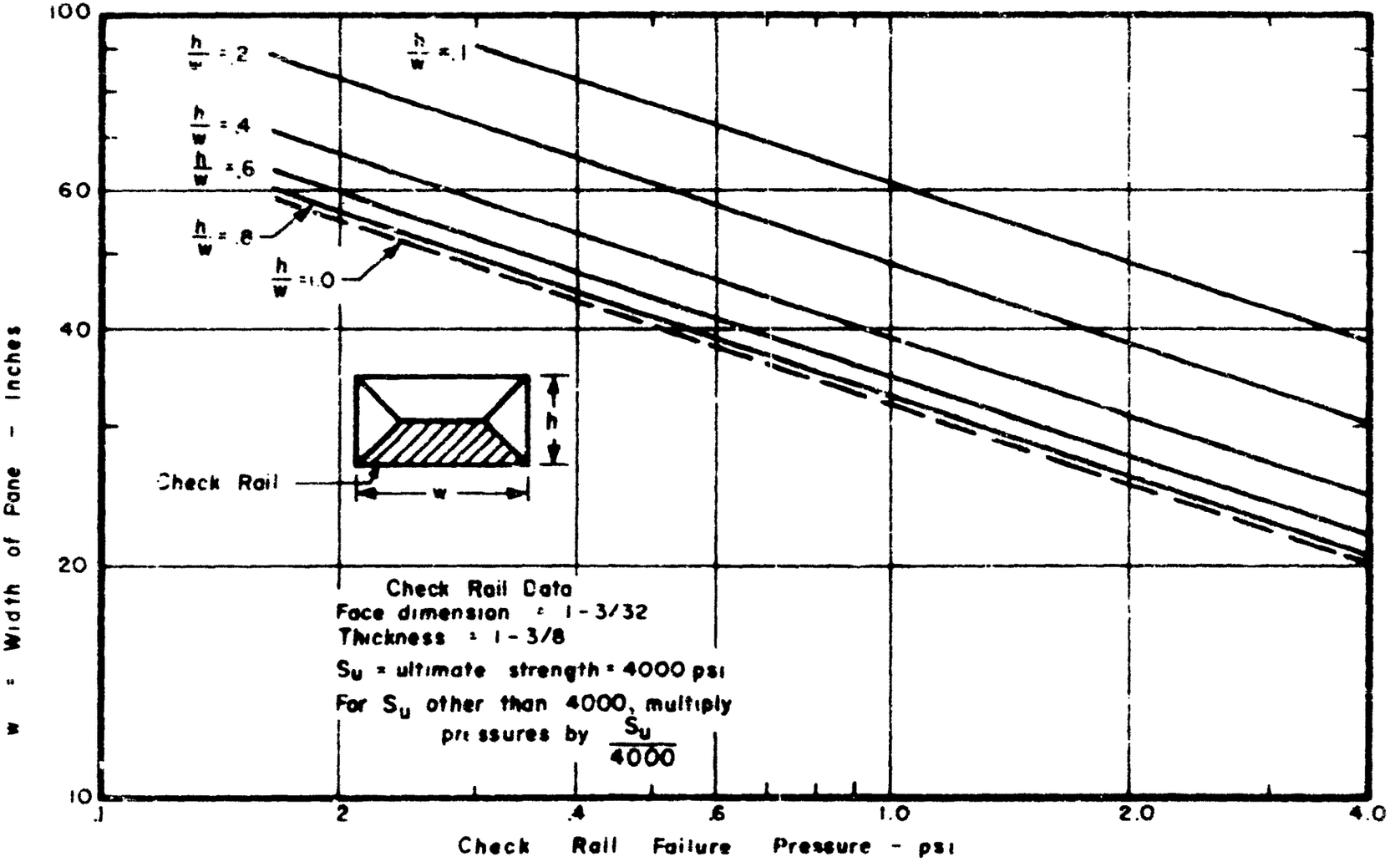

Figure 44 Breaking Strength of ~~Wooden~~ Check Rail With Trapezoidal Loading

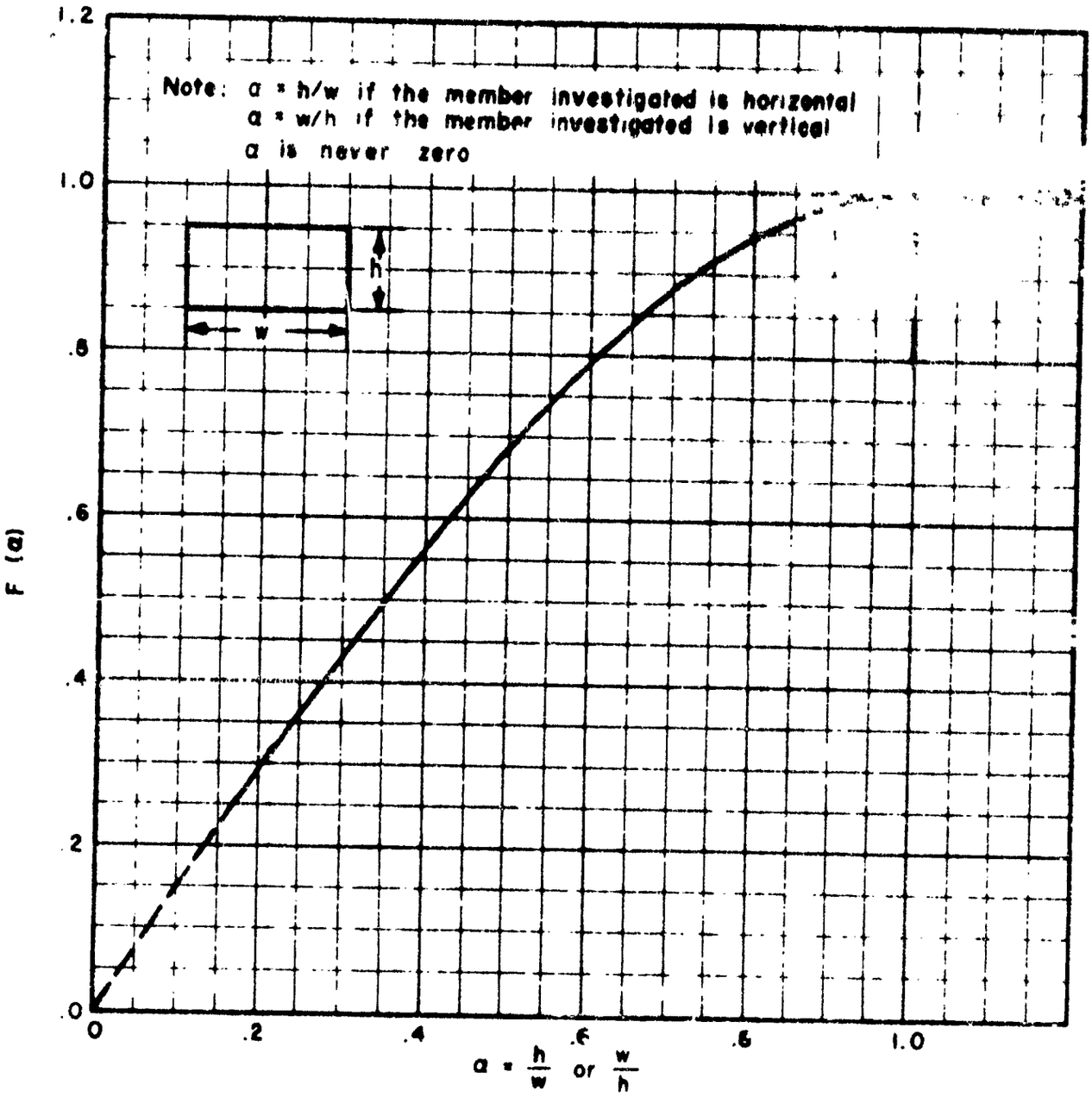

Figure 45 F (α) vs. α

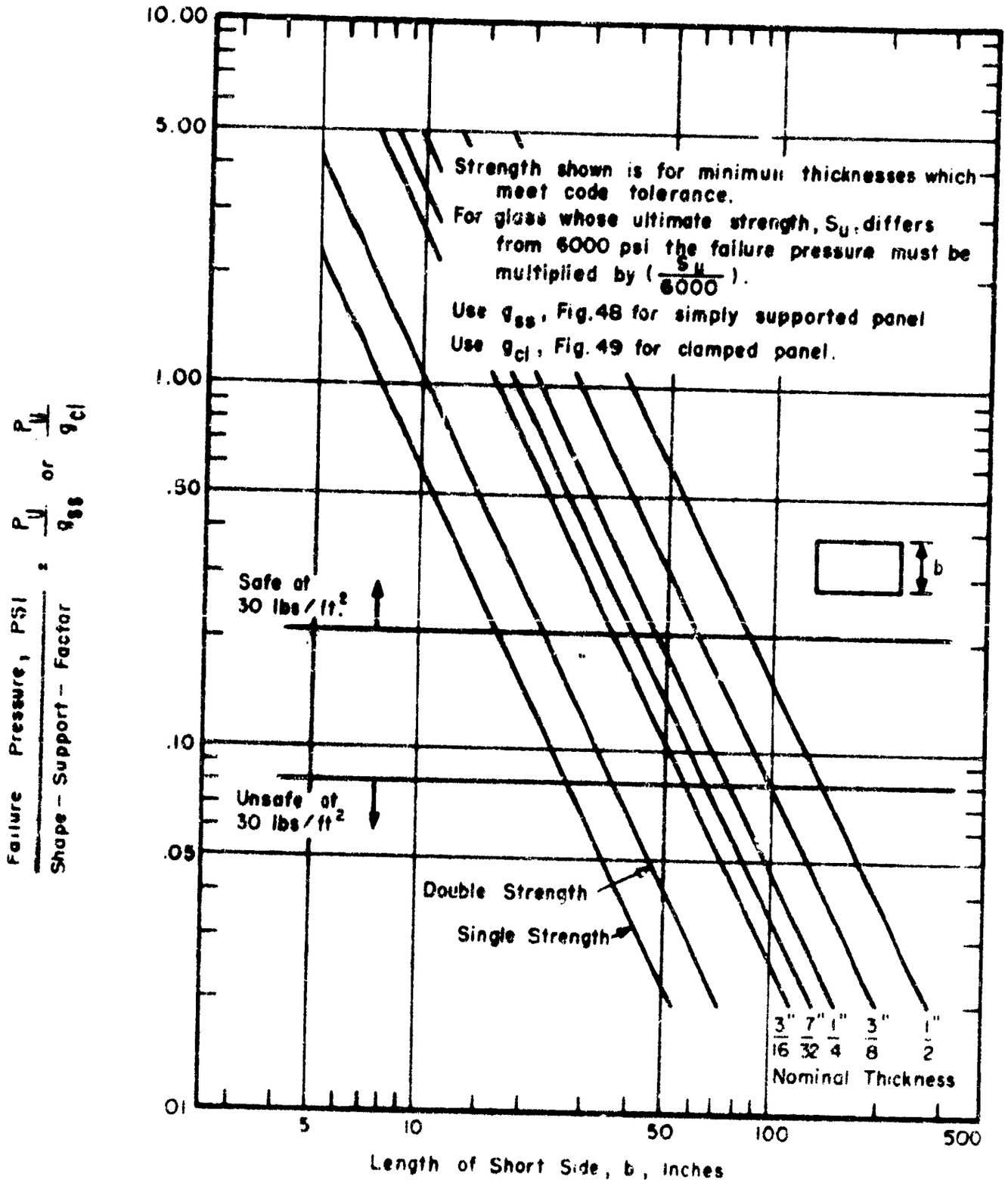

Figure 46 Failure Pressure For Clear Sheet Glass Panels

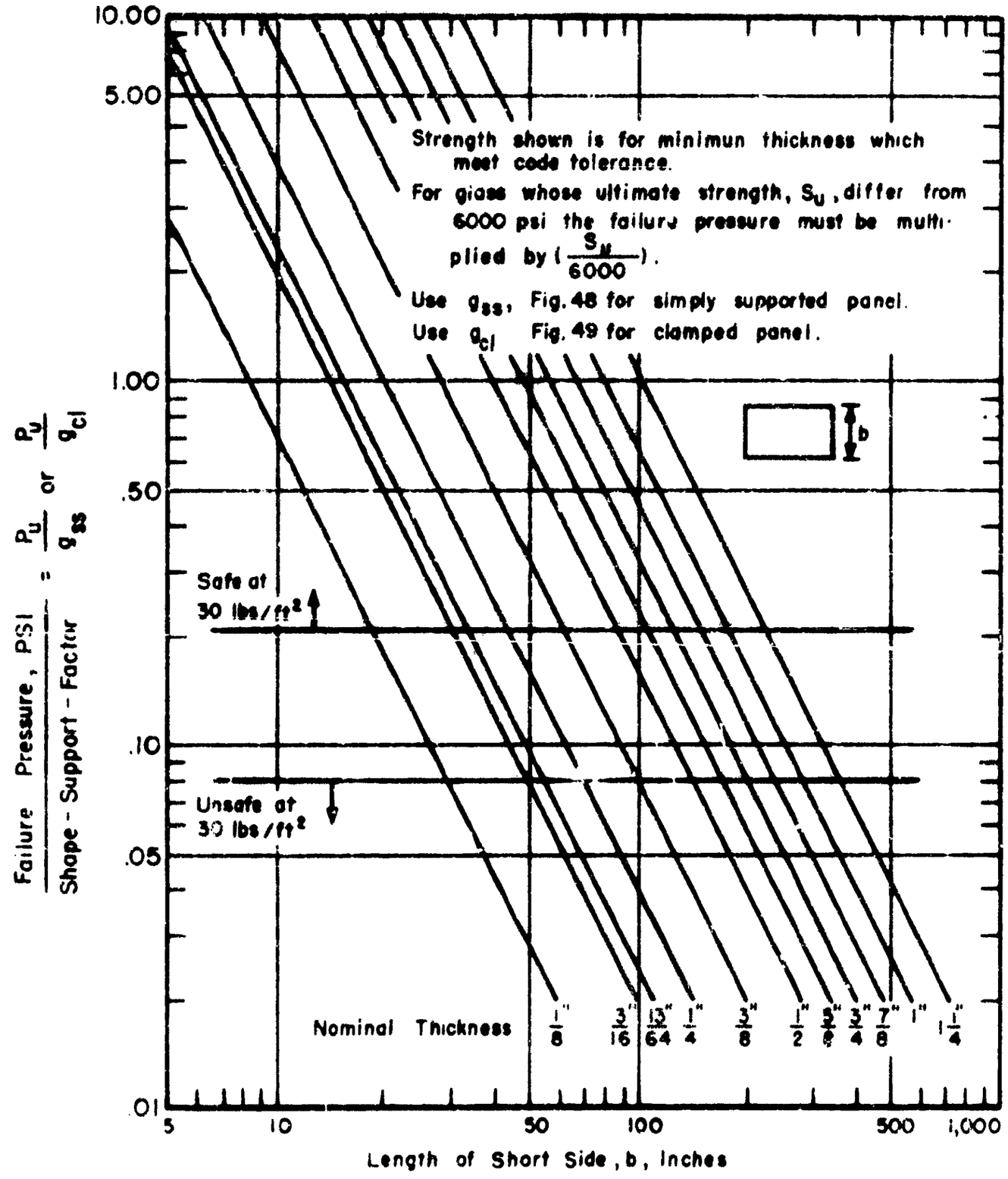

Figure 47 Failure Pressure For Polished Plate Glass Panels

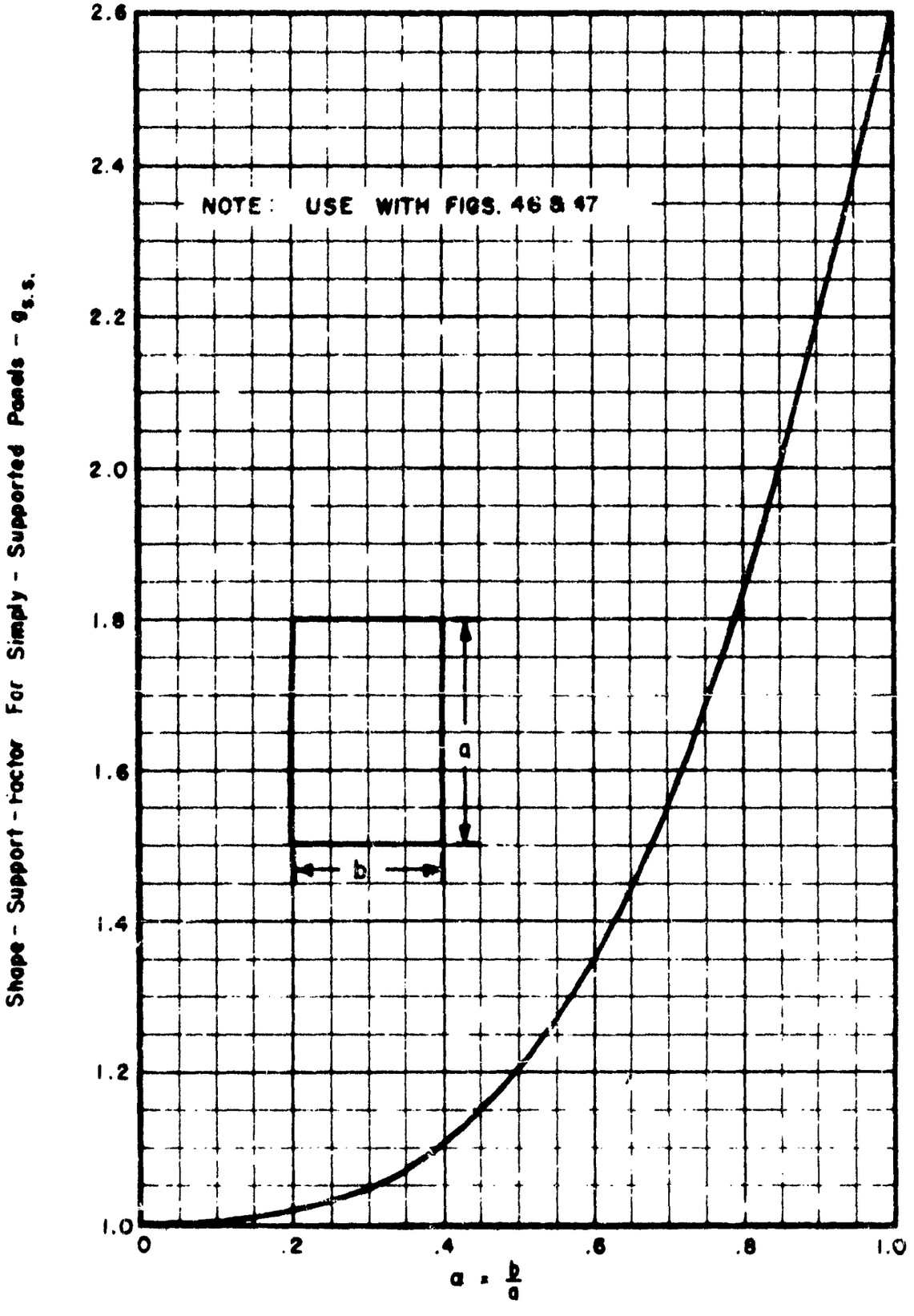

Figure 48 Shape - Support - Factor For Simply - Supported Panels

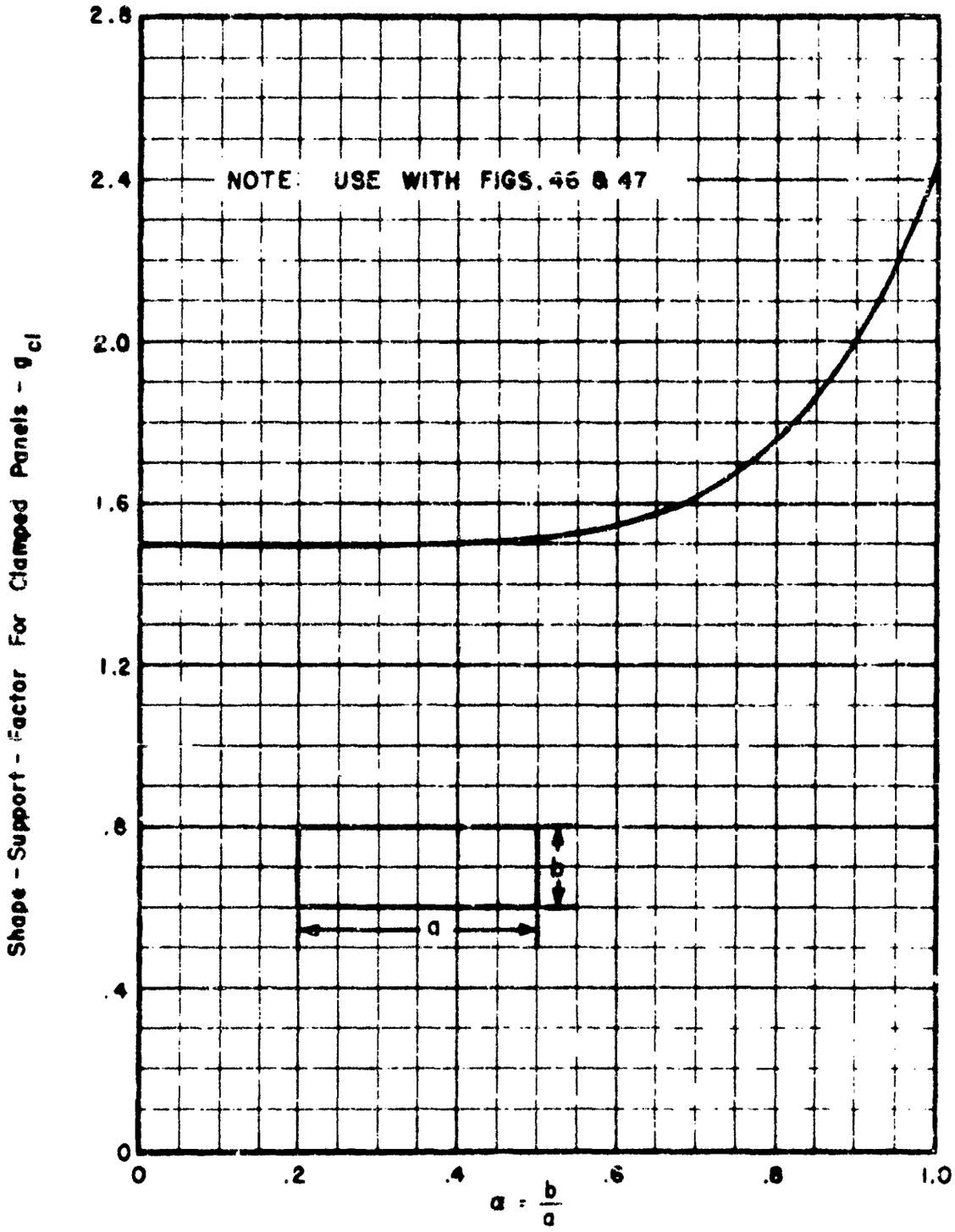

Figure 49 Shape - Support -- Factor For Clamped Panels

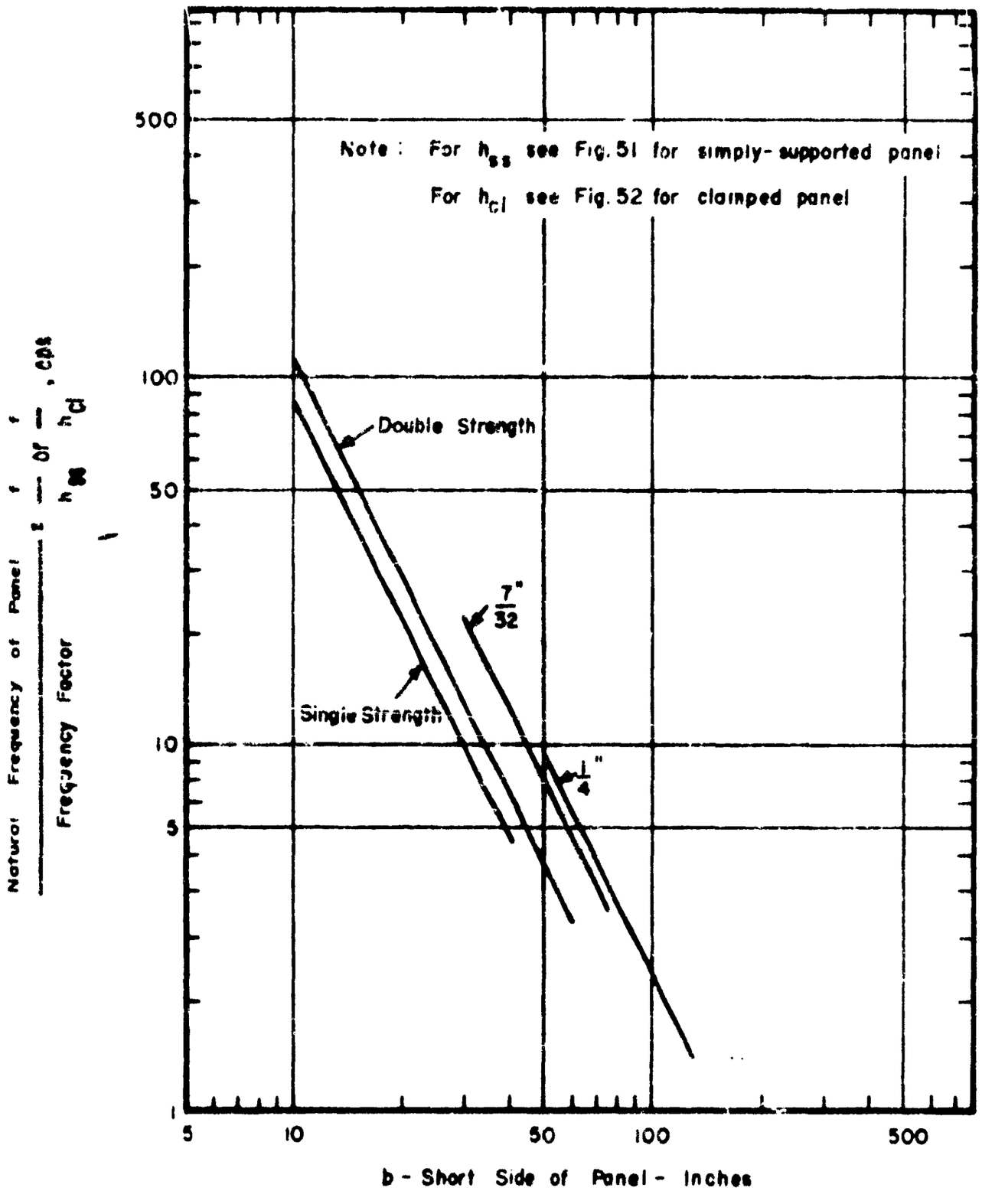

Figure 50 Natural Frequency Of Long Simply - Supported Panels

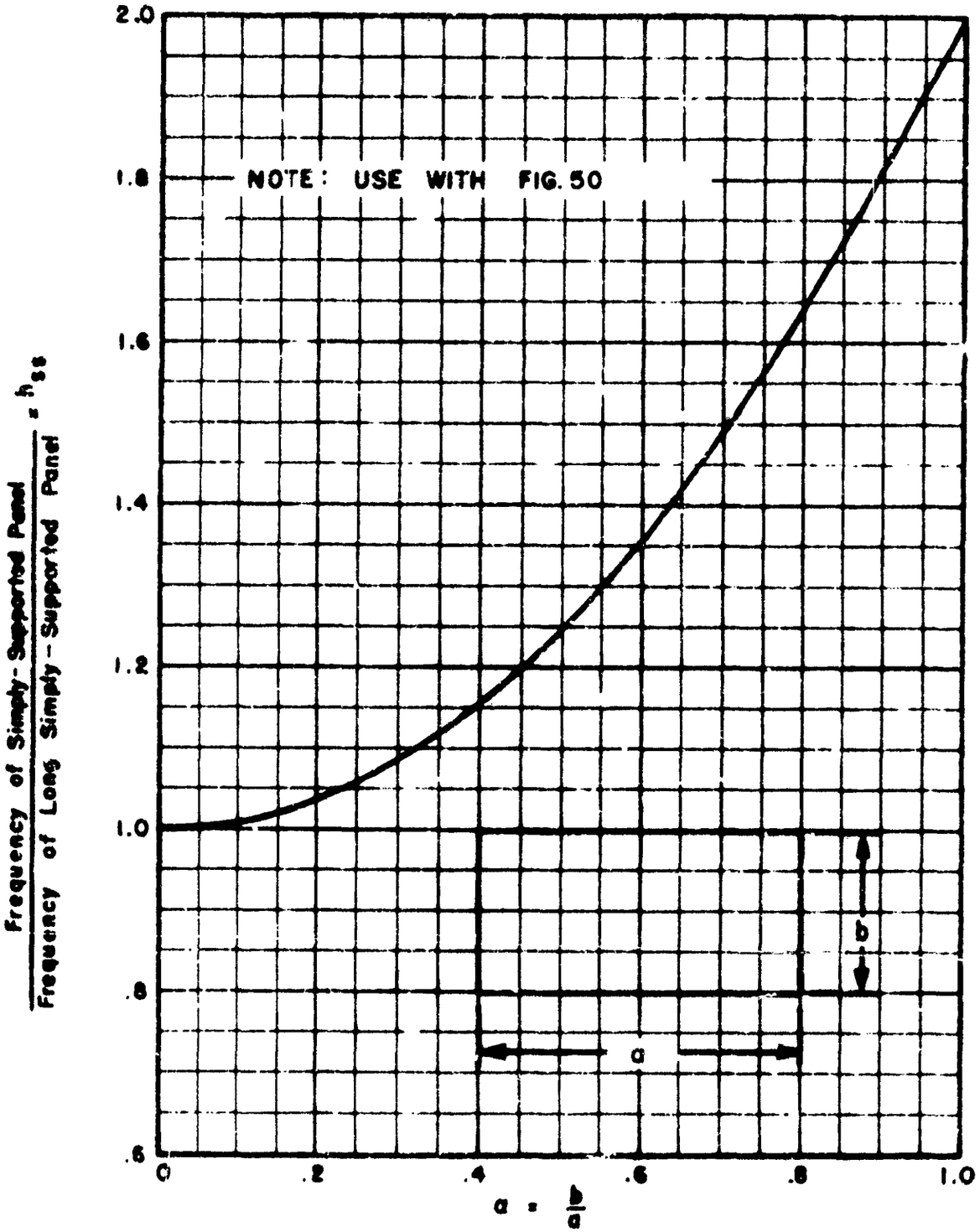

Figure 51 Frequency Factor For Simply-Supported Panels

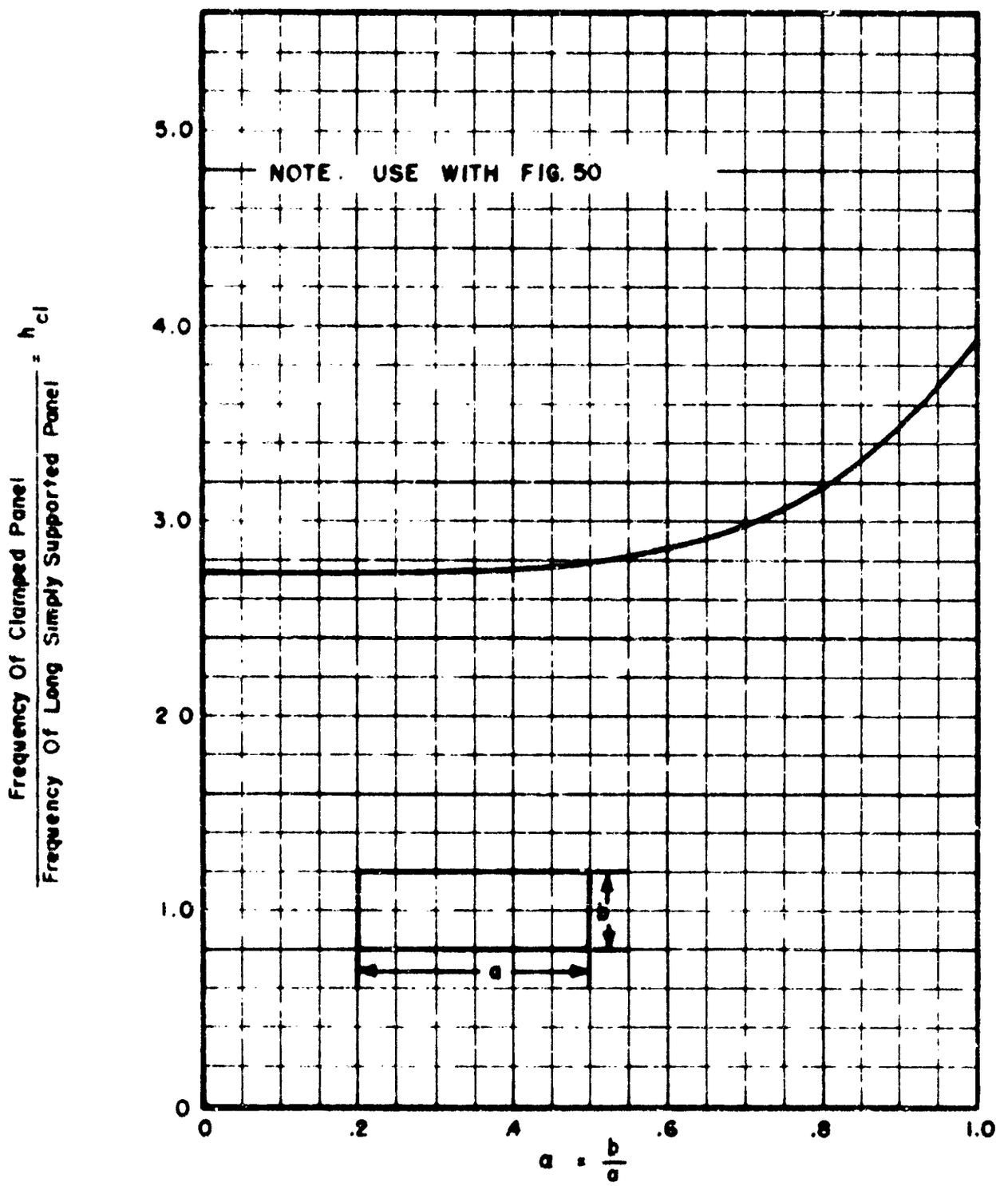

Figure 52 Frequency Factor For Clamped Panels

the effects of various size bomb detonations on three model houses. Extrapolating the data for the smallest size bomb, a 250 pound light case charge, it was determined that the incident pressure acting on these houses was approximately 0.8 psi. At this pressure, many of the window panes were broken in addition to other damages. No conclusions can be drawn from these tests since the minimum pressures were greater than what would be predicted for window pane failures using the methods presented in this report.

The United States Atomic Energy Commission also investigated damage to different types of windows subjected to atomic blasts[44]. Here again, the incident pressures, approximately 2 psi, were above the range of interest for this investigation and no conclusions could be drawn as to minimum free-stream failure pressures.

TABLE VI

CRITICAL JET-STREAM SHOCK WAVE PRESSURES FOR GLASS WINDOWS - NORMAL INCIDENCE
(η =0.1 sec.)

Window Size	Type of Edge* Support	Natural Freq. - f (c.p.s.)	Dynamic Amplification Factor	Failure Pressure (psi)	$\dot{p}_s$ critical
24" x 24" single strength	s.s.	30	2.734	0.261	0.144
	cl.	59	2.0	0.243	0.183
12" x 12" single strength	s.s.	120	2.734	1.04	0.573
	cl.	236	2.0	0.975	0.732
24" x 36" single strength	s.s.	21.7	2.20	0.148	0.112
	cl.	44.1	2.00	0.153	0.120
12" x 36" single strength	s.s.	66.7	2.20	0.424	0.291
	cl.	165	2.0	0.600	0.450
36" x 36" double strength	s.s.	18.0	2.734	0.208	0.114
	cl.	35.4	2.0	0.194	0.147
20" x 20" double strength	s.s.	58.0	2.734	0.678	0.372
	cl.	114.0	2.0	0.634	0.474
36" x 60" double strength	s.s.	12.2	2.20	0.108	0.075
	cl.	22.7	2.00	0.123	0.093
20" x 60" double strength	s.s.	32.2	2.20	0.275	0.186
	cl.	79.8	2.00	0.390	0.291
120" x 200" 1/4" plate glass	s.s.	2.2	0.53	0.036	0.105
	cl.	4.6	1.29	0.042	0.048
50" x 200" 1/4" plate glass	s.s.	10.1	2.20	0.158	0.108
	cl.	26.1	2.00	0.230	0.171
120" x 120" 1/4" plate glass	s.s.	3.2	1.09	0.070	0.096
	cl.	6.3	1.84	0.066	0.054
50" x 50" 1/4" plate glass	s.s.	19.0	2.734	0.400	0.219
	cl.	37.4	2.0	0.372	0.279

* s.s. -- simply supported edges
cl. -- clamped edges

EXAMPLE

In order to illustrate the use of the graphs in determining the data for the above table and to show the method of analysis for stiles and rails, a sample calculation is shown below:

Window Description: 26" x 50" double hung wood frame
pane size 24" x 24" single strength
check rail -- 1-3/32" x 1-3/8" (S_u = 6000 psi)
S_u = 4000 psi (panes)

Assuming the panes have simply supported edges:

$$\frac{P_u}{q_{ss}} = 0.10 \qquad \text{(Fig. 46)}$$

From Fig. 48, with $\alpha = 1$; $q_{ss} = 2.6$

Therefore, $p_u = (.10)(2.6) = 0.26$ psi.

From Figure 50, $\frac{f}{h_{ss}} = 15$

and from Figure 51, $h_{ss} = 2$.

Therefore, $f = (2)(15) = 30$ cps and $T = \frac{1}{30} = .033$ sec.

for $\eta = 0.1$ sec.. $\eta/T = 3$

From Figure 34, $\frac{(\lambda) \times (\mu)}{C} = 2$ and $C = 1.367$ for simply supported square plate.

Dynamic amplification factor = (2)(1.367) = 2.734

Substituting in Equation 15,

$$\dot{p}_s \text{ critical for the panes} = \frac{(3)(.26)}{(2)(2.734)} = 0.144 \text{ psi.}$$

For nonnormal incidence*, $\dot{p}_s$ critical = 0.072

From Figure 37, failure pressure for the check rail equals 2.4 psi.

Using a dynamic amplification factor of 2, and assuming a normal incidence factor of 2,

$$\dot{p}_s \text{ critical for rails} = \frac{2.4}{(2)(2)} = 0.60 \text{ psi.}$$

---

*It is assumed that the angle of incidence β is small so that the window is subjected to a pressure of substantially 4 $\dot{p}_s$ for times the order of its natural period (see Figure 17, Section 2).

SECTION 7

APPLICATION TO WALLS

The National Bureau of Standards conducted a series of tests[39] on a number of different types of wall constructions for low cost residential housing. The purpose of these tests was to determine the structural strengths and properties of the walls under various types of loading conditions. The wall specimens were subjected to transverse, compressive, concentrated and racking loads. The interesting loadings, so far as this investigation is concerned, are those causing initial failure due to transverse and racking loads. The transverse loading simulates the type of loading due to normal pressures, while the racking loads are loads transmitted to side walls by pressure acting on the front and back walls and roof of a structure. These loads are applied to the top of a wall in the plane of the wall and are resisted at the bottom thus producing a shearing action.

Table VII summarizes these test results. The initial failure loads listed in the table are the lowest values, found from a number of tests on each type of wall panel for each type of loading, at which initial failure such as plaster cracks occurred. For comparison, the maximum failure loads are also given. In all cases, the walls tested were solid panels, that is, there were no openings for doors or windows. The last three items in this table are wall constructions typical of those used for foundations for small residences.

A similar series of tests[40] were conducted by the Forest Products Laboratory on wood panel frame walls with plaster on wood lath on one face. These walls were similar in construction to wall QA, Table VII, with the exception that there were door and window openings cut into them. Plaster cracks occurred at the corners of doors and windows for racking loads as low as 57 lbs. per ft. This compares with the NBS tests for wall QA which produced plaster cracks with a racking load of 500 lbs. per ft. This indicates that, for plaster walls with door and window openings, the initial failure loads should be determined by dividing the loads given in Table VII by a factor of approximately 10.

In order to compute amplification factors for walls of these types for their dynamic response to a shock wave, natural frequencies and natural periods are required. For the natural frequency due to transverse, or normal pressure loading, the wall is treated as a uniformly loaded simple beam with a span equal to the height of the wall. For a beam of this type, the first natural frequency is given by (see equations (61) and (64) of Appendix III):

$$\omega = \frac{\pi^2}{12\,L^2}\sqrt{\frac{g\,EI}{w}}$$

and

$$T = \frac{2\pi}{\omega}$$

The flexural rigidity EI is given by (Equation (63), Appendix III):

$$EI = \frac{33\,q\,L^4}{\Delta}$$

TABLE VII

STRENGTH DATA ON VARIOUS WALL CONSTRUCTIONS

BRE[29] Wall Designation	Wall Structure	BRE[39] Report No.	INITIAL FAILURE LOADS* Transverse Loading (lbs./ft.^{2}) Loaded On Inside Face	Loaded On Outside Face	Racking Load (lbs./ft.)	Description of Failure
QA	Wood frame -- bevel siding on diagonal wood sheathing outside -- plaster on wood lath inside	25	262 (289)	26 (63)	500 (1500)	Plaster Cracked
QD	Wood frame -- plaster on wood lath inside and outside	25	48 (52)	48 (52)	380 (880)	Plaster Cracked
BU	Wood frame -- Douglas fir plywood inside -- wood shingles on Douglas fir plywood outside	30	153 (233)	87.5 (271)	875 (1440)	Studs broke due to transverse load -- wallboard and sheathing buckled due to racking load
BG	Wood frame -- wood bevel siding on wood-fiber insulating board outside -- plaster on wood-fiber lath inside	31	75 (400)	75 (422)	1125 (1750)	Plaster Cracked

*Values given are lowest values. Maximum values are indicated in brackets. The number of duplicate tests varied between three and six.

TABLE VII - Continued

BMS Wall Designation	Wall Structure	BMS Report No.	INITIAL FAILURE LOADS: Transverse Loading (Lbs./Ft.^{2}) Loaded On Inside Face	Transverse Loading (Lbs./Ft.^{2}) Loaded On Outside Face	Racking Load (Lbs./Ft.)	Description of Failure
BH	Wood frame -- wood bevel siding on wood-fiber insulating board outside -- 3/4" wood-fiber board inside	31	150 (327)	245 (343)	1375 (1830)	Separation of Wallboard from studs
BI	Wood frame -- wood bevel siding on wood-fiber insulating board outside -- 1/2" wood-fiber board inside	31	233 (319)	250 (318)	1250 (1590)	Stud Ruptured under transverse load -- fiberboard displaced from joint under racking load
BJ	Wood frame -- wood fiber sheathing paper, metal lath and stucco outside -- wood-fiber lath and plaster inside	31	97 (400)	70 (425)	1625 (2250)	Plaster Cracked
BK	Wood frame -- wood fiber sheathing and brick veneer outside -- plaster on wood-fiber lath inside	31	50 (348)	64 (350)	6000 (6250)	Plaster Cracked

TABLE VII - Continued

WSS Wall Designation	Wall Description	16" Support In.	Transverse Loading (lbs./ft.²) Loaded On Inside Face	Loaded On Outside Face	Racking Load (lbs./ft.)	Description of Failure
AL	Wood frame -- wood fiber sheathing, wood furring strips and wood shingle outside -- plaster on wood fiber lath inside	32	75 (350)	60 (475)	1125 (1700)	Plaster Cracked
BK	Wood frame -- sugarcane-fiber insulating board sheathing and wood bevel siding outside -- sugarcane-fiber insulating board lath and plaster inside	42	90 (350)	90 (350)	1125 (1920)	Plaster Cracked
BY	Wood frame -- sugarcane-fiber insulating board sheathing and wood bevel siding outside -- sugarcane-fiber insulating board inside	42	323 (350)	118 (303)	675 (1480)	Stud Ruptured due to transverse loading -- Building board displaced at joint due to racking load

TABLE VII - Continued

BMS Wall Designation	Wall Structure	BMS Report No.	INITIAL FAILURE LOADS: Transverse Loading (Lbs./Ft.^{2}) Loaded On Inside Face	Transverse Loading (Lbs./Ft.^{2}) Loaded On Outside Face	Racking Load ($\frac{\text{Lbs.}}{\text{Ft.}}$)	Description of Failure
CI	Wood frame -- plywood sheathing, sheathing paper and wood shingles outside -- gypsum wallboard inside	47	175 (342)	148 (237)	800 (1370)	Wallboard cracked around nails and studs split due to transverse loading -- nails tore thru edges of wallboard due to racking load
CJ	Wood frame -- gypsum wallboard inside and outside	47	122 (167)	122 (167)	600 (930)	Nails tore thru edges of wallboard due to racking load
CH	Wood frame -- insulating fiberboard inside and outside	48	100 (257)	150 (433)	530 (580)	Studs ruptured due to transverse loading -- fiberboard separated from flame due to racking load
CH	Wood frame -- fiberboard sheathing and wood bevel siding outside -- fiberboard inside	48	275 (440)	180 (393)	740 (800)	Stud ruptured and fiberboard separated from studs due to transverse loading -- fiberboard separated from studs due to racking load

TABLE VII - Continued

BMS Wall Designation	Wall Structure	BMS Report No.	INITIAL FAILURE LOADS: Transverse Loading (Lbs./Ft.^{2}) Loaded On Inside Face	Transverse Loading (Lbs./Ft.^{2}) Loaded On Outside Face	Racking Load (Lbs./Ft.)	Description of Failure
CO	Wood frame -- fiberboard inside and outside	48	200 (318)	200 (318)	540 (920)	Studs ruptured due to transverse loading -- fiberboard separated from studs due to racking load
DK	Lightweight wood frame -- insulating fiberboard inside and outside	72	102 (124)	102 (124)	1150 (1720)	Studs cracked due to transverse loading -- top plate crushed due to racking load
DQ	Lightweight wood frame -- insulating fiberboard and wood bevel siding outside -- insulated fiberboard inside	89	153 (216)	170 (220)	820 (900)	Fiberboard separated from frame
CZ	Non-reinforced monolithic concrete wall -- 6-1/8 in. thick -- 1 part portland cement, 2.71 parts sand and 5.31 parts gravel, by dry weight	61	253 (277)		6250	Specimen ruptured under transverse load -- no failure under racking load

TABLE VII - Continued

BMS Wall Designation	Wall Structure	BMS Report No.	INITIAL FAILURE LOADS: Transverse Loading (Lbs./Ft.^{2}) Loaded On Inside Face	Transverse Loading (Lbs./Ft.^{2}) Loaded On Outside Face	Racking Load ($\frac{\text{Lbs.}}{\text{Ft.}}$)	Description of Failure
DA	Non-Reinforced monolithic concrete wall -- 6-1/8 in. thick -- 1 part cement, 2.53 parts sand and 3.41 parts gravel, by dry weight	61	216 (297)		6250	Specimen ruptured under transverse load -- no failure under racking load
AF	Standard 8 in. concrete block	61	29.6 (36.7)		3000 (3490)	Rupture of mortar and bond between blocks

and w is the weight of the wall in lbs./ft. of span. q/Δ is determined from plots of the transverse load vs. deflection given in the test reports.

For a racking load, the first natural frequency is found from (equation (65), Appendix III):

$$\omega = \left(\frac{12\,k\,g}{w}\right)^{1/2}$$

The spring constant, k, is the slope of the load-deformation curve given in the test data for the racking load tests.

Table VIII gives the dynamic response data for the outside wall types listed in Table VII subjected to transverse or normal pressure loads. The critical free-stream shock wave pressures which would cause initial failure of the walls is summarized in Table IX for various values of η, the duration of the free-stream pressure wave. This pressure is given by:

$$\dot{P}_s \text{ critical} = \frac{P_f}{(2)(A)(144)} \qquad (16)$$

where P_f = initial failure pressure - lbs./ft.^{2}

A = dynamic amplification factor - Figure 33

and the factor 2 in the denominator is the maximum reflected pressure as shown in Figure 4.

Similar data has not been computed for the racking type loads since their dynamic response, which determines the amplification factors, is a function of the weight supported by the walls. This weight depends on the particular construction involved. However, this has been done for the sample house analyzed in Appendix III of this report and the results are summarized in Table XI.

The results given in Tables IX and XI are based on static load test data. Impact tests on wall panels indicated an increase in bending deflection required to produce plaster cracking of 3 to 5 times the static load values. No transient test information is available for racking loads on wall panels or bending loads on roofs. The values of failure pressures given for plaster cracking of wall panels by bending should be multiplied by 3 in order to account for increase in static strength produced by transient loading. No dynamic strength increase factors can be justified for wall panels in shear and roof elements in bending because of the absence of test information. The use of the static strength values leads to conservative estimates of failure pressures for these elements.

TABLE VIII

DYNAMIC RESPONSE DATA FOR WALLS

Wall Panel Type	Weight ($\frac{lbs.}{ft.^2}$)	L (ft.)	q/Δ (lb./ft.^{2}/in.)	EI (#-in.^{2})	k (#/ft./in.)	Transverse Loading	
						ω ($\frac{Rad.}{Sec.}$)	T (Sec.)
QA	10.0	7.5	110	11.5×10^6	2500	89	0.071
BU	4.23	7.5	110	11.5×10^6	1835	137	0.046
BG	8.30	7.5	170	17.8×10^6	4000	118	0.053
BN	5.02	7.5	160	16.7×10^6	2940	151	0.042
BI	4.51	7.5	166	17.4×10^6	3670	153	0.038
BJ	20.00	7.5	227	23.7×10^6	5500	90	0.070
BK	50.5	7.5	88	9.2×10^6	5000	35	0.180
BL	10.6	7.5	180	18.8×10^6	3200	109	0.058
BX	9.1	7.5	160	16.7×10^6	1875	112	0.056
BY	4.7	7.5	140	14.6×10^6	1200	146	0.043
CI	5.46	7.5	170	17.8×10^6	2000	150	0.042
CH	3.60	7.5	160	16.7×10^6	3000	178	0.035
CR	4.38	7.5	200	20.9×10^6	4000	181	0.029
DK	3.13	7.5	35	3.66×10^6	5000	90	0.070
DQ	2.99	7.5	85	8.9×10^6	2850	143	0.044

TABLE IX

CRITICAL FREE-STREAM SHOCK WAVE PRESSURES FOR RESIDENTIAL TYPE HOUSE WALLS (NORMAL INCIDENCE)

Wall Type*	T* (Sec.)	P^*_g ($\frac{lbs.}{ft.^2}$)	η = 0.05 sec. τ/η ** =0.41			η = 0.10 sec. τ/η = 0.205			η = 0.20 sec. τ/η = 0.102			η = 0.40 sec. τ/η = 0.051		
			η/T	A***	$\dot{P}_g$ crit. ($\frac{lbs.}{in.^2}$)	η/T	A	$\dot{P}_g$ crit. ($\frac{lbs.}{in.^2}$)	η/T	A	$\dot{P}_g$ crit ($\frac{lbs.}{in.^2}$)	η/T	A	$\dot{P}_g$ crit. ($\frac{lbs.}{in.^2}$)
QA	0.071	26.0	0.704	1.21	0.075	1.408	1.57	0.057	2.82	1.0	0.090	5.64	1.0	0.090
BU	0.046	87.5	1.09	2.00	0.153	2.18	1.57	0.192	4.36	↓	0.303	8.72	↓	0.303
BG	0.053	75.0	0.94	1.98	0.131	1.88	1.57	0.165	3.76		0.260	7.52		0.260
BH	0.042	245.0	1.19	1.93	0.440	2.38	1.57	0.540	4.76		0.850	9.52		0.850
BI	0.038	250.0	1.32	1.93	0.450	2.64	1.57	0.550	5.28		0.870	10.56		0.870
BJ	0.070	70.0	0.71	1.20	0.202	1.42	1.57	0.154	2.84		0.242	5.68		0.242
BK	0.180	64.0	0.28	0.35	0.630	0.56	0.75	0.295	1.12		0.221	2.24		0.221
BL	0.058	60.0	0.86	1.85	0.112	1.72	1.57	0.132	3.44		0.207	6.88		0.207
BX	0.056	50.0	0.89	1.92	0.090	1.78	1.57	0.110	3.56		0.172	7.12		0.172
BY	0.043	118.0	1.16	1.93	0.211	2.32	1.57	0.260	4.64		0.408	9.28		0.408
CI	0.042	148.0	1.19	1.93	0.265	2.38	1.57	0.326	4.76		0.513	9.52		0.513
CM	0.035	150.0	1.43	1.93	0.269	2.86	1.57	0.330	5.72		0.520	11.44		0.520
CN	0.029	180.0	1.72	1.93	0.322	3.44	1.57	0.397	6.88		0.623	13.76		0.623
DK	0.070	102.0	0.71	1.20	0.294	1.42	1.57	0.225	2.84	↓	0.353	5.68	↓	0.353
DO	0.044	170.0	1.14	1.93	0.305	2.28	1.57	0.375	4.56	1.0	0.590	9.12	1.0	0.590

* Ref. Tables VII and VIII

** $\tau = \frac{3\delta}{U} = \frac{(3)(7.5)}{1100} = 0.0205$ sec.

*** Figure 33

Note: These data do not reflect the increase in strength due to rapid rate of loading. See page 90 for discussion on rapid rate of loading.

SECTION 8

APPLICATIONS TO SMALL BUILDINGS

A small frame residential house typical of those found in the United States is shown in Figure 53. The static strength of the critical structural elements of this house subjected to pressure loadings, and their natural frequencies and periods, are determined in Appendix III. This data, summarized in Table X, was used to determine critical free-stream shock wave pressures due to normal incidence for this structure. These results are presented in Table XI.

The data appearing in Table X are based on a particular geometry and structural design. Considering the many possible variations of these items in the small residential house category, and also that the quality of materials and workmanship play an important part in the structural strength of a house, these data should be considered as order of magnitude numbers. An indication of the possible variation in the structural strength due to material variations and workmanship can be gotten from the data on strength of typical residential type walls given in Table VII. The wide spread in strengths is shown for walls of identical construction.

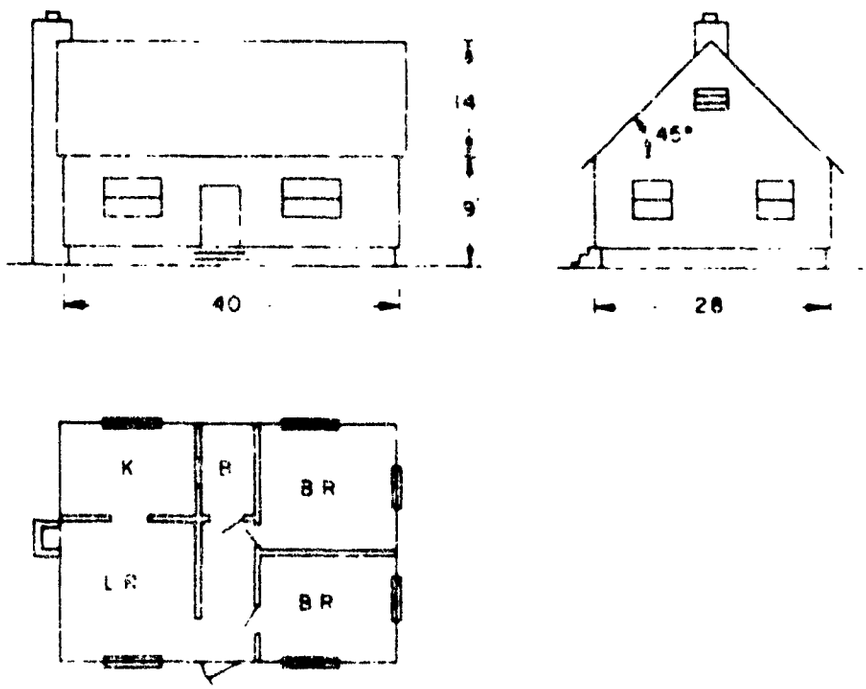

Figure 53. Model House

TABLE X

STATIC STRENGTH OF WOOD FRAME HOUSE

Structural Element	Description*	TRANSVERSE LOADING			RACKING LOAD		
		Max. All. Pressure ($Lb./Ft.^2$)	Natural Frequency (Rad./Sec.)	Natural Period (Sec.)	Max. All. Normal Pressure on House ($Lb./Ft.^2$)	Natural Frequency (Rad./Sec.)	Natural Period (Sec.)
Outside Wall -- Normal to Pressure Loading	Type QA	26.0	62.0	0.101	--	--	--
Side Wall -- No Interior Load Bearing Wall	Type QA (no openings)	--	--	--	38.0	45.3	0.138
Side Wall -- No Interior Load Bearing Wall	Type QA (with openings)	--	--	--	4.3	15.9	0.395
Side Wall -- with Interior Load Bearing Wall	Type QA (with openings)	--	--	--	17.0	18.2	0.335
Interior Load Bearing Wall	Type QD	--	--	--	19.3	52.8	0.119
Roof	2 x 6 Rafters, 24" O.C. -- 3/4" Sheathing -- Roll Roofing Paper -- Asphalt Strip Shingles	74.0	79.0	0.08	--	--	--

*Ref. Table VII

TABLE XI

CRITICAL FREE-STREAM SHOCK WAVE PRESSURES FOR SAMPLE HOUSE
(NORMAL INCIDENCE)

Structural Element	Description*	$\dot{P}_{ss}$ critical (psi)			
		η = 0.05 Sec.	η = 0.10 Sec.	η = 0.20 Sec.	η = 0.40 Sec.
Front Face Wall	Type QA	0.143	0.053	0.072	0.090
Roof	(See Table X)	0.427	0.481	0.467	0.395
Side Wall	Type QA (with openings)	1.450	1.720	0.0306	0.0467
Interior Wall	Type QD	0.171	0.059	0.095	0.117

Note: These data do not reflect the increase in strength due to rapid rate of loading. See page 90 for discussion of strength increases produced by rapid rate of loading.

*Ref. Table VII.

SECTION 9

COUPLING OF SHOCK WAVE LOADS WITH OTHER EFFECTS TO PRODUCE FAILURE

Many structures are on the verge of failure prior to being subjected to shock wave pressure disturbances. The structures could have been considerably weakened or highly stressed from such effects as faulty construction and low grade materials, improper design, foundation settlement, water damage, wood shrinkage and other temperature and/or moisture induced displacements, high wind loads, etc. A detailed account of these various factors is found in insurance company literature.[41]

The application of shock wave pressure loads to these weakened or "initially" highly stressed structures could produce failure even though the free-stream pressure levels are far below those that would produce damage in reasonably well constructed or unweakened buildings. Aircraft generated shock waves could be the "straw that broke the camel's back".

A general evaluation of the coupling of shock wave effects with the other factors possibly contributing to structural damage is not practical because of the many variables involved. Particular situations must be studied in detail.

In some instances, structural elements improve with "age". A study of data[53-58] on plaster construction and manufacture indicates that most plaster strength improves with age. Some lime plasters which are manufactured from rocks containing a mixture of calcium and magnesium carbonates tend to deteriorate in 9-15 years. This is due to expansions which take place as the magnesium oxide converts to magnesium carbonate. This effect can be minimized if the mixture of calcium and magnesium oxides is finely ground before water is added. No data on the effect of age of glass has been found.

SECTION 10

CONCLUSIONS

1. For shock wave pressure levels (small fractions of a psi) the critical types of structures from a failure point of view are wood frame residential dwellings and store fronts having large glass areas. The critical structural elements are glass and plaster walls with openings. Walls are critical in residential structures since the shear area resisting the load in side walls and the bending stiffness of front walls are small compared with other types of structures. Glass is critical for store fronts since large spans are common.

Walls of structures without internal partitions will fail at lower pressure levels compared to similar size structures with internal partitions. Glass fails in tension produced by bending. Failure of plaster walls with openings is generally critical for racking (shearing) loads in the side walls. Shear stress concentration factors around openings can be as high as ten. In some cases, plaster cracking produced by bending of the front wall can be critical.

For an N-wave duration of 0.10 sec., the range of free-stream failure pressures for glass is about 0.02 to 0.38 psi. Corresponding glass panel sizes are: 120 in. x 200 in. x 1/4 in. and 12 in. x 12 in. single strength glass, respectively. For wall construction typical of wood frame residential houses, free-stream pressures required to crack plaster are as low as 0.03 psi for shear in side walls and 0.15 psi for bending of front walls.

The lower bound of free-stream pressures producing damage ($\cong$ 0.03 psi) could be produced, for example, by an F-86 aircraft flying steady level flight slightly in excess of Mach 1 at about 4000 feet above ground. At higher altitudes, higher steady level flight Mach numbers are required to produce a free-stream pressure level of 0.03 psi on the ground. For example, at an altitude of 10,000 feet, the required Mach number is 3.5. Any amplification of the free-stream pressure by reflection or cusp effects would reduce the Mach number (for a given altitude) required to produce this pressure level of 0.03 psi.

Wind load data indicates a lower bound of structural damage at a 45 mph wind. This wind velocity corresponds to a dynamic pressure of about 0.03 psi which is in the range of shock wave pressure estimates.

The computed values of the lower bound of failure pressures given do not account for variations in material properties and workmanship whereas the wind load data do.

2. The failure pressures are functions of N-wave and structural parameters. These parameters vary over a wide range. Whereas it is not practical to present failure pressures for the many possible combinations of structural and shock wave variables, the failure pressures given in this report for the critical structural elements (glass and plaster walls) are for specific values of N-wave and structural parameters which are likely in practice. Other cases may be investigated in detail by employing the methods and basic data presented here.

3. The response of structural elements to shock wave pressures is governed by elastic behavior since at these pressure levels only brittle materials fail, and the more ductile materials such as steel and reinforced concrete, which exhibit substantial plastic deformation before failure, are not strained above their yield points.

4. A critical loading condition occurs when the trace on the ground of the inclined plane of the shock front that contacts the structure is parallel to the

front face of the building. When the angle of the plane of the shock front to the vertical is small, reflection effects can produce up to four times peak free-stream pressure on the front face of the building. This condition is critical for windows near the bottom of the front building face.

5. The strength of glass is increased over its static strength by rapid rate of loading. Test results indicate an increase by a factor of three over static strength of 6000 psi. The strength of plaster walls is also increased by rapid rate of loading. Impact tests in which sand bags were dropped normal to the panel surface (bending action) gave deflections at which plaster cracked of about 3 to 5 times the deflections for plaster cracking under static loading. No data is available for racking transient loads on walls. Any information extrapolated from blast wave tests on buildings would not be meaningful since the pressures employed were too high and the plaster failures noted could have occurred at lower pressures. Test data on plaster walls subjected to transient loads (particularly racking loads) are needed.

6. Experimental measurements of the pressure distribution on structures subjected to N-wave free-stream pressures are required. These tests are needed in order to check the validity of the use of blast wave data and concepts to predict building loads produced by N-waves whose shape and pressure levels are different from blast waves.

7. Existing data on shock wave damage is mostly from insurance claims. The information is spotty and incomplete in a great many cases. Controlled experiments to assess the damage to structures or structural elements produced by N-wave free-stream pressures are required.

SUGGESTED EXPERIMENTAL PROGRAM

1. An experimental program to obtain data on the pressure distribution on structures and the damage to structures produced by N-wave free-stream pressure waves is suggested. The program would be broken down into three phases as indicated below:

Phase 1	Loads on Structures
Phase 2	Damage to Structures
Phase 3	Flight Tests - Loads and Damage

For phases 1 and 2, the N-waves are generated by means other than aircraft flight. In phase 3, actual aircraft generated N-waves are employed. The purpose of the flight tests is to check the results of phases 1 and 2 and to demonstrate to a layman that equivalent effects are produced by actual aircraft generated N-waves and N-waves produced by other means.

2. It is also suggested that extensions be made to Ting's[59] analysis of the diffraction of a sonic disturbance by a rectangular barrier. The extensions would include:

(a) Sonic disturbance corresponding to an N-wave (normal incidence).

(b) N-wave sonic disturbance for nonnormal incidence in a non-vertical plane.

The results would be useful in interpreting experimental data and would represent an advance in the state of the art in diffraction problems.

APPENDIX I

BIBLIOGRAPHY

1. Lilley, G.M., Westley, R., Yates, A.H., and Busing, J.R., "On Some Aspects of the Noise Propagation from Supersonic Aircraft", The College of Aeronautics, Cranfield, Report No. 71, February 1953.

2. Whitham, G.B., "The Behavior of Supersonic Flow Past a Body of Revolution, Far From the Axis", Proceedings Royal Society, 1950.

3. Whitham, G.B., "The Flow Pattern of a Supersonic Projectile", Communications on Pure and Applied Mathematics, Vol. V, 1952.

4. Rao, P.S., "Supersonic Bangs", Part I, Aeronautical Quarterly, February 1956.

5. Rao, P.S., "Supersonic Bangs", Part II, Aeronautical Quarterly, May 1956.

6. Armour Research Foundation, "Theoretical Investigations of Sonic Boom Phenomena", WADC Technical Report 57-412, August 1957, Contract AF 33(616)-3371.

7. Warren, C.H.E., "Noise Associated With Supersonic Flight", Journal Royal Aeronautical Society, Vol. 58, 1954. ~AD - 130823

8. Walters, A.G., "The Noise From Aircraft", Journal Royal Aeronautical Society, Vol. 58, January 1954.

9. Daum, F.L. and Smith, M., "Experimental Investigation of the Shock Wave Pressure Characteristics Related to Sonic Boom", WADC-TN-55-203, Aeronautical Research Laboratory, Wright Air Development Center, August 1955. ~AD-68102

10. Mullens, E.M., "A Flight Test Investigation of the Sonic Boom", AFFTC-TN-56-20, May 1956.

11. Fleming, M., "Measurement of Noise on the Ground from Aircraft in Flight", Journal of Royal Aeronautical Society, Vol. 58, April 1954.

12. Du Mond, W.M., Cohen, E.R., Panofsky, W.K.H., and Deeds, E., "A Determination of the Wave Forms and Laws of Propagation and Dissipation of Ballistic Shock Waves", Journal of Acoustical Society of America, Vol. 18, No. 1, July 1946.

13. Merritt, M.L., "Blast Loading of Idealized Structures Using High Explosives", Proceedings of Symposium on Earthquake and Blast Effects on Structures, Los Angeles, California, June 1952.

14. Merritt, M.L., "Shielding From Blast Waves by Parallel Structures", AFSWP-224, Sandia Corporation, 1952.

15. Hudson, C.C., "Self-Shielding From Blast Waves by Structural Members", AFSWP-225, Sandia Corporation, May 1953.

16. Windes, S.L., "Report of Investigations, Damage From Air Blast, Progress Report 1", U. S. Department of Interior, Bureau of Mines, R.I. 3622, February 1942.

17. Burchard, J.E., Beckwith, H.L., Gelotte, E.W., and Dahl, N.C., "Static Detonation Trials of Three Framed Houses at Area J, Aberdeen Proving Ground, December 19, 1942 to January 11, 1943", Parts I and II, National Research Council Interim Report No. 23, April 1943.

18. Sachs, D.C. and Hornig, S.R., "Air-Blast Loading on Structures", Interim Report No. 3, July 30, 1954, Prepared for Wright Air Development Center, Contract No. AF 33(616)-226, Stanford Research Institute, Stanford, California.

19. Bleakney, W., "Shock Loading of Rectangular Structures", Technical Report II-11, Princeton University, January 1952.

20. Bleakney, W., "A Shock Tube Investigation of the Blast Loading of Structures", Proceedings of the Symposium on Earthquake and Blast Effects on Structures, Los Angeles, California, June 1952.

21. "Study of the Effect of Orientation on Dynamic Loading and Response of Structures", Armour Research Foundation Report No. 3, March 1, 1955, Contract No. AF 33(616)-166, Confidential. (Title Unclassified)

22. Rines, E., Ferguson, M., and Kingery, C., "Air Blast Loading on Three-Dimensional Scale Models of Dome Shape", BRL Memorandum Report No. 889, AFSWP No. 773, April 1955.

23. Newmark, N.M., "An Engineering Approach to Blast Resistant Design", Proceedings ASCE, Vol. 79, Separate No. 306, October 1953.

24. "Windowless Structures, A Study in Blast-Resistant Design", Federal Civil Defense Administration Technical Manual TM-5-4, June 1952.

25. "Proceedings of the Conference on Buildings in the Atomic Age", June 1952, MIT, Cambridge, Massachusetts.

26. "Study of Vulnerability of a Thermal Electric Power Plant to An Air Blast", Armour Research Foundation Report No. 18, March 15, 1954, Contract No. AF 33 (038)-27011, Confidential. (Title Unclassified)

27. Whitney, Anderson, and Cohen, "Design of Blast Resistant Construction for Atomic Explosions", Journal of the American Concrete Institute, Vol. 26, No. 7, March 1955.

28. "A Simple Method for Evaluating Blast Effects on Buildings", Armour Research Foundation, Revised Edition, July 1954.

29. "The Effects of Nuclear Weapons", Prepared by U. S. Department of Defense, Published by U. S. Atomic Energy Commission, June 1957.

30. "Compendium of Air Blast Effects, Vol. II, Loads", Armour Research Foundation, July 1957, Contract AF 33(600)-25734, Confidential. (Title Unclassified)

31. Courant, R. and Friedrichs, K.O., "Supersonic Flow and Shock Waves", Interscience Publishers, Inc., 1948.

32. Liepmann, H.W., and Puckett, A.E., "Introduction to Aerodynamics of a Compressible Fluid", Calcit Aeronautical Series, John Wiley, 1947.

33 Federal Specification DD-G 451a, 1949, "Glass, Flat and Corrugated, For Glazing, Mirrors and Other Uses".

34. Commercial Standard 163-52, "Standard Stock Ponderosa Pine Windows, Sash and Screens", U. S. Department of Commerce, October 15, 1952.

35. "Aluminum Windows - 1957 Specifications", Aluminum Window Manufacturers Association, Great Neck, New York.

36. "Windows and Glass in the Exterior of Buildings", Building Research Institute, National Academy of Sciences, National Research Council Publication 478.

37. Thompson, N.J. and Cousins, E.W., "Explosion Tests on Glass Windows, Effects on Glass Breakage of Varying the Rates of Pressure Applications", Journal of the American Ceramic Society, Vol. 32, 1949.

38. Taylor, W.J. and Clark, R.O., "Shock Tube Tests of Glazing Materials", BRL Memorandum Report No. 626, Ballistics Research Laboratories, Aberdeen, Maryland, November 1952.

39. Building Materials and Structures Reports, National Bureau of Standards, Superintendent of Documents, Washington, D. C.

40. Trayer, G.W., "The Rigidity and Strength of Frame Walls", Forest Products Laboratory Report No. 896, March 1956.

41. "Blasting Claims, A Guide for Adjusters", National Board of Fire Underwriters.

42. Heck, G.A., "Structural Properties of Conventional Wood-Frame Constructions for Walls, Partitions, Floors, and Roofs", Building Materials and Structures Report BMS 25, National Bureau of Standards, September 1939.

43. Den Hartog, J.P., "Mechanical Vibrations", McGraw-Hill, Third Edition, 1947.

44. Clark, W.C., "The Effect of Atomic Weapons on Glazing and Window Construction", U. S. Atomic Energy Commission Report AECD-3643, August 1951.

45. Air Force Judge Advocates Office, Claims Department, Air Force Headquarters, Washington, D. C.

46. File, Kulon Knell CX 57/209, Air Force Judge Advocates Office, Washington, D. C.

47. Whittaker, E.T., "A Treatise on the Analytical Dynamics of Particles and Rigid Bodies", Dover Press, 4th Edition, 1937.

48. Timoshenko, S., "Vibration Problems in Engineering", Van Nostrand Company, 2nd Edition, 1937.

49. English, J.M., "Rupture of Brittle Beams Under Impulsive Loading", Report 51.14, Department of Engineering, University of California, Los Angeles, December 1951.

50. Flynn, P.D., "Elastic Response of Simple Structures to Pulse Loadings", BRL Memorandum Report No. 525, Ballistics Research Laboratory, Aberdeen, Maryland, 1950

51. Baker, W.E. and Hoffman, A.J., "The Shapes of Circular and Square Membranes Under Blast Loading", BRL Memorandum Report No. 556, Ballistics Research Laboratory, Aberdeen, Maryland.

52. Newmark, N.M., "Analysis and Design of Structures to Resist Atomic Blast", Bulletin of Virginia Polytechnic Institute, Engineering Experiment Station Series No. 106, January 1956.

53. Noble, V.H., "Causes and Remedies of Plaster Cracks", Progressive Architecture, November 1951.

54. Commercial Bulletin "Permalite Plaster Aggregate", Perlite Division, Great Lakes Carbon Corporation, Los Angeles.

55. "American Standards Specifications for Reinforced Gypsum Concrete", ASA A59-1 - 1954 American Standards Association.

56. Lowndes, W.S., "Plastering and Stucco Work", Intercontinental Textbook Company, Scranton, Pennsylvania, 1924.

57. Verral, W., "Solid and Fibrous Plastering", Chemical Publishing Company, Inc., New York, 1941.

58. American Standard Specification for Gypsum Plastering and Interior Lathing and Furring", ASA A42.4-1955, American Standards Association.

59. Ting, Lu, "Diffraction of Disturbances Around a Convex Right Corner With Applications in Acoustics and Wing-Body Interference", Journal of the Aeronautical Sciences, Vol. 24, November 1957.

60. "The Effects of Atomic Weapons", Prepared by the U. S. Department of Defense and the U. S. Atomic Energy Commission, September 1950.

APPENDIX II

DYNAMIC PARAMETERS

DYNAMICS OF UNIFORM BEAMS AND PLATES

Since the operations are almost identical for beams and plates, we shall designate beam equations by the symbol B and plate equations by the symbol P.

1. Equation of Motion of an Element

$$\text{(B)} \qquad EI \frac{\partial^4 v}{\partial x^4} + m \frac{\partial^2 v}{\partial t^2} = P(x,t) \tag{17}$$

$$\text{(P)} \qquad D \nabla^4 v + \mu \frac{\partial^2 v}{\partial t^2} = p(x,y,t) \tag{18}$$

2. Boundary Conditions

a. Simple Support

$$\text{(B)} \qquad v = 0; \quad \frac{\partial^2 v}{\partial x^2} = 0, \quad \text{at} \quad x = \begin{cases} 0 \\ L \end{cases} \tag{19}$$

$$\text{(P)} \qquad \left.\begin{aligned} v = 0; \quad & \frac{\partial^2 v}{\partial x^2} + \nu \frac{\partial^2 v}{\partial y^2} = 0, \quad \text{at} \quad x = \begin{cases} 0 \\ L_x \end{cases} \\ v = 0; \quad & \frac{\partial^2 v}{\partial y^2} + \nu \frac{\partial^2 v}{\partial x^2} = 0, \quad \text{at} \quad y = \begin{cases} 0 \\ L_y \end{cases} \end{aligned}\right\} \tag{20}$$

b. Clamped Ends

$$\text{(B)} \qquad v = 0; \quad \frac{\partial v}{\partial x} = 0 \qquad \text{at} \quad x = \begin{cases} 0 \\ L \end{cases} \tag{21}$$

$$\text{(P)} \qquad \left.\begin{aligned} v = 0; \quad & \frac{\partial v}{\partial x} = 0 \qquad \text{at} \quad x = \begin{cases} 0 \\ L_x \end{cases} \\ v = 0; \quad & \frac{\partial v}{\partial y} = 0 \qquad \text{at} \quad y = \begin{cases} 0 \\ L_y \end{cases} \end{aligned}\right\} \tag{22}$$

3. Initial Conditions

$$\text{(B)} \qquad v = g(x); \quad \frac{\partial v}{\partial t} = h(x) \quad \text{at} \quad t = 0 \tag{23}$$

$$\text{(P)} \qquad v = g(x,y); \quad \frac{\partial v}{\partial t} = h(x,y) \quad \text{at} \quad t = 0 \tag{24}$$

For most of our problems $h = g = 0$.

4. Normal Modes

A normal mode ξ_i is one which satisfies the following relations:

(B) $$EI \frac{\partial^4}{\partial x^4} [\xi_i \cos \omega_i t] + m \frac{\partial^2}{\partial t^2} [\xi_i \cos \omega_i t] = 0 \qquad (25)$$

(P) $$D \nabla^4 [\xi_i \cos \omega_i t] + \mu \frac{\partial^2}{\partial t^2} [\xi_i \cos \omega_i t] = 0 \qquad (26)$$

and the boundary conditions. It is known that for beams the solution is:

(B) $$\xi_i = \alpha \sin k_i x + \beta \sinh k_i x + \gamma \cos k_i x + \delta \cosh k_i x \qquad (27)$$

where the values of k_i depend on the boundary conditions. From eq. (25):

(B) $$EI k_i^4 = m \omega_i^2 \qquad (28)$$

so for each k_i there is an ω_i.

For plates, the solutions have also been derived but they are very complex, except for simply supported ends. Here the form of ξ_i, which we shall now call ξ_{ij} is:

(P) $$\xi_{ij} = \sin (i \frac{\pi x}{L_x}) \sin (j \frac{\pi y}{L_y}) \quad , \quad i = 1,2,3 \; ; \quad j = 1,2,3 \qquad (29)$$

and substituting in eq. (26) one obtains:

(P) $$D \left\{ \left[\frac{i\pi}{L_x} \right]^2 + \left[\frac{j\pi}{L_y} \right]^2 \right\} = \mu \omega_{ij}^2 \qquad (30)$$

For beams simply supported:

(B) $$\xi_i = \sin \left[\frac{i \pi x}{L} \right] \quad ; \quad i = 1,2,3 \qquad (31)$$

(B) $$EI \left[\frac{i\pi}{L} \right]^4 = m \omega_i^2 \qquad (32)$$

5. Forced Vibrations

The solution to eq. (17) and (18) with the proper boundary conditions can be described in terms of the normal modes ξ_i multiplied by suitable time functions $\phi_i(t)$. Thus,

(B) $$v = \sum_{i=1}^{\infty} \phi_i \xi_i \qquad (33)$$

(P) $$v = \sum_{i=1}^{\infty} \sum_{j=1}^{\infty} \phi_{ij} \xi_{ij} \qquad (34)$$

Substituting into the equations of motion and using relations (25) and (26) to eliminate $EI \frac{d^4}{dx^4} \xi_i$ and $D\nabla^4 \xi_{i,j}$, respectively, one obtains:

$$\text{(B)} \qquad \sum_{i=1}^{\infty} \left[m\omega_j^2 \xi_i \right] \left[\phi_i + \frac{1}{\omega_i^2} \frac{d^2 \phi_i}{dt^2} \right] = P(x,t) \tag{35}$$

$$\text{(P)} \qquad \sum_{i=1,2}^{\infty} \sum_{j=1,2}^{\infty} \left[\mu \omega_{ij}^2 \xi_{ij} \right] \left[\phi_{ij} + \frac{1}{\omega_{ij}^2} \frac{d^2 \phi_{ij}}{dt^2} \right] = p(x,y,t) \tag{36}$$

Normal modes are known to be orthogonal. Hence

$$\text{(B)} \qquad \int_0^L \xi_i \, \xi_k \, m dx = 0 , \quad \xi_i \neq \xi_k \tag{37}$$

$$\text{(P)} \qquad \int_0^{L_x} \int_0^{L_y} \xi_{ij} \, \xi_{kl} \, \mu dxdy = 0 , \quad \xi_{ij} \neq \xi_{kl} \tag{38}$$

Multiplying equations (35) and (36) by one normal mode and integrating over the full surface, one obtains,

$$\text{(B)} \qquad \left[\int_0^L m\omega_i^2 \xi_i^2 \, dx \right] \left[\phi_i + \frac{1}{\omega_i^2} \frac{d^2 \phi_i}{dt^2} \right] = \int_0^L P(x,t) \, \xi_i dx \tag{39}$$

$$\text{(P)} \qquad \left[\int_0^{L_x} \int_0^{L_y} \mu \omega_{ij}^2 \xi_{ij}^2 \, dxdy \right] \left[\phi_{ij} + \frac{1}{\omega_{ij}^2} \frac{d^2 \phi_{ij}}{dt^2} \right] = \int_0^{L_x} \int_0^{L_y} p(x,y,t) \, \xi_{ij} \, dxdy \tag{40}$$

A great simplification occurs if $P(x,t) = p(x,y,t) = F(t)$. Then

$$\text{(B)} \qquad \phi_i + \frac{1}{\omega_i^2} \frac{d^2 \phi_i}{dt^2} = \frac{F(t)}{m\omega_i^2} \frac{\int_0^L \xi_i \, dx}{\int_0^L \xi_i^2 dx} \tag{41}$$

$$\text{(P)} \qquad \phi_{ij} + \frac{1}{\omega_{ij}^2} \frac{d^2 \phi_{ij}}{dt^2} = \frac{F(t)}{\mu \omega_{ij}^2} \frac{\iint \xi_{ij} dxdy}{\iint \xi_{ij}^2 dxdy} \tag{42}$$

For simply supported ends:

$$\text{(B)} \qquad \phi_i + \frac{1}{\omega_i^2} \frac{d^2 \phi_i}{dt^2} = \frac{F(t)}{m\omega_i^2} \left(\frac{4}{i\pi} \right) , \quad i = 1,3,5 \tag{43}$$

$$(P) \quad \phi_{ij} + \frac{1}{\omega^2_{ij}} \frac{d^2\phi_{ij}}{dt^2} = \frac{F(t)}{\mu \omega^2_{ij}} \left(\frac{4}{i\pi}\right)\left(\frac{4}{j\pi}\right), \quad i = 1,3,5; \; j = 1,3,5 \tag{44}$$

The value of ϕ_i or ϕ_{ij} for even numbered modes is zero. To find the static contribution to the displacement when $F(t) = F_{max.}$ and $\frac{d^2\phi}{dt^2} = 0$, ϕ becomes

$$(B) \quad \left(\phi_i = \frac{F_{max.}}{m\omega_i^2} \frac{4}{i\pi}\right) \sin \frac{i\pi x}{L} \tag{45}$$

$$(P) \quad \left[\phi_{ij} = \frac{F_{max.}}{\mu\omega^2_{ij}} \left(\frac{16}{ij\pi^2}\right)\right] \sin \frac{i\pi x}{L_x} \sin \frac{j\pi x}{L_y} \tag{46}$$

The maximum moment occurs at the center.

Hence, $M_i = -EI \frac{\partial^2}{\partial x^2} (\phi_i \sin \frac{i\pi x}{L})$ at $x = \frac{L}{2}$ is

$$M_i = EI \frac{F_{max.}}{m\omega_i^2} \frac{4}{i\pi} \left(\frac{i\pi}{L}\right)^2 \sin \frac{i\pi}{2}$$

$$(B) \quad M_i = \frac{4}{(i\pi)^3} F_{max.} L^2 \sin \frac{i\pi}{2} \tag{47}$$

$$M_{x_{ij}} = -D \left(\frac{\partial^2}{\partial x^2} + \nu \frac{\partial^2}{\partial y^2}\right)(\phi_{ij}\xi_{ij}) \quad \text{at } x = \frac{L_x}{2}, \; y = \frac{L_y}{2}$$

$$M_{x_{ij}} = D \frac{F_{max.}}{\mu\omega^2_{ij}} \left(\frac{16}{\pi^2(ij)}\right)\left(\left[\frac{i\pi}{L_x}\right]^2 + \nu\left[\frac{j\pi}{L_y}\right]^2\right) \sin \frac{i\pi}{2} \sin \frac{j\pi}{2}$$

$$(P) \quad M_{x_{ij}} = \left(\frac{\left(\frac{i\pi}{L_x}\right)^2 + \nu\left(\frac{j\pi}{L_y}\right)^2}{\left[\left(\frac{i\pi}{L_x}\right)^2 + \left(\frac{j\pi}{L_y}\right)^2\right]^2}\right) \left(\frac{16 F_{max.}}{ij\pi^2}\right) (-1)^{\frac{i-j}{2}} \tag{48}$$

The static moment is:

$$(B) \quad M_x = \frac{1}{8} F_{max.} L^2 \tag{49}$$

$$(P) \quad M_x = \beta F_{max.} L_x^2 \tag{50}$$

See Table IV for β . ($\beta = st^2/6\ pb^2$) with, $F_{max} = p$, $L_x = b$, t = thickness, s = max. stress.

The participation factor is

$$(PF)_i = \frac{\text{stress contributed by } i^{th} \text{ mode}}{\text{maximum static stress}}$$

Hence (B) $$(PF)_i = \frac{32}{(i\pi)^3} (-1)^{\frac{i-1}{2}} \tag{51}$$

(P) $$(PF)_{ij} = \frac{16}{\beta L_x^2 \pi^2 (ij)} \left(\frac{(\frac{i\pi}{L_x})^2 + \nu (\frac{i\pi}{L_y})^2}{[(\frac{i\pi}{L_x})^2 + (\frac{j\pi}{L_y})^2]^2} \right) \tag{52}$$

In the special case of Lx = Ly, i = j = 1, $\beta = 0.0479$, $\nu = 0.3$

$$(P) \quad (PF)_{1,1} = \frac{16}{\pi^4 \beta L^2} \cdot \frac{1}{[4 (\frac{\pi}{L})^2]} = \frac{4(1.3)}{(0.0479)\pi^4} = 1.115$$

If one defines $f_i \ \xi_i^* = \phi_i \ \xi_i$ where ξ_i^* is the contribution to static displacement due to F_{max}, equations (41) and (42) become:

(B) $$f_i + \frac{1}{\omega_i^2} \frac{d^2 f}{dt^2} = \frac{F(t)}{F_{max.}} \tag{53}$$

(P) $$f_{ij} + \frac{1}{\omega_{ij}^2} \frac{d^2 f_{ij}}{dt^2} = \frac{F(t)}{F_{max.}} \tag{54}$$

These equations define the modal dynamic response functions.

APPROXIMATE SOLUTION FOR AMPLIFICATION FACTOR

The solution to the differential equation

$$\frac{1}{\omega^2} \frac{d^2 f}{dt^2} + f = c_1 \quad \text{(where } c_1 = \text{constant)}$$

with the initial conditions $f = a_1$; $\frac{1}{\omega} \frac{df}{dt} = b_1$ at $t = t_1$ is:

$$f = c_1 + F_1 \sin [\omega (t - t_1) - \phi] \tag{55}$$

$$\text{or} \qquad f - c_1 = R_1 \sin \left[\omega (t - t_1) - \phi \right] \tag{56}$$

Therefore, from Eq. (55): $\frac{1}{\omega} \frac{df}{dt} = R_1 \cos \left[\omega (t - t_1) - \phi \right]$ (57)

Eliminating t by summing the squares of equations (56) and (57):

$$(f - c_1)^2 + \left(\frac{1}{\omega} \frac{df}{dt}\right)^2 = R_1^2 = (a_1 - c_1)^2 + b_1^2 \tag{58}$$

In the phase plane, the abscissa is f, and the ordinate $\frac{1}{\omega} \frac{df}{dt}$. Eq (58) is a circle in these coordinates: its center is $(c_1, 0)$ and radius is R_1. Reinterpreting equation (55) in terms of the phase plane, one notes that the angle $\left[\omega (t - t_1) - \phi \right]$ is the angle between a vertical line and the radius to a point on the circle. In an elapsed time $(t_2 - t_1)$, the radius will move clockwise through an angle $\omega (t_2 - t_1)$ radians. See Figure 54.

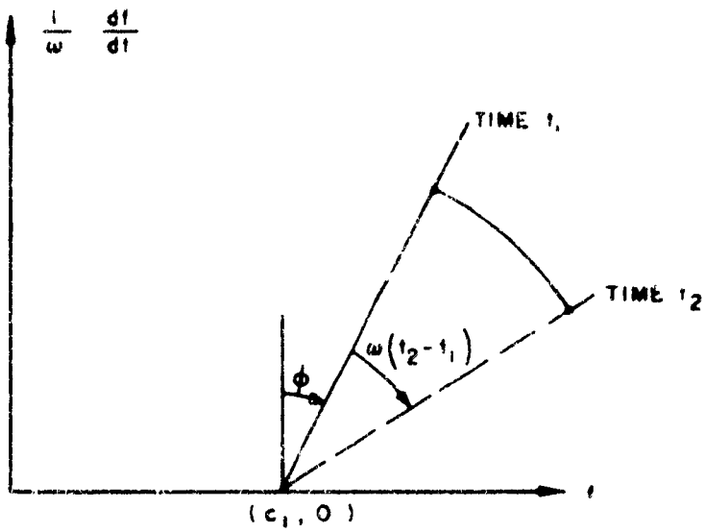

Figure 54. Phase Plane

This is all one needs to know to use the phase plane to construct an approximate solution to the equation

$$\frac{1}{\omega^2} \frac{d^2 f}{dt^2} + f = \frac{F(t)}{F_{max.}} \tag{59}$$

from which an amplification factor can be found. As an illustration, consider Figure 55 in which the loading time happens to equal one natural period. Here we see the N-shaped wave of $F(t)/F_{max.}$ divided into six equal time intervals, one sixth period or 60° in duration on the phase plane. For each time interval, the average ordinate has been noted, i.e., 5/6; 3/6; 1/6; -1/6; etc.

Since the body is initially at rest $f = \frac{df}{dt} = 0$. With a center at $(\frac{5}{6}, 0)$,

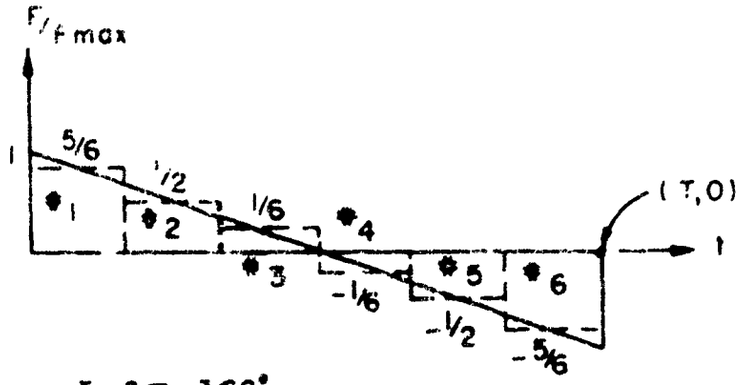

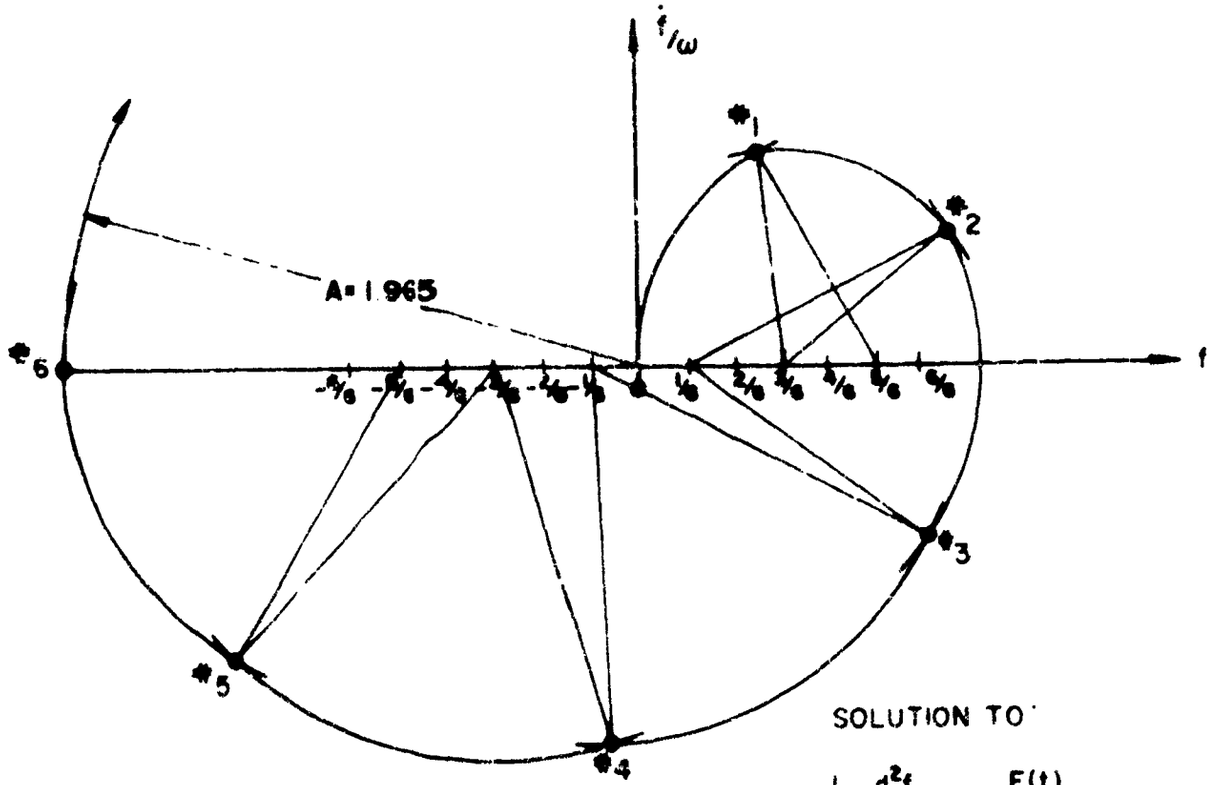

SOLUTION TO

$$\frac{1}{\omega^2}\frac{d^2f}{dt^2} + f = \frac{F(t)}{F\,max}$$

WITH $f(o) = \frac{df}{dt}(o) = o$

FIGURE 55 APPROXIMATE AMPLIFICATION FACTOR FOR N-WAVE USING PHASE PLANE

and a radius to the initial point (0,0), an arc of 60° is swung. The end point is labeled 1. With a center at $(\frac{2}{6}, 0)$ and the radius required to reach point 1, one swings an arc of 60° from point 1 to point 2. The process is repeated till all six points have been determined. The amplification factor is the larger of the radius to point 6 from the point (0,0) or the maximum value of ξ generated by the previous arcs.

DERIVATION OF THE "M" FUNCTION

Let CRITDEF of Figure 56 be a curve of amplification factor versus (η) where η is a characteristic time of the load-time relation and ω is the natural (radian) frequency of the mode considered.

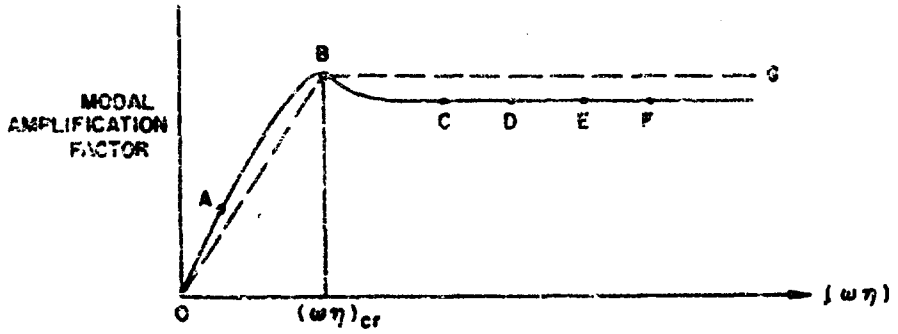

Figure 56. Idealized Modal Amplification Factor

Our objective is to devise factors to exaggerate the contributions due to higher modes.

The formula for A_L is, reference page 47.

$$A_L = \sum_{j=1}^{\infty} (PF)_j A_j$$

If the lowest natural frequency corresponds to C on Figure 56 and the h higher natural frequencies are at E, F, etc., one can use:

$$A_L = A_1 \sum_{j=1}^{\infty} |(PF)_j| \qquad (60)$$

where A_1 is the amplification factor for the first (lowest frequency) mode.

So the first construction would be to use as a general factor on the first mode contribution (which is $A_1 (PF)_1$) the factor,

$$M = \frac{1}{(PF)_1} \sum_{j=1}^{\infty} |(PF)_j|$$

This relation is, however, not conservative when $\omega_1 < \omega_{cr}$, since the contributions from higher modes do not diminish as does the contribution from the first mode.

To overcome this difficulty, we will use an additional factor, M, which is unity for $\omega_1 > \omega_{cr}$ and greater than unity for $\omega_1 < \omega_{cr}$. We simplify the geom-

city of the amplification curve and represent it by the broken line OBG, in Figure 56. In Figure 57, if OBG is multiplied by H, it becomes OB'G'. If one now considers that the contributions due to higher modes is constant independent of ω , the amplification factor would be given by O'B'G'. Designate the ratio of ordinates on O'B'G' to OB'G' as M.

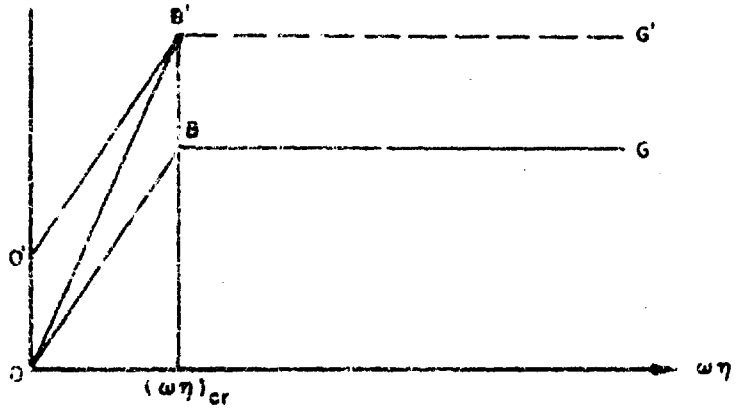

Figure 57. Modified First Mode Amplification Factor

$$M = 1 + \frac{(H-1)\left(1-\frac{\omega_1}{\omega_{cr}}\right)}{H-\left(\frac{\omega_1}{\omega_{cr}}\right)}, \quad \omega_{cr} > \omega_1$$

$$= 1, \quad \omega_{cr} < \omega_1$$

Among all the items in Table V the value for H and hence M would be largest for the simply supported flat plate. The value of H is 1.225. We also note that the largest ratio between the first and second modes was nine. Hence, the second mode frequency will usually have dropped below ω_{cr} by the time $\omega_1 = 1/9\omega_{cr}$. There is no point in carrying M below $\omega_1/\omega_{cr} = \frac{1}{9}$ because the attenuation of higher modes should be considered and since the total response is smaller than static. The use of the "M" factor for the worst value of H is conservative; but, in the interesting regions, its contribution is small.

When the "M" factor is applied to real amplification factor curves, another conservative element appears since the attenuation of the first mode is not quite as rapid as assumed in Figure 57.

The recommended value of the upper limit for the amplification factor is

$$A_L = A_1 (PF)_1 (H) M$$

$$= A_1 M \sum_{j=1}^{\infty} |(PF)_j|$$